The use of ground penetrating radar to map soil physical properties that control water flow pathways in alluvial soils

A thesis presented in partial fulfilment of the requirement for the degree of

Master of Science

in

Agriculture

at Massey University, Manawatu,

New Zealand.

Angela Louise Lane

2016

Abstract

Soil drainage models are vital for informing smart agricultural practices. Predicting soil drainage and zones where denitrification occurs, requires knowledge of the spatially varying subsurface features, for example soil-thickness, flow pathways, and depth to water table. Obtaining information about these features rapidly and non-invasively requires the use of geophysical techniques such as ground penetrating radar (GPR). While applications of GPR are diverse, ranging from geotechnical to archaeological investigations, to mineral and groundwater exploration, GPR has not been extensively applied in soil mapping for agricultural purposes across alluvial soils. The potential use of GPR for identifying subsurface features, such as the depth to gravel and water table which both influence soil drainage and denitrification processes, could benefit future developments in precision agriculture. To assess applicability of GPR for this purpose, this thesis presents research conducted on the alluvial soils at Dairy 1 farm, Massey University, Palmerston North. Radargrams were collected on two 0.4 ha plots, one arable and one pasture, using 200 MHz and 100 MHz antennas, in a 2-m grid pattern. Radargrams were ground-truthed with 13 soil cores and 21 auger holes, targeting different layers detected by GPR. The soil cores were analysed for bulk density, soil moisture and particle size. Using the 200 MHz antennas, soil textural banding was identified with specific reflection configurations within individual radargrams. These were represented when a contrasting textural boundary appeared as a continuous line of two to three bands. However, finer layering features were not identified. The 100 MHz antennas were able to detect depth to water table in the pasture plot. Soil moisture conditions were identified by a change in radar wave velocity. This appeared on radargrams as a difference in depth and radargram configuration shape. The use of Slice View images compiled from radargram data, assisted with identifying potential flow pathways and the depth to the water table across the pasture plot. Validation of radargrams with soil core samples indicates that GPR can obtain meaningful results from alluvial sediments ranging from sandy loams to silt loams. The use of GPR for

delineating subsurface features in alluvial soils is a promising tool that could assist with precision agricultural practices.

Acknowledgements

I would like express my appreciation to my supervisors Dr Sam McColl, Dr Carolyn Hedley and Associate Professor Ian Fuller for your advice, rewording, restructuring, the handy journal articles and chats that I somehow made sense of to form this manuscript. Thanks to the Brian Aspin Scholarship, Colin Holmes Dairy Scholarship, George Mason Sustainable Landuse Scholarship, Helen E Akers Postgraduate Scholarship and Horizons Advanced SLUI Scholarship for the financial support through my postgraduate degree.

Thanks to Paul Peterson and John Dando, for your assistance in the field, measuring plot areas and undertaking soil coring and augering. I appreciate your accurate record keeping and measurements. Thanks also to Eric Breard and Anja Moebis for your assistance with the Horiba Partica Analyzer. This formed such a crucial part of the thesis and I thank you Eric for your time over several months in setting up the Analyser. Thanks also to James Veitch for your assistance with GIS.

I would also like to thank other staff and students based at Massey University, Palmerston North who I came across, whether it was you assisting me with my work or me assisting you, I thank you for your time and the odd chat to keep me sane!

Mum, Don, Gerald and Mike for your positivity and keeping me on track, thanks for the 'check-up' phone calls Mum! Dad, thanks for your support and giving me the determination to complete a Masters.

Finally, Gareth, thanks for being my wing-man through this crazy adventure. Your love, support, strength and encouragement made me realise you can do anything you put your mind to, once the procrastination stops!

I never imagined I would ever write a thesis. I guess it's one of those paths in life…You're never lost, you're just exploring, and what an exploration it's been.

Angela

August 2016

Table of Contents

List of Figures

List of Tables

1 Introduction

1.1 Introduction

There is a need for smarter agricultural practices to minimise contamination to water bodies. Leaching of nutrients such as nitrate (NO^-_3) from agricultural production systems into ground and surface water is becoming a major concern within New Zealand. Nitrate present in ground and surface water at sufficiently high concentrations that is then ingested, is potentially toxic to humans (Cameron et al., 2013; Di & Cameron, 2002). Currently, the maximum acceptable value of nitrate nitrogen present in drinking water is 11.3 mg/l (equivalent to a nitrate ion concentration of 50 mg/l) (Ministry of Health, 2008). In addition to this, nitrate draining into surface waters can deteriorate water quality resulting in eutrophication and fish poisoning (Di & Cameron, 2002). Increasing use of nitrogen (N) fertiliser, effluent, or deposition of animal excreta as agricultural systems have intensified, has increased the risk of NO^-_3 leaching, if not sufficiently taken up by plants. Leaching of NO^-_3 into groundwater occurs when there is an accumulation of NO^-_3 in the soil profile that coincides with excessive drainage (Di & Cameron, 2002). However, where there are oxygen-depleted (reduced) conditions, denitrification is likely to occur (McLaren & Cameron, 1996; Stenger et al., 2013). Denitrification can remove nitrate before it enters groundwater (Stenger et al., 2013). In addition to nitrates, other nutrients (e.g. phosphates) and pathogens are also of concern for freshwater and marine environments (Gachter et al., 2004; Journeaux, 2005).

Future food demand from an increasing human population requires increased agricultural production and thus the demand of N for pasture and crop growth. This in-turn could result in large losses of NO^-_3 and other nutrients and pathogens to water bodies if not managed correctly. The focus of future farming practices should be on sustainable production with minimised nutrient leaching. To understand how NO^-_3 and other nutrients reach ground and surface waters, it is vital to understand the soil physical properties and flow pathways that control movement of potential contaminants. These properties include: soil horizon characteristics; the presence,

depth and geometry of impeding (e.g. fine, cemented) and permeable (e.g. gravel) layers; and the height of the water table. The properties affecting soil drainage and flow pathways start at the soil surface follow through to the vadose zone – a transitional area between the soil and saturated zone – terminating at the groundwater reservoirs (Huisman et al., 2003). Having the ability to map all of these contributing factors from the soil surface through the vadose zone and into the groundwater is potentially useful for improving current precision agriculture applications.

Precision agriculture allows for the application of water, nutrients and other agricultural inputs at a fine scale and variable rate in relation to the crop, pasture or soil demand, minimising the impact of leaching and runoff of nutrients to water bodies. Acquiring information on crop, pasture and soil demand is generally limited to shallow subsurface depths. For example, precision agriculture typically uses electro-magnetic induction (EMI), a proximal sensing method to determine 'apparent electrical conductivity' of soil, which is then related to the spatial variability of soil properties (e.g. moisture content) (Hedley et al., 2004). However, EMI depth penetration is limited to the top ~1.5m and standard EMI equipment cannot differentiate changes with depth (Hedley, 2009). Identifying soil physical features and gathering information below this depth is becoming essential to understand flow pathways, potential zones of denitrification and nutrient loss. Effective tools are needed for exploration at greater depths (Doolittle & Collins, 1995).

Identifying physical features that contribute to soil water flow pathways has not only been time consuming and labour intensive, for example, pit excavations, installation of piezometers and observation wells, but is also limited to the immediate area of observation (Doolittle et al., 2006). Proximal sensing methods provide a more rapid and intensive data collection of subsurface factors over a larger area and without significant ground disturbance (Adamchuk et al., 2004).

A proximal sensing method used to survey the subsurface to greater depths is ground penetrating radar (GPR). This geophysical tool provides an approach for

detecting rapidly and non-invasively the subsurface factors such as soil horizons, the depth to gravels, or the depth to groundwater (Adamchuk et al., 2004). Delineating features that affect soil drainage pathways with the assistance of GPR could effectively result in improved irrigation and farming practices, thereby minimising the loss of water and nutrients via subsurface drainage. However, GPR does not perform equally in all soils, and therefore its effective application may be limited to certain soil types. For instance, soils with high electrical conductivity such as some clays (smectite and vermiculite), will attenuate the radar signal more strongly than non-clay, dry granular materials such as sand or gravel (Doolittle & Collins, 1995).

The purpose of this research is to test the ability of GPR to map subsurface physical features thought to control soil water flow pathways in alluvial soils. The ability to efficiently map subsurface features using a non-invasive technique would be highly desirable to those who need to understand the movement of nutrients and water through alluvial soils.

1.2 Research Aim

To critically assess the use of ground penetrating radar in order to identify soil physical properties, that control soil water flow pathways in alluvial soils.

Objectives

- To classify and evaluate textural (e.g. layering and stoniness), bulk density and soil moisture changes within the vadose zone to compare with radargrams through ground-truthing using soil cores and auger samples.
- To investigate the potential use of GPR to image features that control flow pathways in the vadose zone, and identify how they potentially connect with water tables, if present in alluvial soils.
- To assess the ability of GPR to detect seasonal changes in soil water characteristics (e.g. water table depth and flow pathways).

- To make recommendations on potential GPR surveying methods for identifying features in the soil and vadose zone that influence soil water flow pathways and potential nutrient leaching in alluvial soils.

1.3 Thesis Structure

The remaining thesis is divided into five further chapters. Chapter 2 provides background research and the concept of using GPR for soil investigation in the form of a literature review. Chapter 3 provides a description of the study site and methodologies used. Chapter 4 presents the results, showing a correlation between GPR radargrams and soil cores and auger samples. Chapter 5 discusses the results to explain further the concept of using GPR to delineate soil flow pathways in alluvial soils. Chapter 6 concludes the research and provides advice for future research with GPR when undertaking identification of soil water flow pathways.

2 Literature Review

2.1 Introduction

To understand the theory and application of GPR to image subsurface flow pathways, it is necessary to first discuss the soil physical properties and processes thought to control water movement. The literature review thus begins by examining soil hydrology, emphasising areas of soil physics and the interaction with water storage and movement. Following this, the review explores the theory of GPR and examines its potential application to subsurface flow pathway mapping.

2.2 Soil Hydrology

The vadose zone covers the area from the air-soil interface to the soil-groundwater interface (Shukla, 2011). This forms the area of importance for soil hydrology, including water storage, movement and interaction with soil particles. Soil hydrology processes occur at the pore scale and are controlled by the amount, orientation, size, distribution and connectivity of soil pores (Shukla, 2011). The movement of water through these pores is influenced by their geometry and connectivity. The formation of these pores can be through various means, including physical and chemical reactions, and biological activities (e.g. swelling and shrinking of soils, chemical weathering and microorganism functions). In addition, anthropogenic effects related to land management can also affect soil pore structure. The storage and flow of water within the vadose zone is also controlled by geological properties and processes of soil.

2.2.1 Physical Properties of Soil

Soil physical properties are fundamental to the movement of soil water. Soil is divided up into three phases; solid, water and air. The total volume of soil is equal to the sum of the volume of solids plus the volume of water and air. Volume of pores equates to the volume of water plus air (McLaren & Cameron, 1996). These values along with total mass of the soil form the basis for understanding soil physical properties and their interaction with water movement. The characteristics

of soil dry bulk density (P_b) and porosity (ε) play a vital role in soil water movement. Soil dry bulk density is expressed by:

$$\mathrm{Pb} = \frac{Ms}{Vt} \quad (1)$$

Where *Ms* is mass of dry soil, *Vt* is the total volume of soil, water and air. Bulk density is then expressed as mega grams per cubic metre (Mg m^{-3}). Bulk density affects infiltration rate, root growth, available water capacity and soil porosity. There are many variables relating to bulk density, these include, but are not limited to the amount of organic matter, anthropogenic practices, soil texture and horizon layering. In addition, sandy soils tend to have larger but fewer pore spaces. However, where clay soils are mismanaged leading to compaction, bulk density can increase dramatically, affecting infiltration and root growth. Soil bulk density can alter through time as natural processes (i.e. increasing organic matter) or land use (i.e. pastoral farming converting to cropping) change. As a general rule, bulk density is lower in topsoil compared to subsoil due to increasing load and decreasing soil disturbance down the profile (Marshall, 1996).

As bulk density takes into consideration pore space, this gives an indication into the porosity of a soil and its ability to store and move water. Shukla (2011) identified that an increasing bulk density and lowering porosity results in the reduction of soil water storage and movement.

Pores fall into one of two categories, macropores or micropores (Table 2.1). Macropores allow water to drain freely. Micropores are the water storage pores and the finer pores located within aggregates. Due to the strong capillarity within these finer pores, water is not plant available (McLaren & Cameron, 1996).

Table 2.1: The size and function of soil pores adapted from McLaren & Cameron, (1996).

Pore diameter (μm)	Pore Description	
>300	Air pores	Macropores
300 – 30	Transmission pores	
30 – 0.2	Storage pores	Micropores
<0.2	Residual pores	

Porosity of a soil is displayed as a percentage of the total volume of soil. Porosity can be calculated with particle density (P_p). Particle density generally takes the standard value of 2.65 Mg/m^{-3} for mineral soils thus porosity can be calculated as follows (McLaren & Cameron, 1996):

$$\varepsilon = 1 - \frac{Pb}{Pp} \quad (2)$$

Soil pore space is essential to the storage and movement of water and is directly linked to soil particle size. Particle size plays an important role in physical and chemical properties and is classified in New Zealand using the International Society of Soil Science (ISSS) scheme (McLaren & Cameron, 1996). Soil particles smaller than 2 mm are divided into four texture groups: coarse sand 2 - 0.2 mm, fine sand 0.2 - 0.02 mm, silt 0.02 - 0.002 mm and clay <0.002 mm. Mineral material greater than 2 mm is classified as gravel (McLaren & Cameron, 1996).

The effect of particle size on soil water retention characteristics and ultimately the movement of water within a soil profile is controlled by particles <2 mm (Rawls et al., 1993). Clay particles have the ability to store water and nutrients and are regarded as the most 'surface-active' soil mineral component (McLaren & Cameron, 1996). Sand and silt particles act as an adhesive layer for clay particles to bind to.

Although they are chemically inactive, their ability to manipulate water movement is crucial in a soil profile (McLaren & Cameron, 1996). The structure of a soil relies not only on individual particles, but how these particles are arranged. The bonding of these particles form aggregates that within them can lie a complex system of pores (Marshall, 1996).

The retention and redistribution of water not only relies on particle size, but also the structure and texture of a soil. In saturated conditions, a well-structured aggregated soil, allows for faster water flow due to the arrangement of the structural aggregates resulting in greater hydraulic conductivity. However when soil is unsaturated, drainage through a poorly structured fine silt loam will be faster. This is because soil aggregates in a well-structured soil absorb water and slow the progress of water movement (McLaren & Cameron, 1996). The textural differences between soils also dictate water movement. For example, a sandy loam has a greater proportion of macropores than a clay loam. This increases hydraulic conductivity and water movement when the soil is close to saturation. However, when soils are unsaturated, hydraulic conductivity is higher in the clay loam. This is due to the forces of adhesion and capillarity, also known as the matric potential (discussed in the following section) controlling water movement amongst the micropores. Water moves from an area of high potential (saturated) to an area of low potential (unsaturated). The likes of a sandy loam however, has fewer micropores than a clay loam, the effect is a slowing of water movement in this soil type when unsaturated (McLaren & Cameron, 1996).

The physical properties of the vadose zone control the storage and movement of water and dissolved chemicals or nutrients through the soil profile (Shukla, 2011). The formation of these layers can either enhance permeability, water movement or impede flow (e.g. clay layers have higher water holding capacity and can create perched water layers) (Boulding, 1995). In addition to natural layering controlling water movement, land use and management has a large influence on soil hydrological properties. For example, cultivation tends to break down aggregates and can lead to poor soil structure and the creation of plough pans.

2.2.2 Interaction of Soil and Water

The physical properties of water in conjunction with the physical properties of soil, determines soil water movement (McLaren & Cameron, 1996). Understanding how these properties and their potential variability through the soil profile affects water movement, may help to assess to what extent geophysical equipment might be used to detect these properties.

Water molecules are arranged in such a way to achieve polarity. Polarity is achieved through the bonding of a water molecule's two hydrogen atoms with an oxygen atom resulting in positive and negative charge. This polar nature results in individual water molecules being attracted through cohesion to one another and the attraction of water to other surfaces resulting in adhesion (McLaren & Cameron, 1996). These forces are important as they allow soil to store and move water. The adhesive nature of water to other surfaces can result in capillarity of water which results in water being held through tension. Smaller pores (micropores) are able to have a greater ability to hold and store water than the likes of larger pores (macropores). The potential for water to move into these pores is based on the energy needed for water movement (McLaren & Cameron, 1996).

Water flows from a position of high potential to a position of low potential, creating a change in energy potential (Marshall, 1996; McLaren & Cameron, 1996). Although gravity plays a major part in the movement of water, it is not the only force acting on this movement. McLaren and Cameron (1996), describe the following equation as the sum of total soil water potential:

$$\Psi t = \Psi g + \Psi m + \Psi p + \Psi s + \cdots \quad (3)$$

where Ψt is the total potential, Ψg is the gravitational potential, Ψm is the matrix potential, Ψp is the pressure potential, Ψs is the solute potential, and other minor potentials are indicated by the dots. The gravitational potential can either be

negative or positive. Water moving against gravity (upwards) has a negative potential and likewise water moving with gravity (downwards) has a positive potential (Marshall, 1996). The matric potential relies on capillarity and adhesion (Marshall, 1996; McLaren & Cameron, 1996). Matric potential is always lower in comparison with free water due to these acting forces. Thus, soils with high capillarity (e.g. clay lens) will have even lower matric potential (i.e. water held more tightly cannot freely move until a zone of even lower potential is created). The pressure potential is always positive in a saturated soil as water moves from this zone to an unsaturated zone (McLaren & Cameron, 1996). Further to this, water from an unsaturated zone has a zero pressure potential. The solute potential or osmotic potential follows that of the process of osmosis, where water moves from an area of lower concentration (e.g. pure water) to an area of higher concentration (e.g. saline solution) (McLaren & Cameron, 1996). Understanding what controls soil water movement through a profile will aid in understanding where potential flow pathways are located. Gish et al. (2002) identifies that flow pathways are influenced through the local differences in subsurface stratigraphies (largely because of their differences in texture and therefore water storage and potential). Therefore, mapping soil stratigraphy would be beneficial to identify soil properties that could act on water movement. Further to this, the potential acting on water will dictate water movement. For example, matric potential will prevent water moving down a soil profile due to the presence of a clayey lens. Water may therefore move along this lens. In comparison, the gravity potential in an unsaturated sand layer may cause preferential flow of water vertically down a soil profile as the large amount of macropores are unable to hold water against the gravity potential (McLaren & Cameron, 1996).

2.2.3 Soil Water Redistribution

The redistribution of water once applied to a field, either through rainfall or irrigation, travels through several stages. In a uniform dry soil initially a saturation zone forms at the surface. Below this, a transmission zone forms where water uniformly filters down due to gravity and other potential gradients. A wetting front

is formed below the transmission zone and represents the area where all micropores are filled. The stability of the wetting front is determined by the hydraulic conductivity and volumetric water content of the soil (Hill & Parlange, 1972; Miyazaki, 2005). Recharge of the water table, nutrient and water movement are all reliant on the stability of a wetting front making its way down a soil profile (Hill & Parlange, 1972). When a wetting front encounters a change in texture from a fine texture overlying a coarse texture, this will alter the movement of this wetting front and create “fingers”(Hill & Parlange, 1972). For example, a silt loam overlying a sand layer creates a change in texture due to pore size. Water will move uniformly through the silt loam, until it reaches the sand layer. From here, the soil in the above layer becomes saturated and builds up water potential, before allowing water to enter the larger pores in the sandy horizon (McLaren & Cameron, 1996). At this stage the front then forms rapidly moving “fingers” of water down through the coarse layer (Hill & Parlange, 1972). In addition to a change in soil texture, the presence of cracks, earthworm burrows and root channels also alter this flow (Hill & Parlange, 1972).

A major issue with water redistribution and drainage is nutrient and solute movement. Nutrients and solutes move through a soil profile via water movement. This can result in contamination of surface and groundwater. Water movement is influenced by the changes in soil horizon characteristics (e.g. degree of permeability) or layering boundaries (e.g. a change in texture or density causing a discontinuity of soil pores (Gish et al., 2002). These characteristics can initiate funnel (preferential) flow (Gish et al., 2002). By mapping these layers and the potential flow pathways that these layers induce will enable a better understanding of subsurface water and nutrient fluctuations at the field scale. Other spatially varying subsurface features (e.g. soil-thickness, soil structure, depth to gravel and depth to water table) could also have an effect on flow pathways. The importance of identifying these features cannot be overlooked when identifying the spatial distribution of water for future precision agriculture management (Huisman et al., 2003).

2.2.4 Geomorphic Controls for Alluvial Soil Formation

Soils are made up of multiple layers or horizons that have an influence on soil water movement (Gish et al., 2002). The deposition of materials that make up horizon layers is determined by fluvial and aeolian processes, leaching and accumulation of ions, cementation of primary particles, and translocation of clay particles (Gish et al., 2002). Sediments derived from the fluvial environment form the parent material of the soils at the study site, located on the Manawatu Terrace. They influence both the stratigraphy of the subsurface and grain size of soil particles. In addition to this, fluvial processes have influenced the landforms of the greater Manawatu Region, New Zealand. Such generalised landforms include terracing found along the Manawatu River and more localised abandoned (paleo) channels expressed at the surface.

Understanding the distribution and layering of alluvial sediments in a floodplain setting involves understanding the fluvial system. This system is dependent on the interaction between streamflow with erodible materials making up the channel boundary (Knighton, 1998). Objects such as hillslopes, the channel network and floodplains all influence water movement and sediment load (Charlton, 2007).

The process of erosion and deposition within a river system determines the history of a floodplain (Boulding, 1995). Large scale deposition has led to the formation of the Manawatu floodplains.

Infilling of the Manawatu Flood Plain with fluvial sediment from the Manawatu River began during the Holocene sea-level highstand (ca. 6500 - 2500 cal BP) (Clement, 2011; Sloss et al., 2010). The effect of this covered the former estuarine environment of the lower Manawatu Valley and created a substantial coastal plain (Clement, 2011). During the early Holocene, tectonic activity created uplift of the Ruahine Ranges, increasing sediment movement downstream. The late Holocene however, has still resulted in high sediment transport rates from a change in climate patterns (Clement & Fuller, 2007). Northerly air flows across New Zealand have

increased resulting in relatively short lived, high intensity rainstorms and floods (Clement & Fuller, 2007).

Changes to channel form are results from either a short term effect of low frequency/high magnitude flood events that affect the channel spatially and temporarily, or having a long term effect where a channel sustains a new level due to climatic, tectonic or volcanic activity. These variables in turn affect vegetation of the surrounding area and consequently alter river flow, sediment production, supply and transportation (Knighton, 1998).

The supply of sediment and energy expended from streamflow determines the deposition of sediment as rivers migrate across the floodplain. Previous flooding events that have inundated the floodplains deliver a new layer of alluvium (Cowie, 1978). The natural shape of these floodplains will dictate where alluvium will be deposited. For example, flooded abandoned channels create areas where water can pond and finer sediment will be deposited. In addition to this, the inclusion of stop banks along the Turitea stream have prevented floodwaters encroaching onto the Manawatu Terrace but also prevent surface water draining efficiently resulting in deposition of finer sediment and ponding in lower lying areas (i.e. abandoned channels). Infilling of these abandoned channels is dictated by their geometry and position on the floodplain in relation to overbank events (Charlton, 2007).

The abandoned channels and the natural progression of levee building by the Manawatu river create areas of poor drainage (Cowie, 1978). However, these levees rise from low-lying poorly drained soil to well drained sandy ridges where ephemeral channels often occur along their crest (Cowie, 1978). Surface water drains rapidly at these sites where the underlying gravels will act as an aquifer (Cowie, 1978).

The evidence of morphologic channel change can be detected through abandoned, infilled channels. The climate type and status of the environment can also be determined due to sediment deposition (Knighton, 1998). The deposition of sediments at different flow intensities creates a distinct bedform (Charlton, 2007).

Hence throughout a core sample of an infilled channel, the change in horizon boundaries relates to a change in sediment supply and the power of streamflow (Knighton, 1998).

2.3 Introduction to Ground Penetrating Radar

Having the ability to map soil features rapidly and inexpensively can be achieved through the use of proximal sensing methods. Currently there is a major limitation to understanding soil profiles to depths beyond ~2m (Doolittle & Collins, 1995). Understanding soil structure and its ability to manipulate soil flow pathways will ultimately improve site specific management processes (i.e. environmental protection and improving agricultural product quality) (Adamchuk et al., 2004).

GPR, a proximal sensing method, is able to measure characteristics such as reflectance, absorption or transmittance of energy that penetrate subsurface materials or objects (Allred et al., 2008). These characteristics then relate to important features such as boundary layers and depth to gravel. Ultimately this assists with determining subsurface water movement (Adamchuk et al., 2004).

The history of GPR use is varied, ranging from forensic investigations, archaeological, land mine detection and surveying an array of geological strata (Daniels, 2004). GPR was initially used as a geophysical technique during the early 1960s, where it was used to detect the subsurface characteristics of polar ice sheets, the work of Bailey et al. 1964 (as cited in Allred et al., 2008). Geophysical surveys became popular in the latter half of the 20th century (Allred et al., 2008; Davis & Annan, 1989). Investigations into soil moisture during the 1930s and 1940s using resistivity methods started the soil research trend (Allred et al., 2008). The use of GPR within agriculture was first applied to study the variability of soils in Florida in the late 1970s. GPR was then used for soil investigations throughout the United States (Allred et al., 2008).

2.3.1 Concept of GPR

The GPR method is similar to that of seismic and sonar methods (Davis & Annan, 1989), in that it uses the theory based on Maxwell's equation where the propagating radar wave has both a "magnitude and orientation" (Allred et al., 2008). From a transmitting antenna, a short pulse, high frequency (10 – 1000 MHz) electromagnetic wave is transmitted into the subsurface (Davis & Annan, 1989). The measurement of this wave is recorded by its two-way travel time, in nanoseconds (ns) where 1 ns = 10^{-9} s. This includes the time taken to leave the transmitter, reflect off a subsurface feature and return to the receiver. Variations to the electrical properties in materials results in these waves penetrating through the subsurface at differing velocities. This change in velocity results in a portion of the electromagnetic wave being reflected and a real-time image being produced of the subsurface (Davis & Annan, 1989). In addition to radar waves penetrating the subsurface, radar waves are also sent out across the ground and through the air from the transmitter. These waves are also recorded by the receiver and form part of the signal trace (Allred et al., 2008). This signal trace is a record of the radar wave amplitude versus the two-way travel time. Using an on-the-go approach (i.e. instant data collection), this signal trace is then plotted as a cross-sectional image (radargram) and the two-way travel time converted to depth, to highlight subsurface conditions (Allred et al., 2008). The depth of penetration of the radar signal depends on the antenna frequency and high frequency electrical properties of the material being penetrated (Allred et al., 2008; Davis & Annan, 1989).

2.3.2 Dielectric Constant & Velocity

The variation in wave velocity is dependent on the contrasting electrical properties of the subsurface. Dielectric constant or relative permittivity (ϵ_r) describe the high frequency (10 – 1000 MHz) electrical properties of materials (Davis & Annan, 1989). Thus, the polarisation (displacement) properties at these high frequencies dominate over the conductive properties of geological materials (Davis & Annan, 1989). Soil particle size and the electrical nature surrounding these particles affect the

behaviour of a dielectric constant. Within a soil profile, there is a mixture of dielectric constants as is there is a mixture of soil particle sizes.

Electrical properties of subsurface materials are strongly linked to the water content (Davis & Annan, 1989). This is highlighted in Table 2.2, where a change in water content between dry and saturated sand subsequently affects dielectric constant. In addition to this, the strength of the penetrating radar wave is dependent on these contrasting boundaries to dictate velocity of the returning wave (Doolittle et al., 2006).

Table 2.2: Dielectric constant, velocity and attenuation found in typical geological materials (Davis & Annan, 1989).

Material	ϵ_r (dielectric constant)	Velocity (m/ns)	Attenuation (dB m^{-1})
Air	1	0.3	0
Fresh Water	80	0.033	0.1
Sea Water	80	0.01	10^3
Dry Sand	3 - 5	0.15	0.01
Saturated Sand	20 - 30	0.06	0.03 - 0.3
Silt	5 – 30	0.07	1 – 100
Clay	5 - 40	0.06	1 – 300

To explain this further, if a saturated sand layer lay above a dry sand layer this would create a highly contrasting boundary as dry sand has a much lower dielectric constant than wet sand (Allred et al., 2008). This contrast in water content provides an avenue for radar waves to either attenuate into a layer or reflect back to the surface at the appropriate velocity. The relationship between dielectric constant

and velocity of a radar wave penetrating through subsurface material is represented by:

$$V = \frac{c}{\sqrt{\epsilon r}} \quad (4)$$

where *c* is the velocity of light through air (3 x 10^{8} m/s) and ϵ_r refers to the relative dielectric constant of material (Davis & Annan, 1989). Referring to Table 2.2, this explains the dependency of velocity on the water content of a material (Davis & Annan, 1989). Velocity is determined when surveying from one of two modes; reflection sounding mode or common midpoint (CMP). Reflection sounding mode comprises of radar antennas separated by a fixed distance. This setup is then moved along a transect above the ground surface to develop a cross-sectional image of the subsurface. When GPR detects an object of differing dielectric constant, a hyperbole is formed as the GPR is moved over this buried object. This is because radar waves are emitted in all directions. When the GPR is directly overhead of the object this creates the shortest travel distance (time) (Huisman et al., 2003). Once a hyperbole has been identified, albeit at a depth to include all relevant features (i.e. depth to gravel), this hyperbole can then be used in post processing. Using specific software, the average velocity can be found by adjusting an interactive hyperbole to fit the width of a chosen hyperbole from the data (Sensors & Software, 2003). This determines the average velocity between the ground surface and the subsurface object (Huisman et al., 2003). Common midpoint survey (CMP) allows an estimation of velocity by varying antenna spacing from a fixed location and measuring the two-way travel time to subsurface reflections. This method does however rely on a known reflector being identified, generally from a reflection survey. Antennas are then positioned over the target point and moved perpendicularly apart after each data collection (Sensors & Software, 1999).

2.3.3 Depth Penetration & Resolution

There are three main features that determine the depth of penetration of subsurface materials, these are the radar system performance (i.e. antenna

frequency, time window), the attenuation in the ground and the reflection properties at a boundary or object where dielectric permittivity changes (Davis & Annan, 1989). High resolution and depth penetration are both desired features of GPR (Huisman et al., 2003), but there is an inverse relationship between the two. Increasing resolution (by choosing a higher antenna frequency) will minimise the depth penetrated and likewise, increasing the depth of penetration comes at the expense of resolution. Antenna frequency is a major component that dictates these features of surveying. GPR is able to detect features from centimetres to tens of metres deep depending on the frequency bandwidth used (Huisman et al., 2003). The bandwidth of a GPR system is approximately equal to that of its frequency, therefore increasing frequency results in increased resolution (Davis & Annan, 1989). However, depth of penetration decreases as antenna frequency increases. For example, increasing from 50 MHz to a 500 MHz antenna would provide high resolution and highlight finer features within the shallow subsurface, but depth penetration would be limited to the initial 1 – 2 metres (Huisman et al., 2003). On the other hand, using a 50 MHz antenna to penetrate to greater depths will decrease resolution and may make finer features within the shallow subsurface less distinct (Allred et al., 2008).

In addition to antenna frequency affecting depth penetration, the time window (i.e. a set time for the two-way travel time to penetrate the subsurface and return to the surface) must also be set according to the maximum depth to be penetrated in relation to the antenna frequency. The time window can be estimated using the equation (Sensors & Software, 1999):

$$W = 1.3\,\frac{2d}{v} \tag{5}$$

where *W* is the time window, *d* equals maximum depth to be penetrated and *v* equals the minimum velocity that will be encountered within the survey area. This equation allows for variations in conditions by increasing total two-way travel time by 30% (Sensors & Software, 1999). Being too conservative and opting for a greater

depth or lower velocity will unnecessarily lengthen the survey time. On the other hand selecting for a shallower depth or greater velocity may cause valuable data to be overlooked. Once an approximate time window has been chosen, dependent on the depth of penetration, an accurate depth can then be determined from the following equation:

$$D = \frac{ct}{(2\sqrt{\epsilon r})} \quad (6)$$

where *D* is the depth in metres, *t* is the two way travel time (ns) and ϵr refers to the relative dielectric permittivity (Collins et al., 1994). Using this equation, the time scale can be adjusted to depth.

Although depth and resolution can be controlled to some extent with antenna frequency and time window, GPR also relies on the soil electrical conductivity and water content. The depth of penetration by GPR can be severely limited by an increase in electrical conductivity, this results in signal attenuation that decreases the wave magnitude including both the initial and returning wave (Annan & Chua, 1992; Chow & Rees, 1989). For example, signal attenuation is increased and further penetration of GPR is prevented when energy is lost from the polarisation effect of electromagnetic waves interacting with colloidal clay particles (Table 2.2) (Harari, 1996). This has the flow on effect of GPR having a declining ability to detect boundaries farther down the soil profile (Daniels, 2004). Although doubling the total depth of penetration as shown in equation 5, is necessary to avoid such issues, attenuation of the radar wave may be too great and further depth penetration will be minimal (Allred et al., 2008).

GPR has the ability to identify shallow features through increased resolution and identify depth to a boundary or object. However, detecting the thickness of a layer (soil horizon) may not always be possible with GPR. Any areas of abrupt contrast in soil moisture content (i.e. dielectric constant) are amplified in a radargram image. Although these features can be highlighted, their thickness may not be determined.

Kung and Lu (1993) tested this theory with a 450 MHz antenna to detect a 1 cm PVC plate in water lowered to depths between 0.3 – 1m. A triple band appeared in the radargram image on detection of the PVC plate. However, these bands did not correlate with the plate thickness. Allred et al. (2005) was able to detect buried drainage pipe as small as 5 cm wide at depths of 0.5 – 1 m using a 250 MHz antenna. Once again, depth to the feature could be determined, yet pipe thickness could not be detected. In relation to depth, the conductivity of a layer or object determines the power reflected. For example, clays, silts and seawater increase attenuation of a radar wave (Table 2.2), thus decreasing the strength of the returning wave (Davis & Annan, 1989). Attenuation of a signal is greater as the radar wave penetrates farther down a soil profile.

Research performed by Doolittle & Collins, (1998) suggests GPR is a valuable tool in identifying soil water flow pathways and characteristics of soil water movement. However, supporting radargram images with ground-truthed verifications is recommended to reduce ambiguous results and increase the confidence in interpretations. Shih and Doolittle (1984), compared auger samples with radargram imagery and concluded that ground-truthing radargrams with augering gave a high correlation coefficient (0.84). Furthermore, the deviations between augering and radar imagery was within 12 cm in all samples, suggesting GPR has a high accuracy in determining depths to layer boundaries.

2.3.4 The Effect of Soil Water on GPR application

As previously discussed, a change in textural boundaries or a change in soil moisture throughout a homogenous horizon produces a highly reflective plane. An important feature relating to this is the capillary fringe (a transitional zone) occurring above the water table. This is an area of partly saturated to saturated soil. The thickness of this zone is highly dependent on the porosity (Doolittle et al., 2006). For example, a finer-textured soil (e.g. silt loam) will have a larger proportion of micropores. This increases capillary rise compared to a coarser textured soil (e.g. sandy loam). As a consequence the capillary fringe is larger in finer textured soil. This in-turn causes wave reflections to have lower amplitudes and produce a less distinguishable water

table depth. In contrast, the coarse textured soil has a very narrow capillary fringe and produces a stronger reflection that can then be interpreted as a distinguishable saturated zone (i.e. water table) (Doolittle et al., 2006). Furthermore, a stagnant or rapidly rising water table is easier to delineate with GPR than a falling or retreating water edge (Allred et al., 2008). This is due to the water table impinging into drier material therefore creating a highly reflective plane. A falling water table however, leaves a saturated zone, weakening the reflected wave signal, resulting in less energy returning to the surface.

As GPR relies on water content to produce reflections, this provides a great avenue to investigate the seasonal changes in soil water movement (Doolittle & Collins, 1995; Zhang et al., 2014). Assessing the optimal time to use GPR is dependent on the type of soil and season. Zhang et al. (2014) identified during wet seasons (i.e. winter and early spring), deep soil profiles (>2 m to gravel) highlight water restricting layers. Such layers are able to accumulate water above the restricted horizon, this is amplified more so in wet seasons. Shallow soils (< 0.5 m to gravel) provide and avenue to assess preferential flow pathways and to identify soil-bedrock and weathered-unweathered rock during the dry seasons (summer, early autumn). The ability of GPR to detect contrasting dielectric permittivity between two adjacent layers (due to changing water content), makes it possible to understand the seasonal change in subsurface water storage and flow pathways (Zhang et al., 2014). As previously mentioned, the size of the transitional zone affects the strength of the radar signal and consequently the image produced. This adds great value to GPR images when assessing the seasonal change in subsurface flow pathways. Repeated GPR surveys can disclose the changes in soil moisture at contrasting boundaries through a change in the strength of reflection. This will also determine the optimal time to evaluate a soil profile in relation to flow pathways. An alluvial soil can differ dramatically over a confined area. Shallow soils can be located in one area while deeper soils dominated by silt and sand layers may lie adjacent to these shallow soils. This may require repeated GPR surveys over contrasting seasons to highlight water content changes within these soil types.

Determining where and when flow pathways are active, could assist with efficient crop planting, this in turn could lead to minimal nutrient loss and maximum crop yield. Further to this, depths to impeded layers (i.e. clay lens), can influence root growth and plant uptake of water (Gish et al., 2005). The application of GPR to identify soil moisture and flow pathways was used by Gish et al. (2005) to identify the variability in corn yield. Preferential funnel flow was identified at sites based on increased soil moisture values across a 3.2 ha field. This information was then used to monitor grain yield with results supporting an increase in corn yield closer to identified flow pathways during a drought year.

Identifying areas of a paddock that are more hydrologically active than others can potentially decrease the uncertainty of hydrology impacts on crop yields. The ability to identify these features in alluvial soils within a New Zealand context can not only benefit the decision making process regarding farm and soil management but also emphasise features that contribute to the effective use of GPR. Alluvial soils can vary dramatically in soil thickness, layering and depth to gravel. Understanding how these features affect the ability of GPR to map contrasting alluvial soils can benefit future farm management practices, as intensification over alluvial land will only continue to increase within New Zealand.

2.4 Conclusions from the Literature

The vadose zone is an important area for water storage and movement and is determined by soil pore size, soil texture and the potential acting on water to move. The GPR technique – which relies on a change in electrical properties that are primarily linked to a change in soil moisture conditions, which in turn are related to particle size and drainage – can be used for mapping these soil physical properties. Identifying potential soil water flow pathways using GPR has previously been successful in organic and sandy soils and karst landscapes. The amount of salt in solution or clay particles within the vadose zone is one of the major factors that will inhibit the function of GPR.

There is an absence of research applying GPR to mapping alluvial soils. Alluvial soils of the Manawatu and Rangitikei series have low clay contents as these soils are relatively young and unweathered, and therefore are likely to be suited to GPR applications. In these soils, the GPR signal is likely to be most sensitive to soil moisture conditions. Alluvial soils are characterised by the layering of sediments such as silt and sand. This layering affects the movement of water through the vadose zone due to a change in soil pore size at textural boundaries throughout a soil profile. A change in soil texture causes a change in water potential. If water potential increases above a coarser layer, this can cause rapid infiltration into the available pore spaces below. In comparison, water lying above a saturated finer layer has low hydraulic conductivity and will cause water to perch, creating reducing conditions, ideal for the denitrification process. GPR may be useful for differentiating and mapping these structures and therefore useful for identifying potential flow pathways. Such structures have previously been identified in sandy and organic soils, using high frequency (e.g. >200 MHz) GPR antennas that have provided a rich resolution, with lower frequency (e.g. 100 MHz) antennas used to identify features at depth (i.e. water table).

Seasonal changes to soil water movement can also have an effect on the ability to determine these layering properties. When soil moisture conditions are higher, this can highlight restricting layers in a soil profile, indicating potential flow pathways, likewise, identification of soil-gravel interfaces or weathered-unweathered rock is more effective when GPR surveys are conducted in drier soil moisture conditions. Identifying these seasonal changes in soil properties can be completed rapidly and efficiently with GPR surveys compared to multiple laborious point collections (i.e. soil cores).

GPR takes a non-destructive approach to investigation of the vadose zone. Although some point collections are needed to validate radargrams, the frequency with which these are collected when compared to point collections alone can be dramatically decreased when used in conjunction with GPR.

Although the use of GPR to identify subsurface features and water movement within the vadose zone are known, there is still uncertainty about its ability to identify the physical and hydrogeological properties within alluvial soil.

3 Study Site and Methodology

3.1 Study Site

The study site consists of two research plots near the southern end of Dairy 1 farm (Fig 3.1), Massey University, Palmerston North, New Zealand. The total farm area is 142.7 ha (119.6 ha eff.) and is managed as a profitable, low input, sustainable pasture-based dairy farm with a once-a-day (OAD) milking, spring calving system (Massey University). The farm itself is approximately 3 km east of Palmerston North and lies adjacent to the Manawatu River to the west and the Turitea stream to the south. The average rainfall is 969 mm/year, with monthly average air temperatures of 8.7°C (July) and 18.2°C (February) (NIWA, 2016).

Figure 3.1: Study site showing the two plots located at Dairy 1 farm. (1) pasture plot, (2) arable plot.

Two 0.4 ha (40 x 100 m) plots were established for this research trial; one a pasture plot (24.8 – 23.9 m above sea level (ASL)) and the other an arable plot (26.7 – 25.2 m ASL). The pasture plot consists of ryegrass and clover pasture and is grazed by the OAD milking dairy herd. The arable plot was previously sown in turnips that were being grazed by mixed-age ewes. Only the far west corner of the arable plot had turnips remaining at the time of the surveys, the remainder of the plot had been grazed and was left fallow. The arable plot is used for cropping trials year round and is also under irrigation when necessary via a variable rate centre pivot. The arable plot was chosen due to the existing research carried out on this plot involving variable rate irrigation. The pasture plot was chosen to provide a site with a difference in soil types and soil thickness, topographic variation and the proximity to piezometers for correlation of radargrams with depth to the water table.

3.1.1 Geomorphological Setting

The study site is situated on the Manawatu Terrace (Fig 3.2) (Cowie, 1978; Palmer, 2016). Although this surface exists 4 – 6 m above the present level of the Manawatu River it has been generically mapped as Holocene alluvium (Clement, 2011). To the far east, the Tararua – Ruahine Ranges rise over 1500 m. These were uplifted during the Pliocene – Pleistocene (Heerdegen & Shepherd, 1992). To the east and south of the study site lays the Tokomaru Marine terrace. This is a low angle marine terrace formed by marine processes during the last interglacial (c 125,000 years BP). The exposure of this terrace was caused by a lowering sea level during the last glacial maximum (LGM) (c 20,000 years BP) and constant tectonic uplift (Heerdegen & Shepherd, 1992).

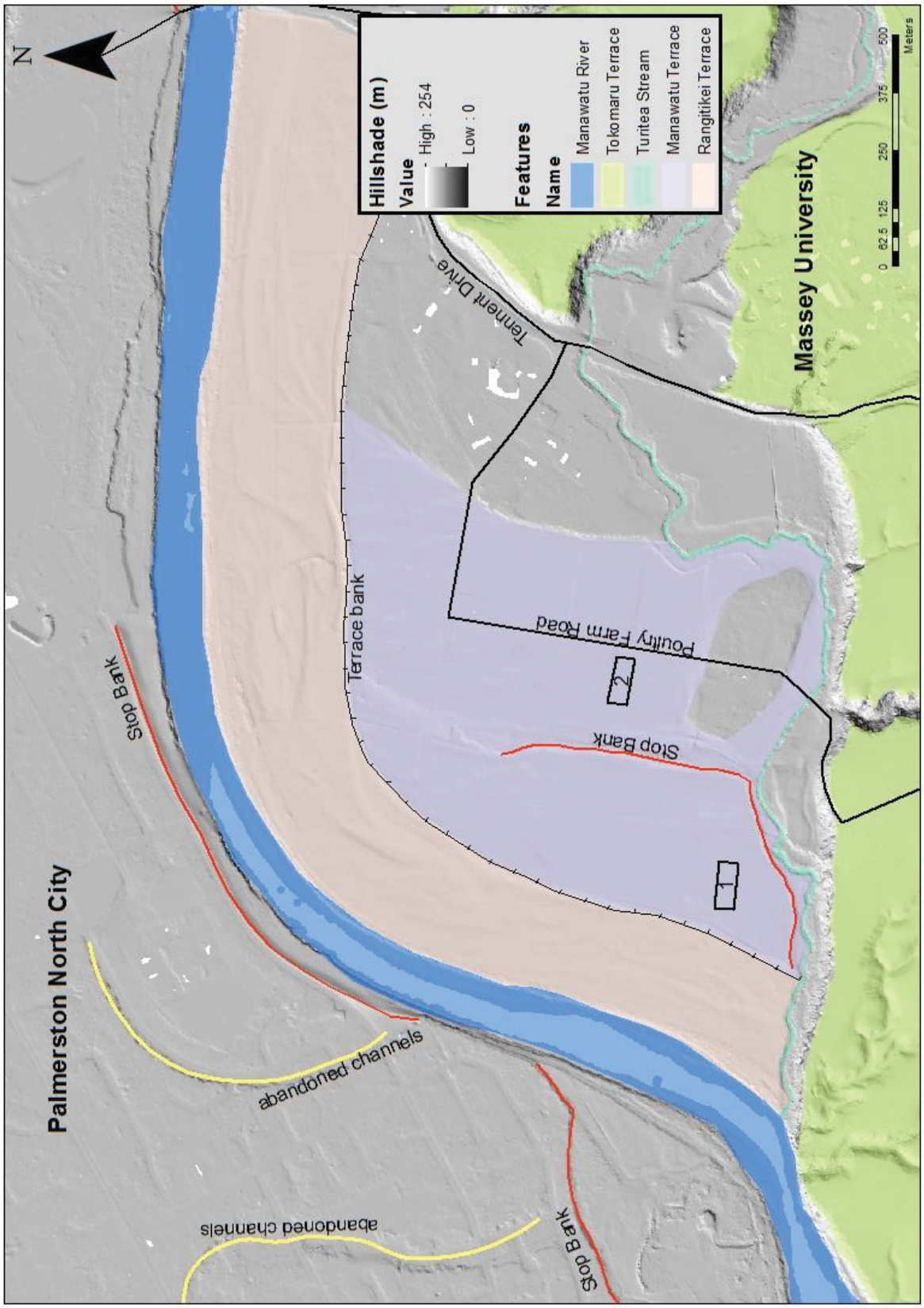

Figure 3.2: Geomorphological setting developed from LiDAR hillshade, showing the two research plots on the Manawatu Terrace (purple). The Tokomaru Marine Terrace to the east and south (green) and the Manawatu River to the west of the study site (Source: LiDAR hillshade provided by Horizons Regional Council).

The Manawatu River has been the dominant force in shaping the greater Manawatu region. The influence of the Pohangina anticline directs the course of the Manawatu River southeast towards its mouth at Foxton Beach (Clement et al., 2010; Heerdegen & Shepherd, 1992). The catchment area of this River is nearly 6000 km² and flows from north of Dannevirke on the eastern Ruahine Ranges before cutting through the axial Tararua - Ruahine ranges at the Manawatu Gorge (Page & Heerdegen, 1985). Downstream from this, the Pohangina River joins the Manawatu River and provides a significant source of coarse bedload gravels. It then travels adjacent to Palmerston North city where it has been subject to extensive river works since 1944 (Page & Heerdegen, 1985). The stretch upstream of Opiki has a bed slope of 1.2 m/km and a sinuosity of 1.4, where sinuosity = channel length/straight line valley length (Page & Heerdegen, 1985). Gravel bars are common amongst the single thread wandering channel (Heerdegen & Shepherd, 1992). Figure 3.3 highlights the numerous abandoned channels and cut-off meanders and suggests the river from the Manawatu Gorge to Opiki has recently changed (last 100 years) from a meandering silt/sand bed river to a straighter gravel bed river (Heerdegen & Shepherd, 1992). The change to a straighter gravel bed river is indicative of tectonic activity within the area, slowly adjusting the stream power and subsequently providing coarser sediment for transport (Heerdegen & Shepherd, 1992). In addition to this, engineering of the river channel (e.g. channel straightening, stop bank inclusion and gravel extraction) have caused net river degradation and lowering of the river bed (Page & Heerdegen, 1985).

The geological composition of the Manawatu catchment is primarily made up of gravel (40.3%), mudstone (18.5%), sandstone (14.7%) and greywacke (14.6%) (Vale et al., 2016). Most of this sediment is sourced from the Tararua - Ruahine Ranges (Heerdegen & Shepherd, 1992). The finer material transported in the Manawatu River can make up to 90% of total sediment load and is generally a product of weathering and erosion of the softer Tertiary rocks (Mudstone) located mainly in the eastern sub catchments (Tiraumea) (Heerdegen & Shepherd, 1992; Vale et al., 2016).

Recent flooding events that inundated Dairy 1 farm, have occurred when the Manawatu River's median flow of 73 m^3/s (Horizons, 2016) is approximately >30 times greater. On 22 June 2015, the Manawatu River produced a discharge of 2,043 m^3/s, causing flooding of Dairy 1 farm, mainly over the lower Rangitikei Terrace (Horizons, 2016). The previous major flooding event covered 90% of Dairy 1 farm on 16 February2004, the Manawatu River produced a discharge of 3,500 m^3/s at peak flow, equivalent to a one in 100 year flood event (Fuller, 2005). This flood has probably been the biggest within the Manawatu region since 1902 (Fuller, 2005). The most severe and frequent flooding occurs on the low flats bordering the rivers (Cowie, 1978). The study site however, sits above these frequently flooded areas. Soil patterns and development have been influenced through the rate of accumulation of flood deposits and the change in bedload material. Alluvial deposits range from gravels to clays and the deposition of these materials is dependent on their distance from the main channel. Finer sediment tends to travel farther during flood events with coarser sediment deposited closer to channel banks (Cowie, 1978).

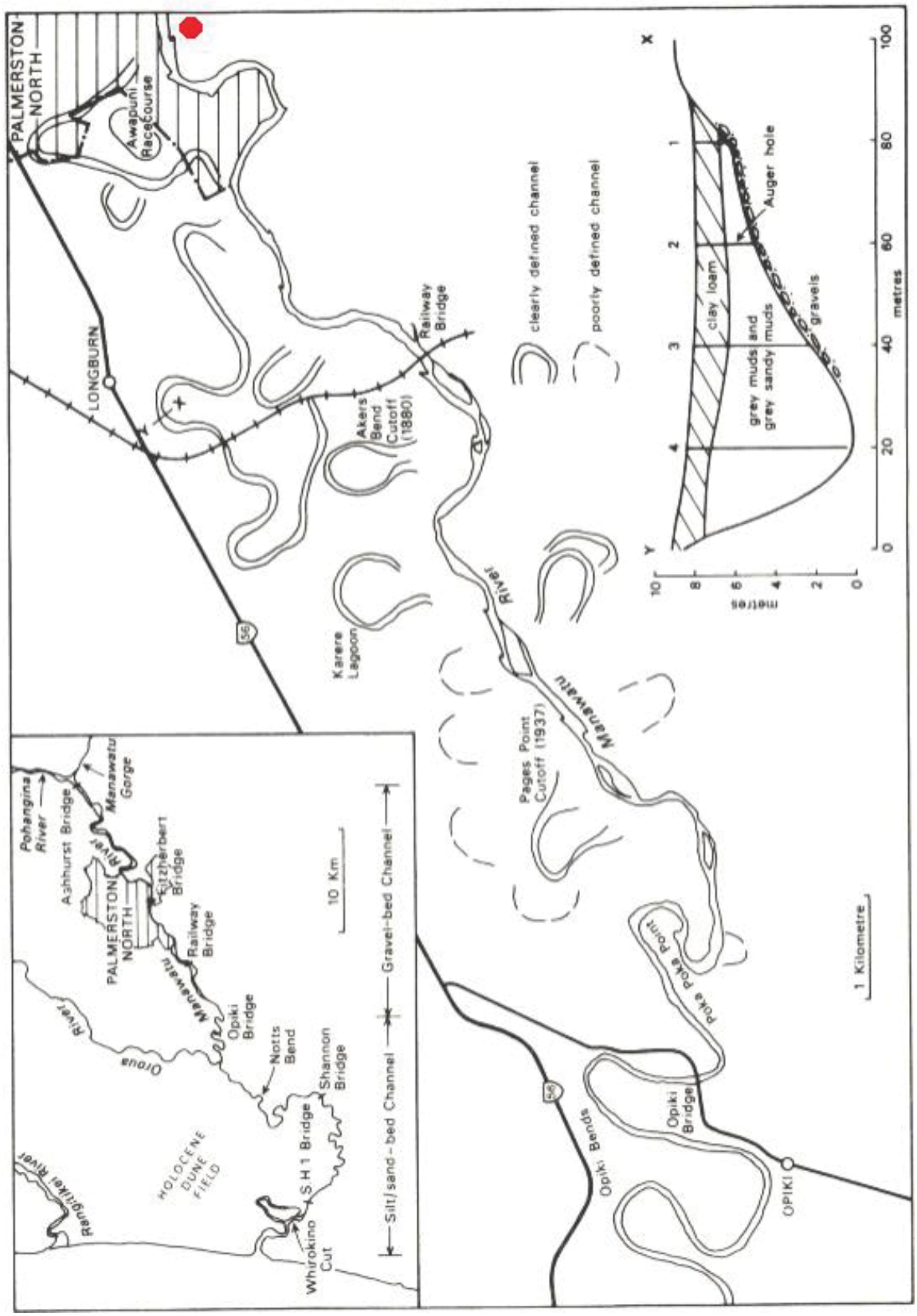

Figure 3.3: The lower Manawatu River, highlighting areas of previous channels and the change in channel bedload from gravel to silt/sand at Opiki. Approximate study site location denoted by the red dot, after Page & Heerdegen (1985).

3.1.2 Soils

Alluvial and marine materials are located on the floodplains, terrace and rolling lands of the Manawatu Region (Cowie, 1964). The soils present over the two plots are formed from recent alluvium dispersed by the Manawatu River and Turitea streams. Recent soils can range in texture from silt loam to loamy sand and are moderately-well to excessively well-drained. Subsoils are weakly developed yellowish grey or olive brown (Cowie, 1978). Parent materials are sediments derived from Jurassic greywacke and Tertiary sandstones, mudstones and limestones that are sourced from the Tararua – Ruahine ranges (Cowie, 1978).

Two soil series are present over the study site, the rapidly accumulating Rangitikei series and the more slowly accumulating Manawatu series. The Rangitikei soils have a tendency to flood frequently, although this is largely controlled by the inclusion of stopbanks since the early 1900s (Cowie, 1978). This reduces the time for organic matter to form resulting in thin topsoil and weakly developed structures. The Manawatu series occur in areas that flood less frequently resulting in the slow accumulation of alluvium and a slightly higher organic matter content (Cowie, 1978). Manawatu soils tend to show more profile development than the Rangitikei soils and are used throughout the region for intensive stocking and cultivation. This however can result in soils becoming compacted with degraded structure. This in turn can affect the rate of water percolation through the soil profile (Cowie, 1978).

Figure 3.4 indicates the soil types present over the south end of Dairy 1 farm as mapped by Pollock et al. (2003). A distinct change in soil type is seen across both the pasture and arable plots and could be indicative of former river channels. The Rangitikei silt loam over sand and the Manawatu fine sandy loam are encountered within the pasture plot and likewise the Manawatu silt loam over sand and the Manawatu sandy loam are encountered within the arable plot. LiDAR imagery suggests a good relationship between elevation and soil type as shown by the inset maps in Figure 3.4.

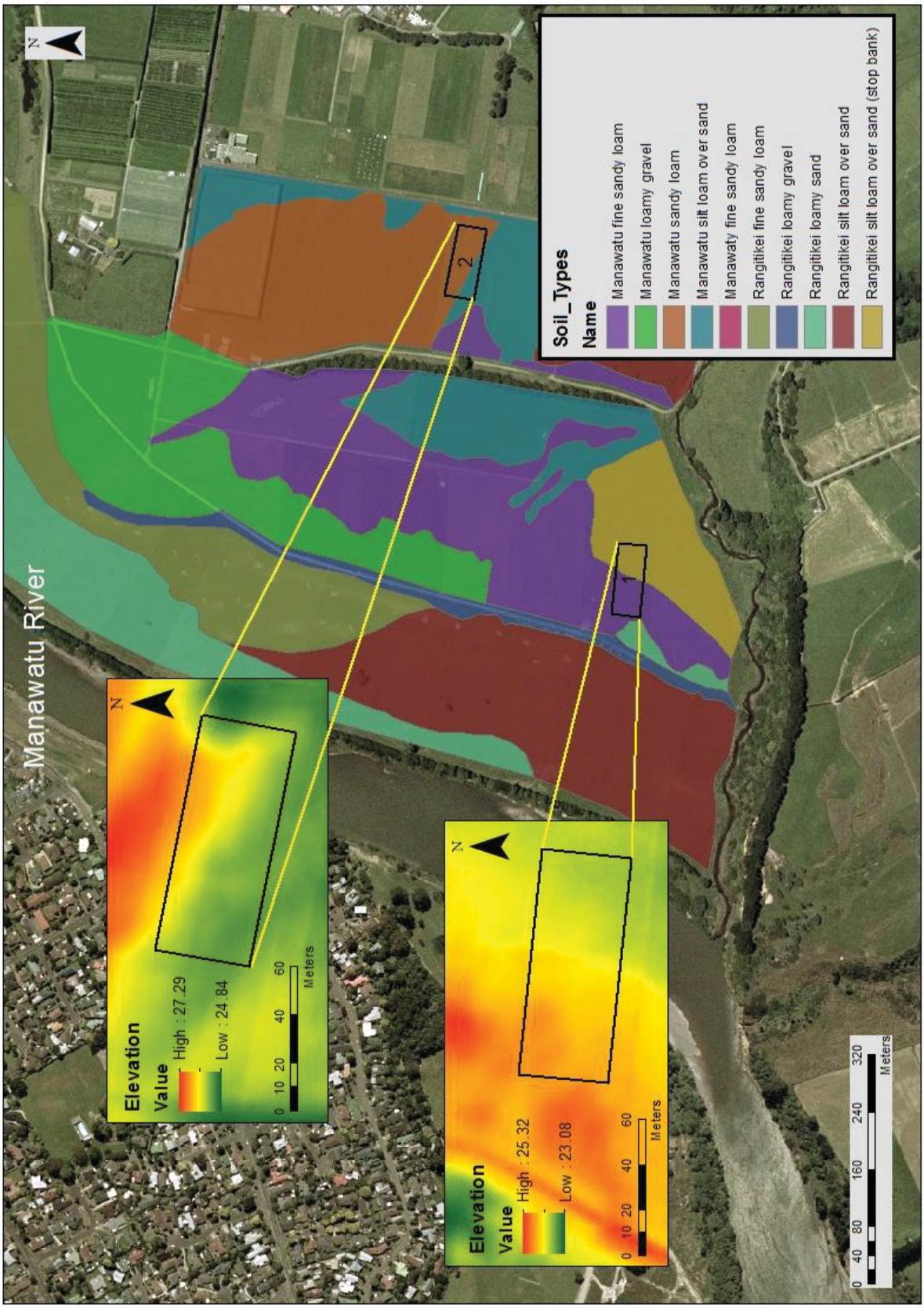

Figure 3.4: Soil types mapped at Dairy 1 Farm. Insets give an indication of elevation over the two research plots and signify the changes in soil type relevant to elevation change Adapted from (Pollock et al., 2003d).

S-map is the new national soils database. This has been used to describe some key physical properties and factors to consider when making management decisions for three of the four soils located within the study site (Table 3.1). Although this specific area has not been S-mapped, the characteristics described in S-map relate to those found at the study site. In addition to this, the Manawatu fine sandy loam located in the pasture plot has similar features to the Manawatu sandy loam, both free draining recent soils with the exception of a slightly different topsoil as shown in Figures 3.5 and 3.6. All soils have a similar bulk density throughout their profile with either high or very high structural vulnerability. The lack of organic matter formation, especially through the subsoil can increase bulk density and the structural vulnerability of these soils. Being well drained alluvial soils, waterlogging is not an issue.

Table 3.1: Physical properties found in the Rangitikei silt loam, Manawatu sandy loam and Manawatu silt loam over sand according to S-map data (Landcare Research, 2015a, 2015b, 2015c).

Soil Factors		**Rangitikei silt loam**	**Manawatu sandy loam**	**Manawatu silt loam over sand**
Site		Pasture	Arable	Arable
S-map Reference		Selw_12a.1	N_252_3a.1	Hind_5a.1
Profile Available Water (0-100 cm)		High (171 mm)	Moderate to High (139 mm)	High (239 mm)
Dry Bulk Density	Top Soil	1.09 g/cm³	1.09 g/cm³	1.09 g/cm³
	Subsoil	1.30 g/cm³	1.38 g/cm³	1.30 g/cm³
Structural Vulnerability		High (0.64)	High (0.68)	Very High (0.71)
Water Logging Vulnerability		Very low	Very low	Moderate
Drought Vulnerability (not irrigated		Low	Low	Low
Clay %		20	14	13
Sand %		10	65	19

Figure 3.5: Pasture plot soil descriptions (Pollock et al., 2003a, 2003e).

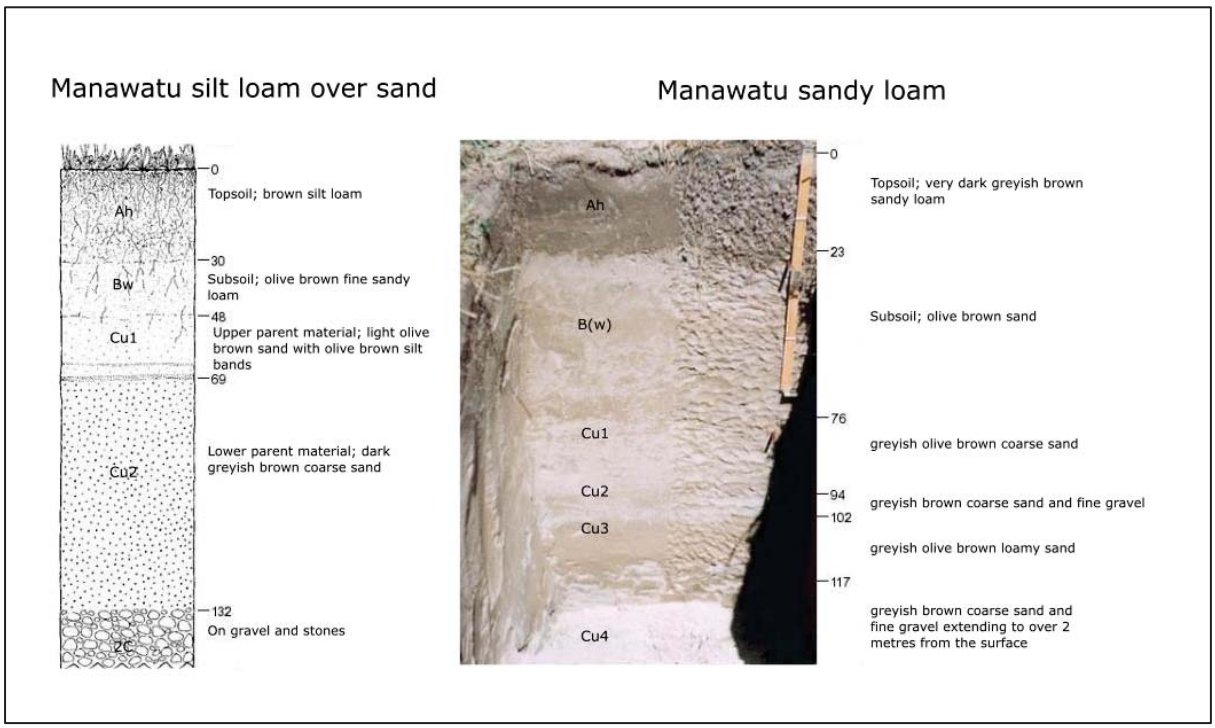

Figure 3.6: Arable plot soil descriptions (Pollock et al., 2003b, 2003c).

In summary, the study site situated on the Manawatu Terrace includes soils from the well-drained Rangitikei and Manawatu series. Previous literature has suggested the Manawatu River meandered through this section and has been the dominating force in shaping this area. LiDAR imagery suggests former river channels paved their way through the area, indicated through topographical change. Deposition of sands, silts and gravels from previous flooding events have formed these soil horizons. Exploration of soil profiles with GPR should identify these former channels and the variation in soil depth and layering. In addition to this, depth to river gravels should vary as an indication of channel migration and extent of previous flooding.

3.2 Materials and Methods

3.2.1 Introduction to the Experiment

The study site consisted of two plots, arable and pasture. These plots were chosen to show a comparison between land use and soil type. Within both plots, GPR grid surveys and associated soil measurements were conducted. These soil measurements focused on soil physical attributes that affected soil water flow and were used to ground truth GPR imagery (radargrams). Surveys were conducted in September 2015 (spring, increased soil moisture conditions and higher water table) over both plots and February 2016 (late summer, decreased soil moisture conditions and a lower water table) on the pasture plot only as access to the arable plot was limited due to an established cropping rotation.

3.2.1.1 Grid Setup

To help guide the soil sampling and GPR surveys, two 40 x 100 m (0.4 ha) grids with 10 m spacing was set out using tape measures over the arable and pasture plots respectively (Fig 3.7). The long axis (Short GPR Lines) of both grids had an east – west orientation. The grid nodes (spaced 10 m apart) were marked with PVC pipe. These markers were used as reference points for Global Positioning System (GPS) measurements used to georeference the grids. GPS coordinates were then coded using a letter (Short GPR Lines axis) and corresponding number (Long GPR Lines axis). A finer grid of 2 m spacing was defined within the coarser grid, using spray

paint to mark the more-approximately located nodes (Fig 3.7). This finer grid was used to guide the GPR survey lines, which were spaced 2 m apart.

Seventy-two GPR lines were collected at each plot to form a grid pattern (black lines in Fig 3.7). This totalled 21 long lines (100 m length) and 51 short lines (40 m length). Lines were labelled according to distance along the short or long GPR lines axes. For example, Long_12 refers to a long 100 m GPR line, located 12 m along the Long GPR Lines axis and Short_92 refers to a short 40 m GPR line, located 92 m along the Short GPR line axis (blue lines in Fig 3.7).

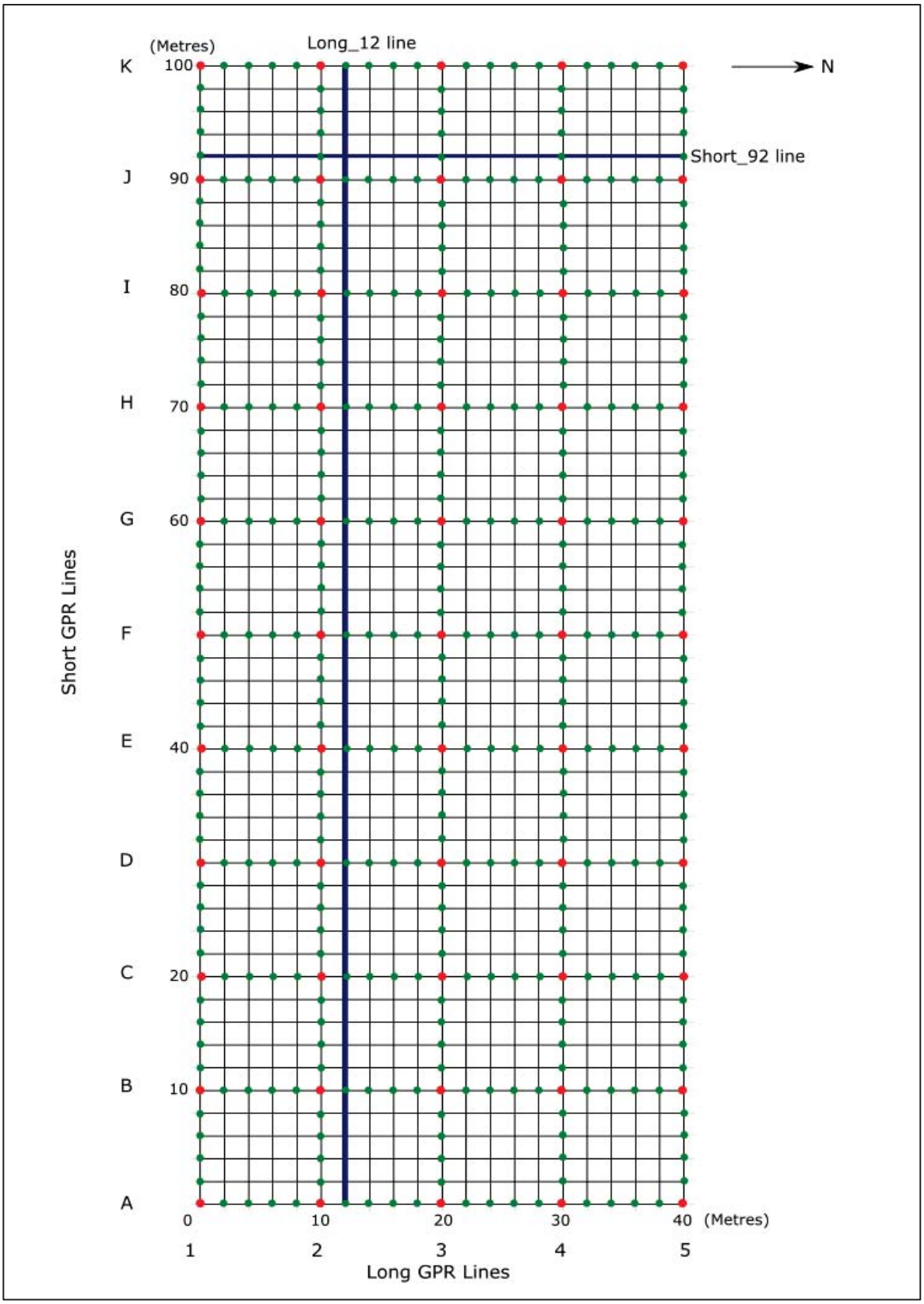

Figure 3.7: Grid setup, 10 m markers (red dots), 2 m markers (green dots), GPS points were recorded at each red marker. GPR lines (black lines) are spaced every 2 m. Example GPR names of two lines (blue).

3.2.1.2 Georeferencing the survey grid

A Trimble® R8 RTK-dGPS was used to survey GPS coordinates of the 10-m grid nodes from both plots. An R8 base station was set up adjacent to the arable plot, on a random point. Using an R8 Rover, the position of each 10 m GPS marker was recorded (Fig 3.8). GPS positions were recorded in New Zealand Transverse Mercator (NZTM2000) coordinate system.

Figure 3.8: collecting GPS points using the R8 Rover at the pasture plot. Note the white PVC markers are spaced 10 m apart and GPS recordings were taken at each marker.

3.2.1.3 Elevation using LiDAR

Elevation was sourced using LiDAR data from Horizons Regional Council. Each georeferenced point across both grids was entered into ArcMap 10, a geographic information system. This allowed for accumulation of respective elevation points from LiDAR data. In addition to data collection of elevation height, Natural Neighbour raster's were produced in ArcMap 10 to assess ground surface and gravel surface topography. Gravel surface was first evaluated using soil auger data (Section 3.2.4.1) that was interpolated across the arable and pasture plot from respective radargrams. Depth to gravel was then subtracted from ground surface topography to form points for the Natural Neighbour raster. A Raster Math calculation was conducted to show the difference between the ground surface and

the surface of the gravel underlying the soils. This was represented as a soil thickness layer.

3.2.2 Ground Penetrating Radar

The GPR system used for this research was a Sensors & Software Pulse EKKO Pro ground penetrating radar. In September 2015, the 200 MHz antennas were used to collect line data over both the arable and pasture plots, and repeated in February 2016 for the pasture plot. It was not possible to resurvey the arable plot in February, due to land use restrictions. While the results of the 200 MHz antennas surveys in September 2015 provided good resolution information of the top few metres of soil, it was decided that 100 MHz antennas would be required for imaging the base of the soils (i.e. the soil-gravel interface) and the water table. So in November 2015, a trial of four transects using the 100 MHz antennas was undertaken, and from this it was decided to also deploy the 100 MHz antennas in the pasture plot in February 2016, in addition to the 200 MHz survey.

3.2.2.1 Setup

A PVC trolley was used to push the GPR system by hand within the grid formation (Fig 3.9). With the transmitter antenna located at the front of the trolley, the antennas were spaced 0.5 m and 1 m apart for the 200 MHz and 100 MHz surveys respectively, following the optimal spacing recommended for these antennas. Antennas were secured to the trolley approximately 0.15 m above ground level. Five metre long fibre optic cables were run from both the receiver and transmitter antennas to the display unit. The antennas were always oriented perpendicular to the measurement transects along which data was collected. The time-window was adjusted in the field from the default values to maximise the data acquisition at depth. All other values were set to default.

Figure 3.9: GPR setup showing the 100 MHz antennas with battery packs and display screen assembled on a PVC cart

3.2.2.2 Kinematic Surveys

The Pulse EKKO pro GPR was run in continuous reflection mode, with the trolley pushed at a constant speed that attempted to achieve the recommended step size of 0.1 m and 0.25 m for the 200 MHz and 100 MHz surveys respectively. While not as accurate as using the step-mode for data collection, the continuous method and the use of the trolley, made data collection much faster and possible with a single operator. Lines were collected in a serpentine pattern to eventually form a grid over the 40 m x 100 m areas (Fig 3.10). Fiducial markers were added to the data every 10 m to assist with post processing. Due to a portion of the turnip crop remaining over the south-western corner of the arable plot, GPR lines were shortened as shown in Fig 3.10. Each grid survey took on average five hours to complete.

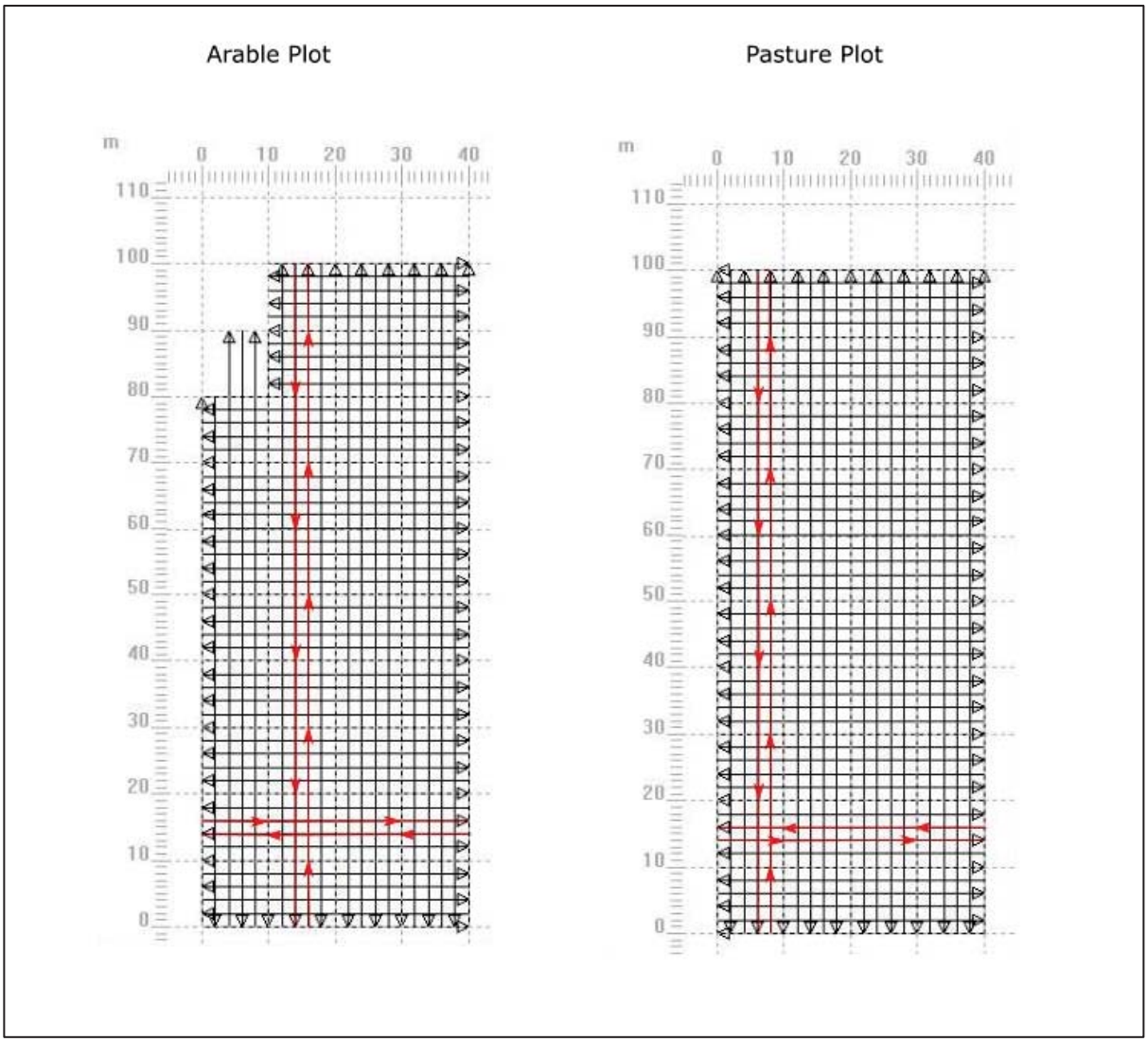

Figure 3.10 Arable and pasture GPR grids created in GFP Edit 4. Transects were collected in a serpentine pattern over the whole plot for more efficient collection of data. An example of the serpentine pattern is shown by the directional red lines.

3.2.3 Post Processing of Radargrams

A total of four grids were produced in addition to the 4 trial 100 MHz GPR lines. Seventy-two (72) surveyed lines were gathered per grid survey. These data were grouped according to antenna frequency and month of survey:

- Arable_200 MHz_Sep
- Pasture_200 MHz_Sep
- Pasture_100 MHz_Feb
- Pasture_200 MHz_Feb

Data was processed using three software packages, EKKO_View Deluxe, GFP Edit 4 and EKKO Project 4. Initially radargrams were corrected for distance in EKKO_View Deluxe. Arrangement of GPR lines to form the four grids was then completed in GFP Edit 4 and finally further editing of individual radargrams including adjustment of velocity, filters and gains was completed in EKKO Project 4.

3.2.3.1 Distance Editing with EKKO_View Deluxe

To help eliminate the effects of speed variations (i.e. changing step size) when surveying in continuous mode, the radargrams needed to be adjusted using a process called rubberbanding. Rubberbanding is used to stretch and squeeze a line to reposition the individual radar traces to where they should be along the transect. Fiducial markers that were inserted into the radar file at marked positions along the transect are used as reference points for this process (Sensors & Software, 2003). However, occasionally fiducial markers were missed (human error), and in this situation, an additional fiducial marker was later added in the trace comments section of EKKO_View Deluxe, in the approximate expected position. The rubberbanding process resulted in all radargrams being automatically trimmed to their correct lengths (i.e. either 40 m or 100 m length).

3.2.3.2 Creating Grids with GFP Edit 4

During field setup, lines were collected continuously in a serpentine pattern. This was the most efficient method of field collection. However, this resulted in extra handling of GPR data in post processing. Although this step could have been avoided if the initial setup included collecting lines in grid form; this relied on each individual grid having the same start and end location (i.e. all long lines start at 0 and finish at 100 m, instead of the serpentine pattern) this would have increased the time in the field dramatically. It was therefore more efficient to produce a grid in post processing.

Using the GFP Edit 4 software, each group of rubberbanded lines were then collated to form a grid. Lines were selected as either Y (long GPR lines) or X (short GPR lines) axes and if they were either taken as normal or reverse direction. Once all lines

were brought into the software, the start points were adjusted to allow the grids to line up. These grids formed a complete collection of GPR lines related to one another spatially (Fig 3.10). These grids were then uploaded to EKKO Project 4 software for further processing and analysis.

3.2.3.3 Displaying Grid Data in EKKO Project 4

EKKO Project 4 software was used to display both the individual radargrams and each grid in a Slice View mode. Slice View mode provides a map (in the X-Y plane) of radar-reflector intensities at specified depths below the grid surface.

Processing in EKKO Project 4 included altering velocity/depth and adding topography files, filters and gains. Converting the two-way travel time of the radar waves to a corresponding depth involved an estimation of the average radar wave velocities. As surveys were recorded in the reflective method, a representative radar velocity was assessed by using the hyperbole method. This method fits a modelled hyperbole curve to hyperboles in the radargrams, with the shape of the fitted curve being related to the average velocity of the soil above the hyperbole point source. Not all radargrams contained hyperboles, but the velocity between different radargrams was very similar, and as a result an average velocity of 0.09 m/ns was chosen and applied to all of the data. However, velocity was adjusted to 0.065 m/ns for the September pasture plot Short 36 line. This appeared to compare to the most accurate depth scale for this individual radargram. The February 100 MHz surveys were adjusted to 0.1m/ns to show an accurate depth scale when soil moisture conditions were drier as this resulted in a faster radar wave velocity penetrating the subsurface. The February 200 MHz surveys were kept at 0.9 m/ns to highlight the difference in reflection configurations when soil moisture conditions change without altering velocity. The common midpoint survey (CMP) is another survey technique that is used to obtain an estimate of the radar wave velocity. This involves varying antenna spacing from a common midpoint and assessing velocity from the distance covered across the surface and the slope of the ground wave shown on the radargram (Davis & Annan, 1989). This was not conducted in this research but should be noted for future research programmes using GPR.

Other editing included spatial and time filters. These are adjusted to improve a radargram image. Spatial filters enhance or eliminate features through altering the shape of a trace. This includes background subtraction which removes the average trace from all traces in a GPR line. This feature removes horizontal bands and the ground and air waves located at the top of the radargram (Sensors & Software, 2016). The time filter "Dewow" was applied to remove any slowly decaying low frequency "wow" on a trace (Sensors & Software, 2016). This "wow" (low frequency signal) attaches itself to the high frequency waves and its magnitude is dependent on ground conditions and antenna spacing. A default running average filter was applied to each trace to remove wow (Sensors & Software, 2016).

Gains were applied to the radargrams to amplify the weaker signals, because radar signal strength decreases with increasing time window (Sensors & Software, 2016). In other words, reflections near the top of a radargram have a stronger signal than those nearer the bottom of a radargram, regardless of the nature of the object or material creating the reflected signal. Applying a gain may have no benefit to enhancing deeper subsurface features if radar signal is particularly strong near the surface (Sensors & Software, 2016), and if the gains at depth are applied too strongly, there is a risk of amplifying noise instead of real reflections. The gain used in all radargrams was the Spreading Exponential Calibrated Compensation (SEC2). This applies an increasing gain as a function of depth, and is the default recommended gain type for the software being used. This gain type allows the response from similar targets or material at different depths throughout the radargram to appear alike (Sensors & Software, 2016).

3.2.4 Soil Measurements

Physical soil measurements were made to ground truth the GPR data and assess the ability of the GPR to detect differences in various soil properties. Thirteen sites (five from arable plot and eight from pasture plot) were chosen for soil coring (i.e. recovery of soil for logging and measurement) and 29 sites (21 from arable plot and eight from pasture plot) were selected for soil augering (Fig 3.11) to establish the depth to the gravel layer below the soils. These will be further discussed in the

following sections. The sites for soil coring and augering were chosen to intercept strong reflections and anomalies noted in the radargram images. Soil sample locations were numbered 1 through 13 for ease of reference, where cores 1 – 5 and 6 -13 were located in the arable and pasture plot respectively (Fig 3.11).

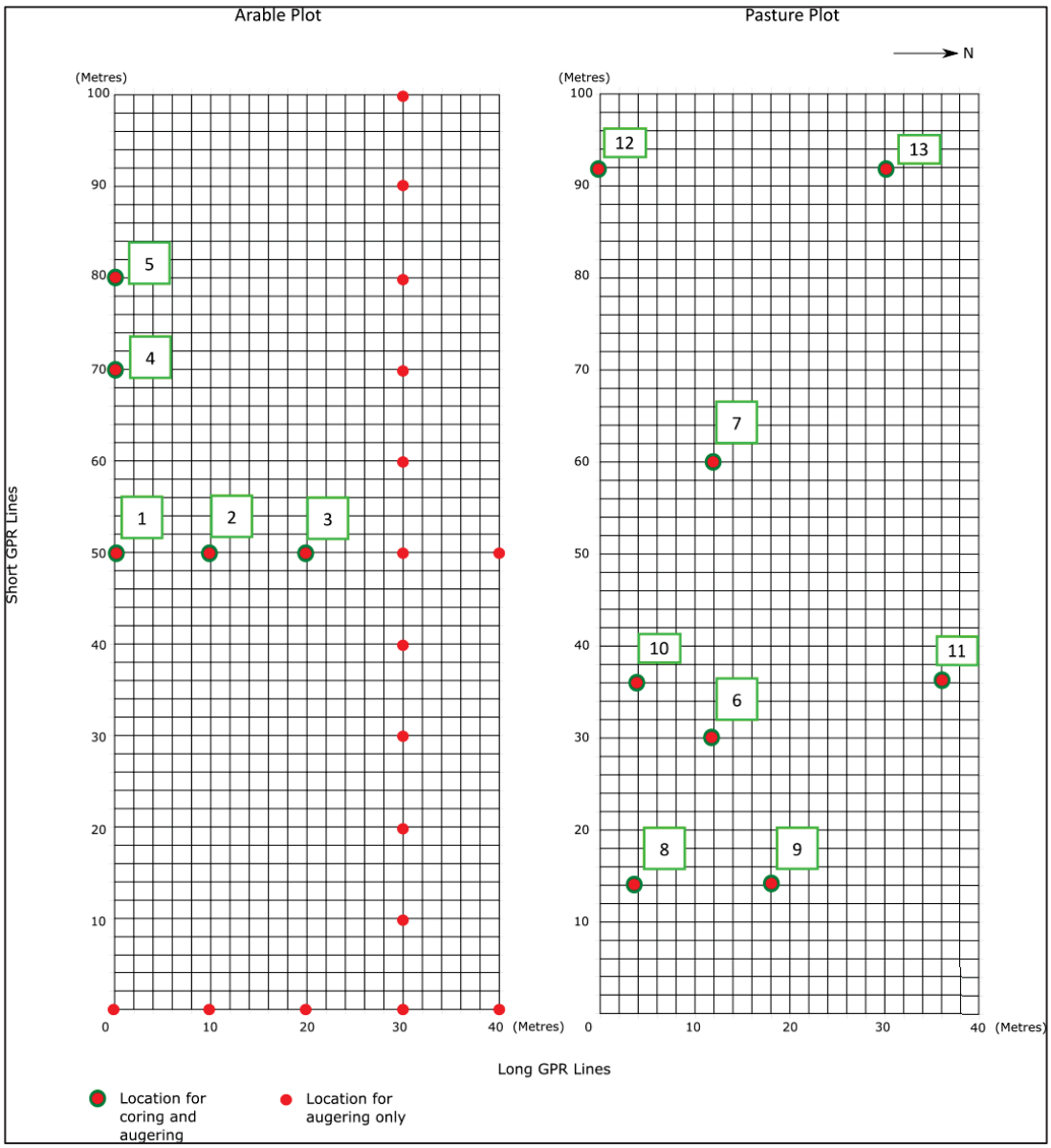

Figure 3.11: Soil core and auger locations across the two plots. Soil cores are numbered for ease of reference when interpreting with the results section.

3.2.4.1 Soil Augering

Soil augering was used to confirm that a strong reflector in the radar data at both plots corresponded to the assumed boundary between gravels and the overlying soils (fine sediments). Augering also assisted with determining the depth of

subsequent soil cores to avoid damage to the soil corer upon reaching gravel. A hydraulic auger attached to a Giddings drilling rig (Fig 3.12), was used to penetrate to gravel up to 3.46 m below the surface. Auger locations are shown in Figure 3.11.

3.2.4.2 Soil Coring

After preliminary examination of the radargrams, five soil cores were collected at the arable plot and eight soil cores were collected from the pasture plot (Fig 3.11). The Giddings rig corer was slowly deployed at each site and samples collected in sections (generally 0.3 m sections at a time) until gravel depth was reached.

Figure 3.12: Giddings rig corer with soil corer attached.

Figure 3.13: Measuring and labelling core lengths. Cores were collected in half – round PVC pipe for ease of movement off the Giddings rig.

The diameter of each core was 0.067 m (radius 0.0335 m). However, the length of each core differed depending on depth to gravel (0.7 – 3 m depth). All sections were then positioned together using PVC plastic pipe tubing (Fig 3.13). Cores were logged according to horizon depth, texture and colour. Photos were taken of each core. Depths and descriptions of soil horizons were recorded according to the New Zealand Soil Classification (Hewitt, 2010). A typical core profile consisted of a sandy loam or silt loam A horizon (≈ 0.10 m in pasture plot and ≈ 0.25 m arable plot), a sandy or silt loam B horizon in the Manawatu series soils or a sandy loam AC horizon in the Rangitikei series soil. This was followed by a mottled interbedded silt and sand C horizon across all soil types. Bulk density and soil moisture samples were collected from each representative layer by selecting a 0.05 – 0.10 m section and placing in an airtight bag labelled with its core location and depth (i.e. core 6, depth 0.64 – 0.69 m). In addition to the bulk density and soil moisture samples, a small (50 g) soil sample was also collected for particle analysis that represented each bulk density and soil moisture sample.

3.2.4.3 Supplementary Profile Observations

Measurements of water table depth were recorded at the pasture plot with an electronic dip-meter. An average depth to the water table was recorded from four piezometers. Measurements were collected after each GPR survey performed at the pasture plot (i.e. 30 September 2015, 26 November 2015 and 24 February 2016), to help to identify the water table in the radargrams.

3.2.5 Lab Analyses

3.2.5.1 Soil Dry Bulk Density

Each 0.05 – 0.10 m soil section that was collected in-field from individual cores was then placed into pre-weighed plastic containers, the wet weight recorded, dried at 75°C for 72 hours, and then re-weighed and dry weight recorded. Although the standard temperature for oven-drying soils to assess bulk density is 105°C, the oven used to dry these samples was pre-set to 75°C as an average for other geological samples being analysed. This may have an effect on the final weight of the bulk

density samples as a second dry weight was not recorded to confirm constant weight. The following equation was then used to determine dry bulk density:

$$\mathrm{Pb} = \frac{Ms}{Vt} \tag{7}$$

where *Ms* represents the weight of the dry soil (Mg) and V*t* represents the soil section volume (m^{-3}). Soil section volume was calculated as follows: πr^2 x soil section length = π x (0.0335^2) x soil section length.

A total of 68 soil sections were analysed for dry bulk density and soil moisture (23 arable plot and 45 pasture plot).

3.2.5.2 Volumetric Moisture Content

Volumetric moisture content (Θv) was estimated using the following equation:

$$\Theta v = \Theta m \text{ x } \frac{soil\ bulk\ density}{density\ of\ water} \tag{8}$$

where *Θm* is the gravimetric water content. Since density of water is assumed to be 1.0 Mg/m^{-3}, this equation can be expressed as the gravimetric water content (Θ*m*) multiplied by soil bulk density (P_b).

3.2.5.3 Soil Porosity

Total porosity of each soil section was calculated using soil bulk density divided by average particle density (2.65 Mg/m^3) as explained in McLaren & Cameron, (1996). Total porosity is expressed as a % of volume of pores to the volume of soil as follows:

$$\varepsilon = 1 - \frac{Pb}{Pp} \quad (9)$$

3.2.5.4 Soil Texture

Soil samples were analysed for particle size distribution. Over the two plots, particle size was assessed for the < 2000 µm fine earth fraction. This was performed using the Horiba Partica LA-950V2 laser scattering particle size distribution analyser (PSDA). On average 8 to 16 small soil samples (50 g) were collected per core, depending on horizon layering. Half of these samples were then chosen to be analysed for particle size, with the other half discarded (due to resource limitations). A total of 70 soil samples were analysed to represent the 13 soil cores.

To prepare each sample, approximately 4 g of moist soil was placed in a 600 ml beaker after removal of any roots. To further remove organic matter (which was not permitted in the PSDA), beakers were placed into a fume hood and a 36% hydrogen peroxide (H_2O_2) solution was added to just cover the soil sample. Samples were checked daily for signs of drying and extra H_2O_2 added. Beakers were covered with paper towels and left for two to three weeks until effervescence had stopped in all samples, signifying that all organic matter had been removed. Residual H_2O_2 needed to be removed before samples could go through the PSDA. Samples were left until the majority of H_2O_2 had evaporated once effervescence had ceased, then deionised water was added to each beaker. Each soil solution was then spread evenly amongst six centrifuge tubes and centrifuged for 4 minutes at 7000 rpm. Water was then decanted off each tube and deionised water added before further centrifugation. This process was repeated 3 – 4 times until water appeared clear and colourless (representing minimal H_2O_2 remaining). Each soil solution was then added to a PSDA glass tube and ¾ filled with deionised water.

The refractive index chosen for the PSDA was 1.54. This represented Manawatu flood sediment and consequently was typical of the study site (Moebis, 2015). The PSDA was operated according to standard procedures. Each sample was analysed

three times by the PSDA with rinsing and debubbling between each sample. The PSDA was refilled with deionised water regularly.

The PSDA analyses samples from 0.011 µm to 3000 µm and gives results of particle size as a % of the sample analysed. It was recommended samples > 2000 µm should be dry sieved and analysed separately from the PSDA. All samples collected were < 2000 µm therefore all samples were analysed using the PSDA. This data was then put into Gradistat (Blott & Pye, 2011) to interpret mean particle size per sample. A further analysis was completed in Microsoft Excel to calculate the proportions of sand (2000 - 20 µm), silt (20 - 2 µm) and clay (<2 µm) per sample.

4 Results

This chapter is divided into two sections, with the first section presenting the measured physical and hydrological soil properties and their relationships. The second section describes the relationships found between the radar images and these measured physical and hydrological properties. Soil cores have been labelled across the two plots as follows, to assist with interpreting the features described in the core logs and radargrams.

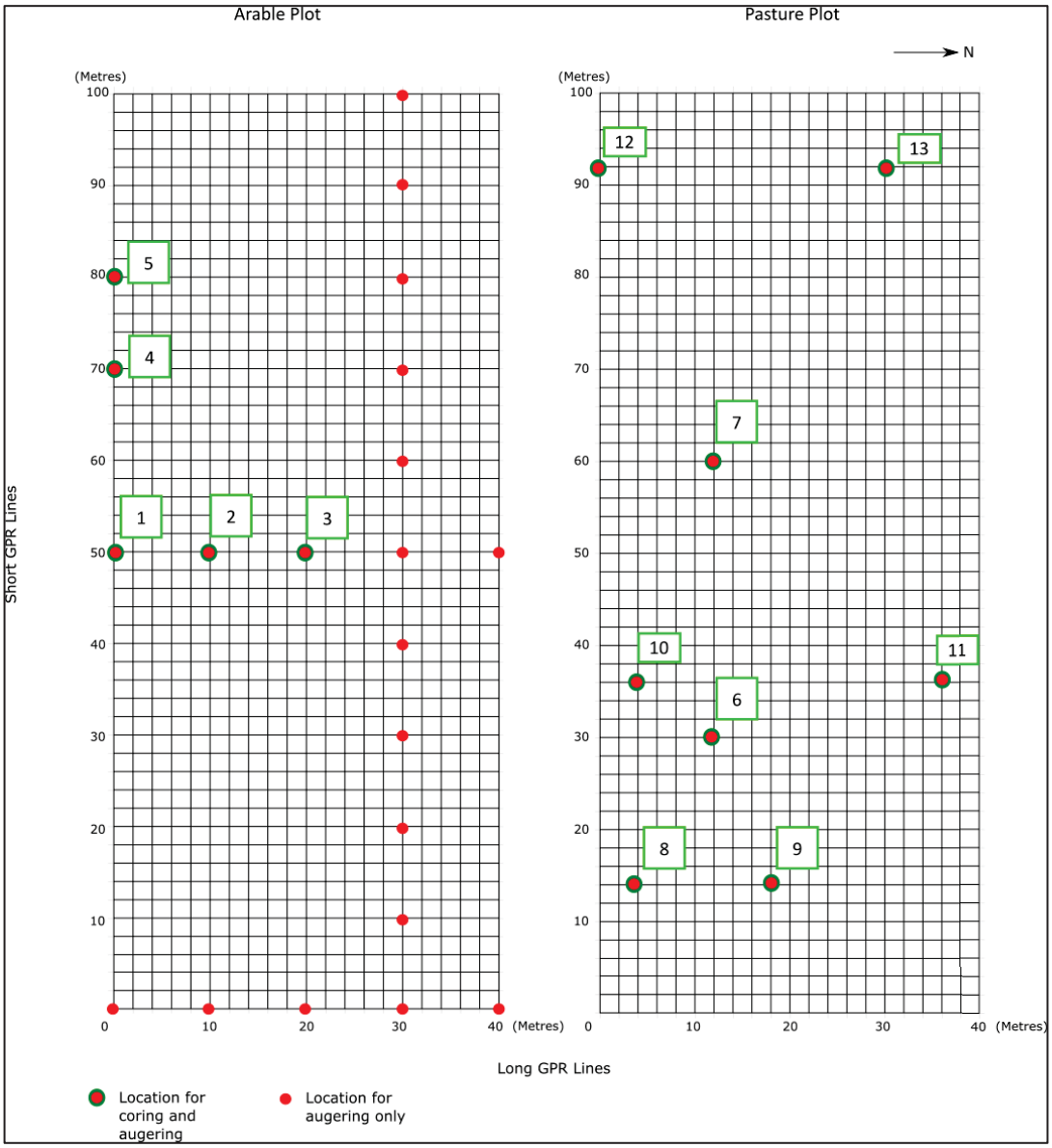

Figure 4.1: Soil core and auger locations across the two plots. Soil cores are numbered for ease of reference when interpreting with the results section.

4.1 Soil Properties

4.1.1 Soil Texture

All soils were of either a sandy loam or silt loam topsoil texture following down to sandy loam, loamy sand and sand sub soils (mapped according to Pollock et al. (2003). Sand fractions from each horizon ranged from 17.04 to 99.12% across the arable and pasture plots (Table 4.1).

Table 4.1: Average percentages of sand and clay ranges across the arable and pasture plots.

Location	Sand % per horizon		Clay % per horizon	
	Min	Max	Min	Max
Arable	34.47	99.12	0	7.2
Pasture	17.04	98.05	0	4.94

Sand fractions dominated the soil profiles across the study site and generally increased and fluctuated down the soil profile, especially through the deeper profiles located in the pasture plot. For example, Core 9 (Fig 4.2), (see Figure 4.1 for the core naming convention and see Appendix 1 for all of the raw core log data) in the pasture plot has a sand percent of 33 % in the A horizon, increasing to 80 – 90% down the profile to 2.11 m depth, then declining to 65% at 2.20 m depth before increasing again to 94 % at 2.44 m depth.

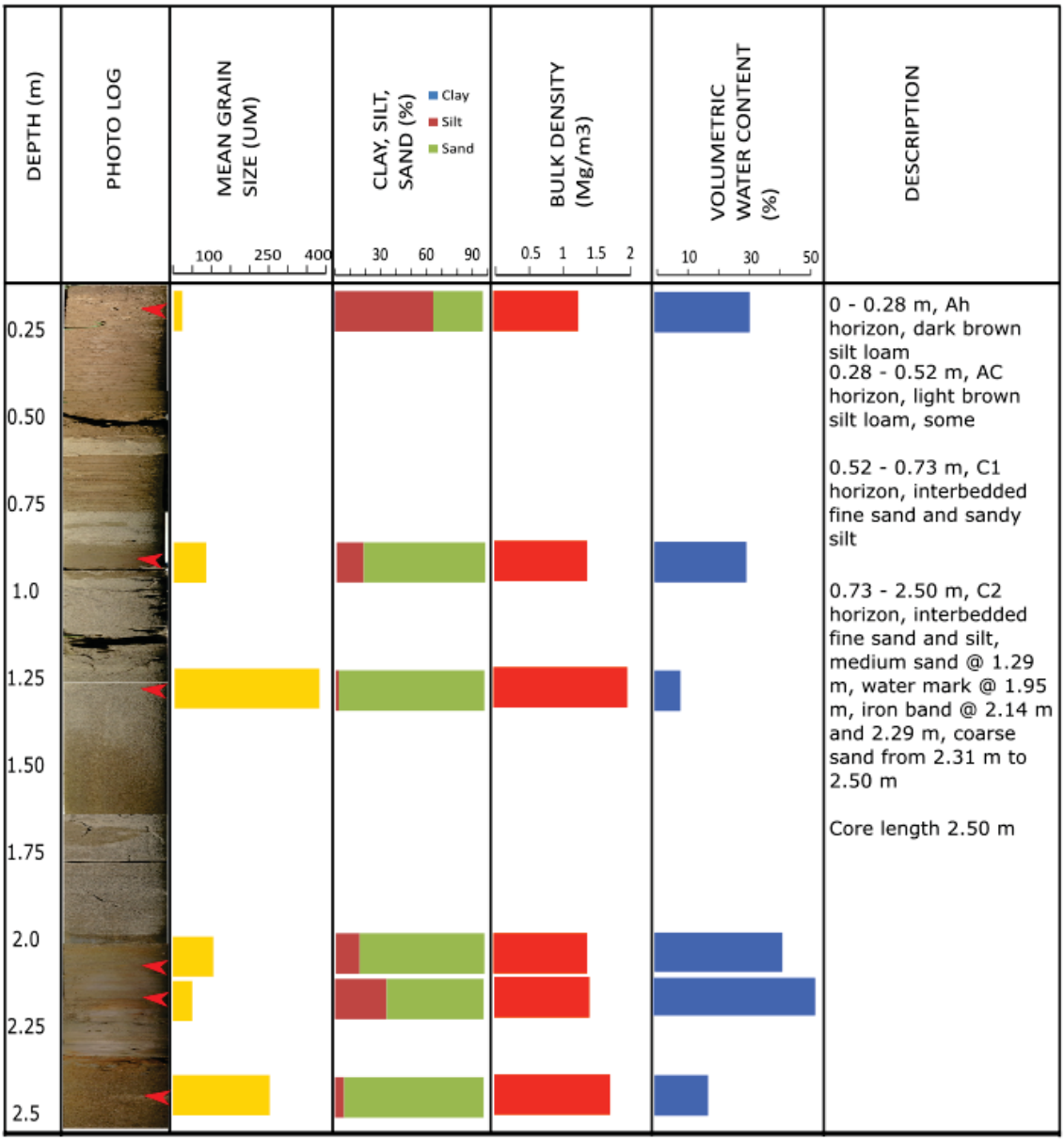

Figure 4.2: Core 9 from the pasture plot, showing an increase in sand content down the soil profile to 2.11 m. At 2.20 m sand percent declined to 65% then increased to 94% at 2.44 m depth. Red arrows represent location depth of each sample.

The highest proportion of clay was associated with the A horizon of both plots. The Ah horizon of core 8 (Fig 4.3) of the pasture plot had 4.94% clay and the Ap horizon of Core 2 (Fig 4.4) of the arable plot had 7.2% clay. These proportions of clay are significantly less than that of the same soils mapped using S-map (Table 3.1).

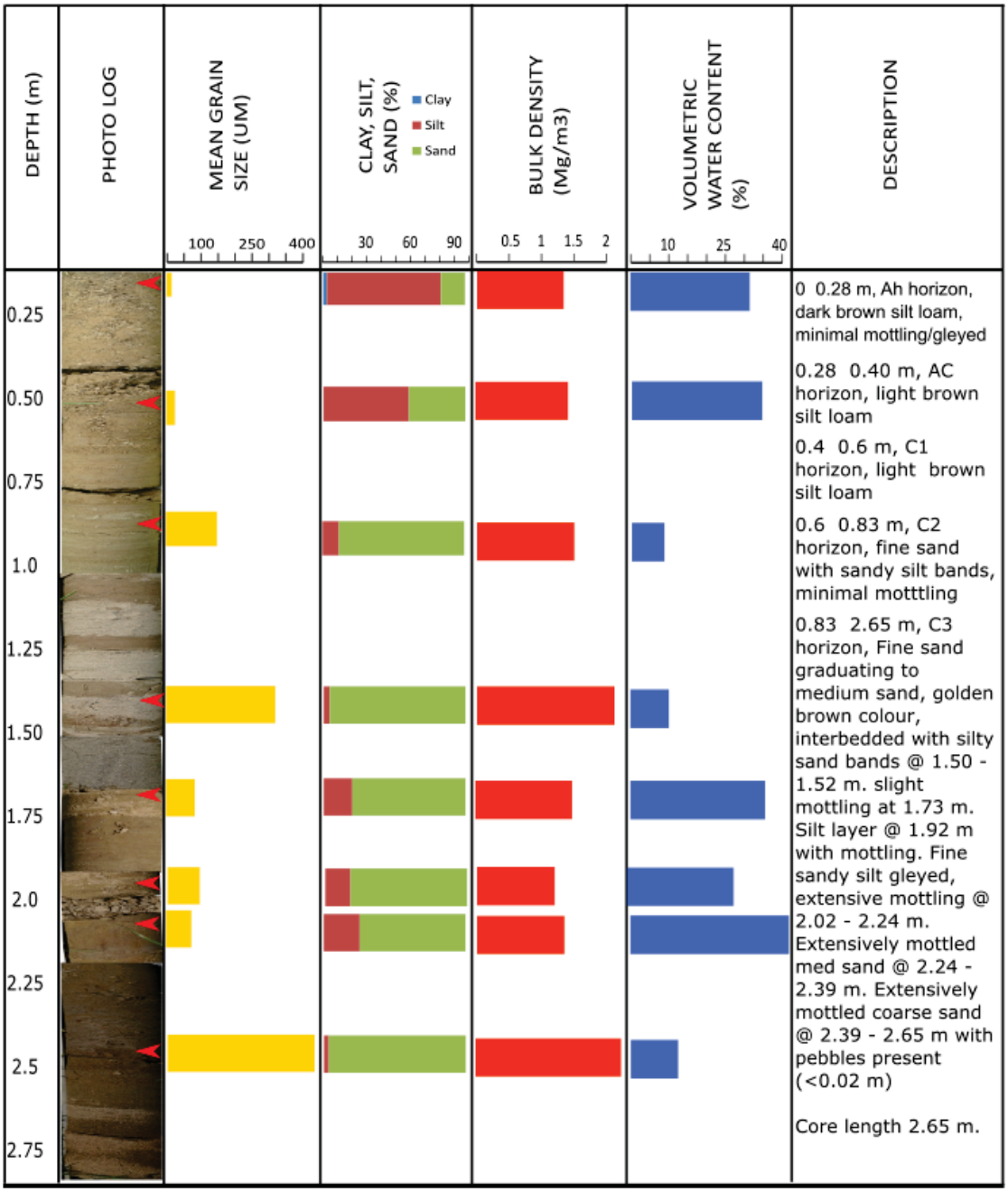

Figure 4.3: Core 8 from the pasture plot, showing 4.94% clay in the Ah horizon, indicating very recent, young soils that have not had sufficient time to develop. Large textural changes are shown between 1.39 m and 1.69 m where mean grain size changes from 322 µm to 85 µm respectively and again at 2.09 m to 2.46 m grain size changes from 75 µm to 433 µm respectively.

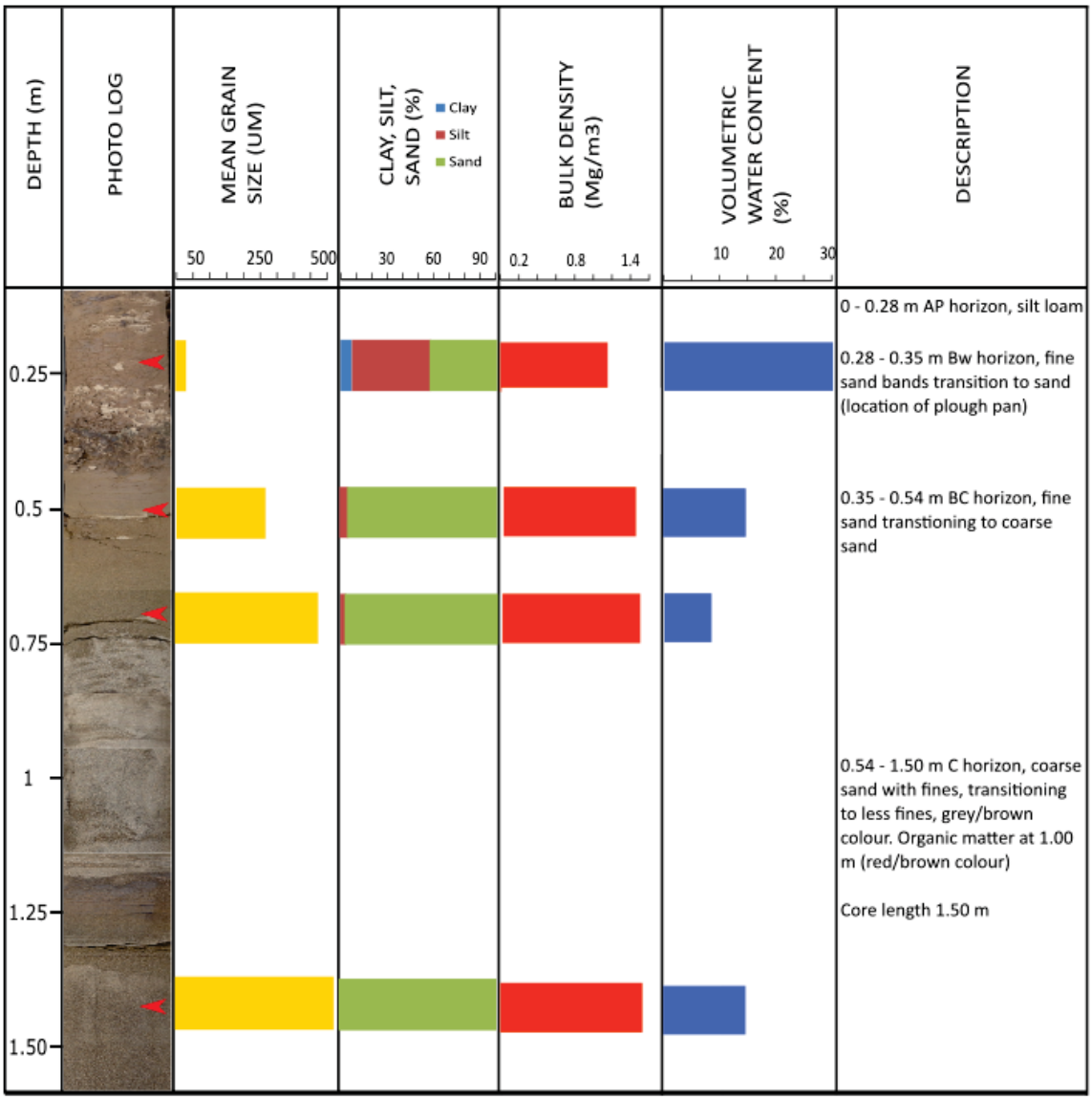

Figure 4.4: Core 2 from the arable plot, showing 7.2% clay fraction in the Ap horizon, this value is still significantly less than the same soil type mapped using S-map.

Significant textural changes in grain size (>200 µm between sample collection locations down a soil profile) were common throughout the C horizon of both plots (Appendix 1). Core 4 and Core 5 from the arable plot and Cores 6, 8, 9, 10 and 13 from the pasture plot had significant textural changes within the C horizon.

Iron staining was located within a few core locations across both plots. These were all found within the C horizon and were encountered when there was a sharp textural break. For example, core 4 (Fig 4.5) within the arable plot had an iron band located at 0.72 – 0.74 m depth where coarse sand preceded a fine sand layer. In

addition, a further iron band is located at 1.05 m depth where very coarse silt lays over medium sand. A small percentage of mottling (~5%) and gleying were common where texture was very fine (i.e. very coarse silt or very fine sand at 0.91 – 1.05 m depth).

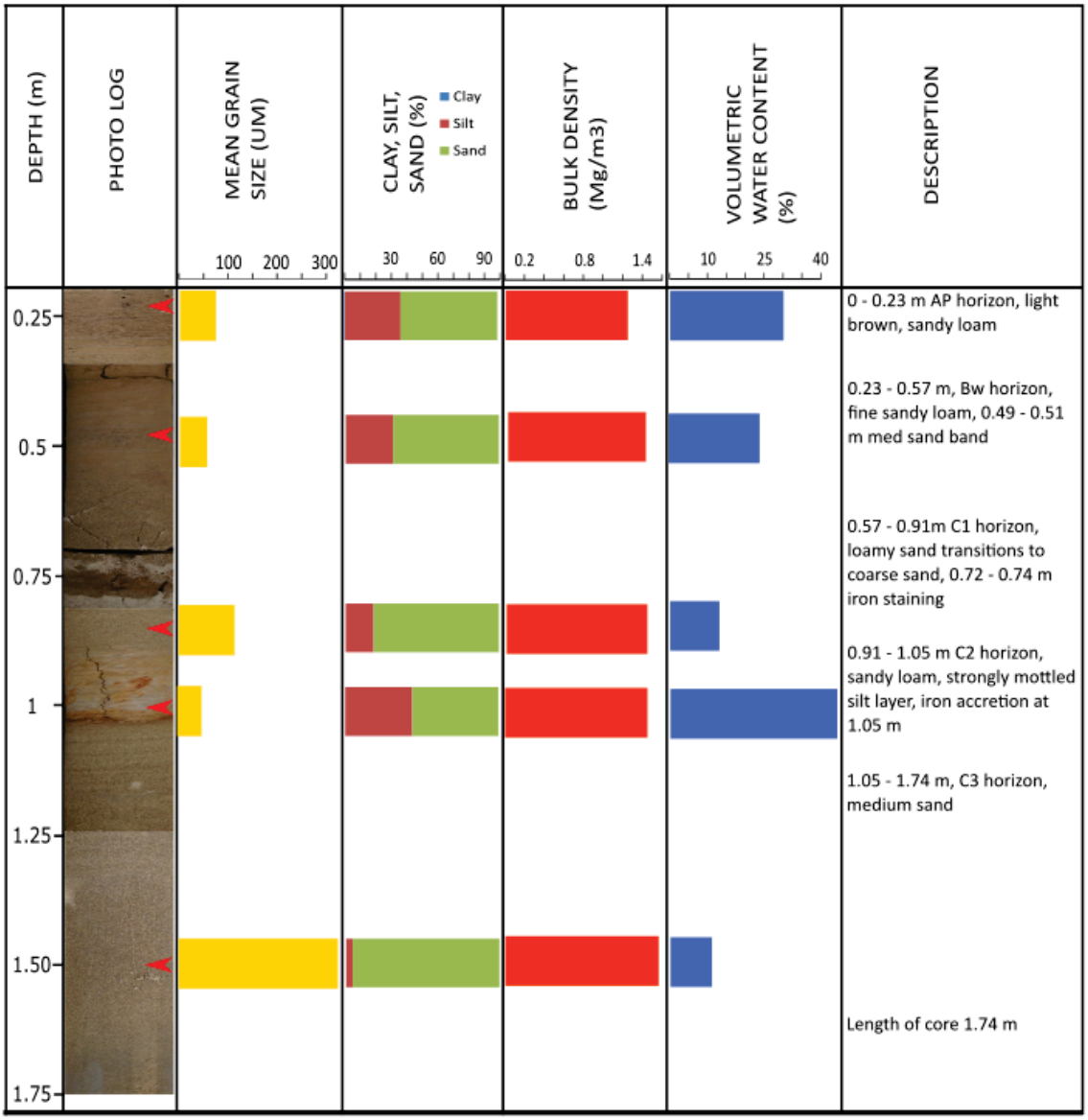

Figure 4.5: Core 4 of the arable plot. Iron banding is located at 0.72 – 0.74 m and 1.05 m depth at the boundary of a textural break.

4.1.2 Soil Type

According to the soil types mapped by Pollock et al. (2003), the arable plot has the Manawatu silt loam over sand and Manawatu sandy loam soil types located within

it. Core 4 (Fig 4.5) and 5 (Fig 4.15) had an increased amount of sand located in the topsoil. From the initial mapping these cores are located within the Manawatu silt loam over sand. However, their soil profile aligns more to that of the Manawatu sandy loam. The topsoil has a larger sand fraction, giving it a sandy loam texture and additionally a finer textured layer is found at ~1 m depth at both of these core locations. In comparison, the Manawatu silt loam over sand does not contain any finer sediment below 0.69 m depth. The three cores located within the Manawatu silt loam over sand fraction, Core 1 (Fig 4.7), 2 (Fig 4.4) and 3 (Fig 4.17) had silt loam topsoils made up of <42% sand and classed as coarse to very coarse silt. Further down the profile, sand fractions increased within the C horizon.

The area where the pasture plot is located was mapped by Pollock et al. (2003) as Rangitikei silt loam over sand and Manawatu fine sandy loam. A distinct topographical change approximately halfway along the plot defines the change in soil types (Fig 3.4). The cores located in the Manawatu fine sandy loam included Core 12 (Fig 4.24), 13 (Fig 4.25), 11 (Fig 4.22) and 7 (Fig 4.6). Although there were slight differences down the profile of each core related to the layering of silt and sandy loams, they all had similar topsoil and depth to gravel was < 1.30 m at these locations as reflected in the mapped Manawatu fine sandy loam soil type. Cores located in the Rangitikei silt loam over sand included Core 6 (Fig 4.19), 10 (Fig 4.21), 8 (Fig 4.3) and 9 (Fig 4.2). These cores all had a deeper profile and no B horizon. At depths, interbedded layers of sands and silts were common.

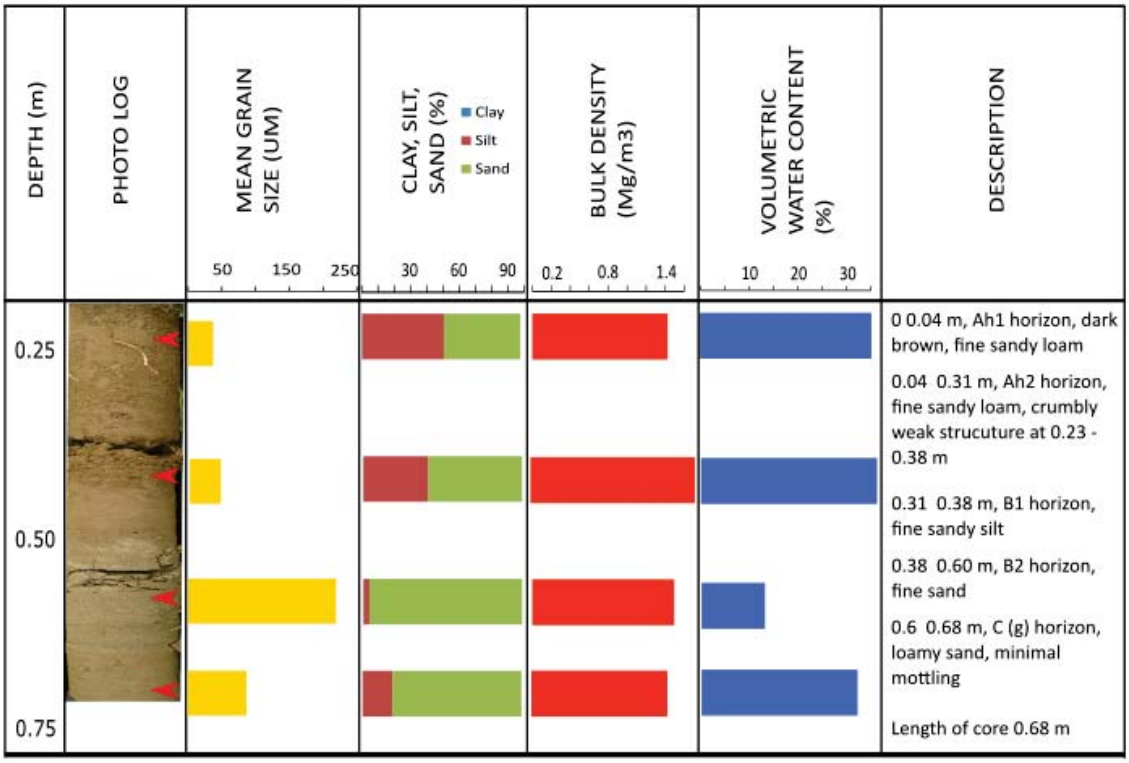

Figure 4.6: Core 7 from the pasture plot, with a soil depth of 0.68 m, located in the Manawatu fine sandy loam.

4.1.3 Soil Bulk Density

Sample depth and textural changes show differences in soil dry bulk density values across the arable and pasture plots. Generally soil bulk density increased with increasing depth across both the arable and pasture plots (Table 4.2).

Table 4.2: Average soil dry bulk density values across the arable and pasture plots. Note pasture plot soil cores with an A horizon >0.20 m were used for these calculations.

Horizon	Arable Plot (Mg/m³)	Pasture Plot Mg/m³)
A	1.30	1.33
B	1.44	1.47
C	1.53	1.52

Exceptions were seen in the arable plot at Core 1 (Fig 4.7) and 5 (Fig 4.15) where bulk density was lower at the top of the C horizon compared to the A horizon. The effect of cultivation of the top 0.3 m of soil within the arable plot has resulted in a weak topsoil structure thus increasing bulk density in the A horizon due to soil compaction. Bulk density values in the pasture plot alternated with depth, especially through the C horizon. This variation in density is thought to be related to sequences of flood deposits (alternating layers of silts and sands), with an example of this layering provided by Core 8 (Fig 4.3) where a medium sand layer had bulk density values 66% greater than that of a very fine sand layer at 2.46 m and 2.09 m depth respectively. This layering is also prominent from 1.0 – 1.5 m depth within this core. In general medium sand had the highest bulk density values, but exceptions were seen in Core 5 of the arable plot and Cores 12 and 10 of the pasture plot where very coarse silt had the highest bulk density values for these cores (Appendix 1).

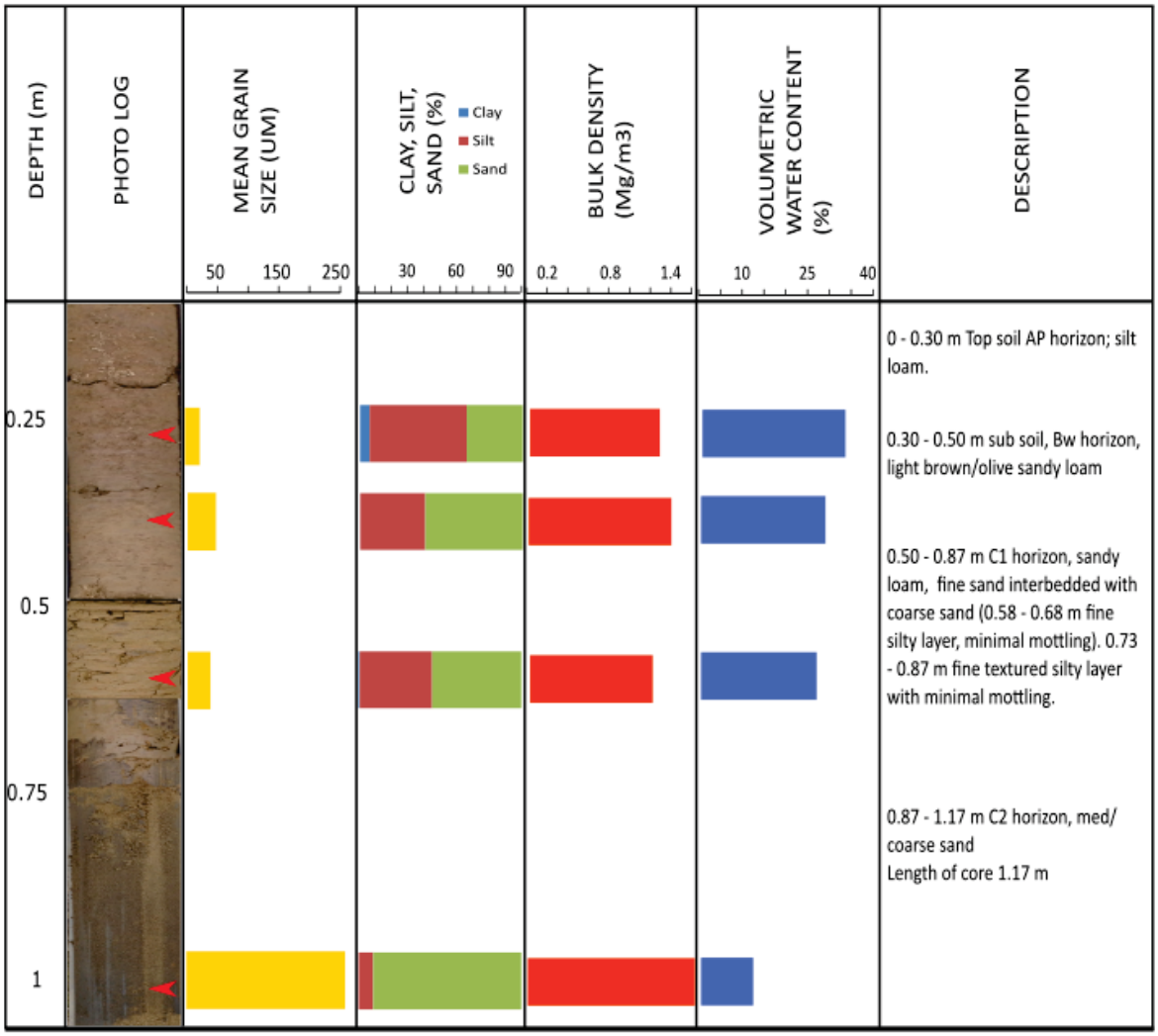

Figure 4.7: Core 1 showing an increase in bulk density from topsoil to subsoil, before a slight decline at 0.66 m before a further increase at 1.06 m depth.

4.1.4 Soil Volumetric Water Content

Average volumetric water content decreases down the profiles across both plots (Table 4.3). However, the highest volumetric water content was 53% found in Core 9 (Fig 4.2) at 2.26 m depth. The lowest volumetric water content was 7% located in Core 6 (Fig 4.19) at 0.64 m depth. The pasture plot tended to have higher volumetric water contents. On average both the B and C horizons of the pasture plot carried 6% more water than the B and C horizons of the arable plot. In general, where grain size was >200 µm, volumetric water was <19%, an exception was Core 11 (Fig 4.22), where grain size >200 µm a volumetric water measurement of 24% was recorded. The highest volumetric water content related to a smaller grain size

(<75 µm) among cores from both plots. Further results will be discussed in Section 4.1.6 *Relationships between Soil Properties,* where volumetric water content is compared to other soil properties.

Table 4.3: Average volumetric water content across the arable and pasture plot within each horizon.

Horizon	Arable Plot	Pasture Plot
A	31%	32%
B	23%	29%
C	20%	25%

4.1.5 Piezometer Measurements

In September 2015 groundwater depth averaged 4.02 m and ranged from 4.04 m to 3.98 metres across the four piezometers, located adjacent to the pasture plot and spaced approximately 1.0 m apart (Table 4.4). During November 2015, approximately two months after the initial groundwater reading, depth to groundwater had decreased on average 0.68 m to an average depth of 4.70 m with a range of 4.72 m to 4.66 m. A further reduction in groundwater was recorded in February 2016 where the average depth to groundwater had decreased by 0.33 m from the November reading to 5.03 m and ranged from 5.06 m to 4.96 m. The depth of groundwater decreased on average 1.01 m from September 2015 to February 2016 (5 months difference) at the pasture plot location. This drop in groundwater level represents a drying out of the soil in the summer months; it is expected that both the drop of the water table and the drying out of the soil in the vadose zone above could be detectable in radargrams (which is explored in Section 4.2 and 4.3).

Table 4.4: Depth to groundwater level taken from four piezometers (P1, P2, P3, and P4) located adjacent to the pasture plot.

Date	P1 (m)	P2 (m)	P3 (m)	P4 (m)	Average (m)
30 Sep 2015	4.04	4.04	4.025	3.98	4.02
25 Nov 2015	4.72	4.72	4.70	4.66	4.70
24 Feb 2016	5.04	5.06	5.06	4.96	5.03
Difference Feb 2016 to Sep 2015	1.00	1.02	1.03	0.98	1.01

4.1.6 Relationships between Soil Properties

The comparison of bulk density and soil moisture across the differing textures of the study site are shown in Figure 4.8. Soil moisture increases from silt loam to sandy loam textures, then decreases sharply from loamy sand to sand texture. Having less micropores amongst the sand particles will limit the amount of water that can be stored, hence the decrease in volumetric water content.

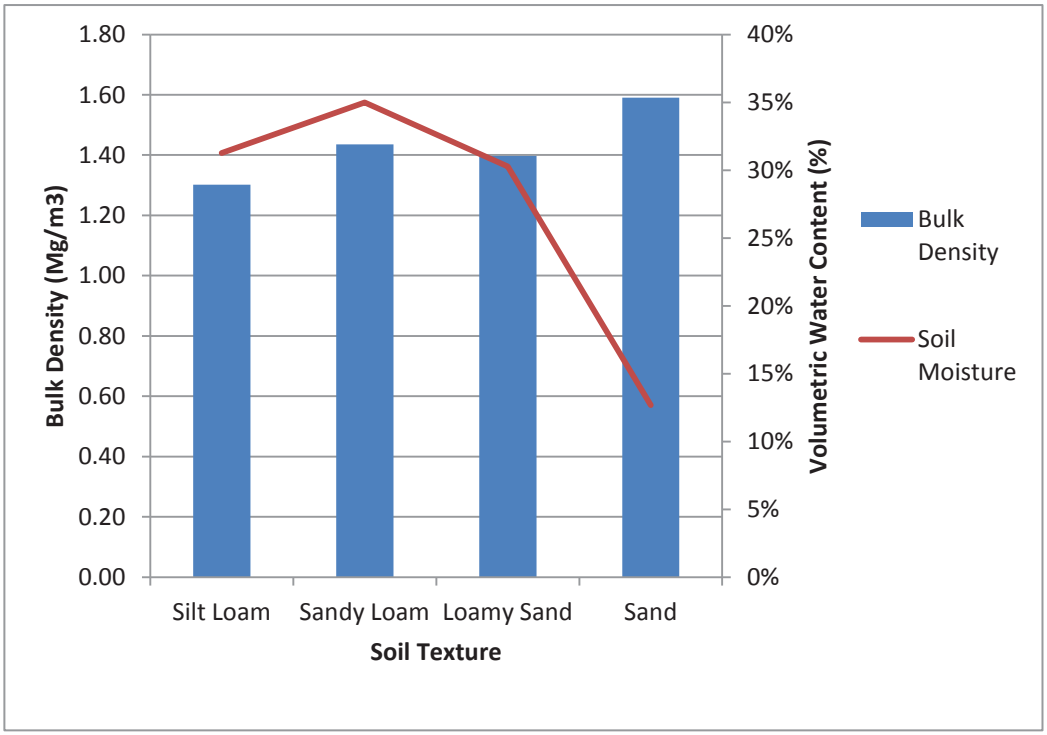

Figure 4.8: A comparison of bulk density and soil moisture across the four different soil textures located at the study site.

Volumetric water content varied between 7% - 51% and the corresponding mean grain size varied between 14.98 µm - 473.46 µm across the study site. To assess the influence of grain size on water content, the relationship between the two variables was assessed visually in a scatter plot (Fig 4.9). There is a moderate, negative, non-linear correlation between mean grain size and volumetric water content (r^2 = 0.6241). Water potential is dependent on soil texture and structure as these properties define pore size (McLaren & Cameron, 1996). Finer particle sizes are likely to have an increased amount of micropores. These micropores have an increased capillarity where water is held more tightly than that in coarser sediment (i.e. sand). Larger grain sizes have more of a variation on volumetric water content. This could relate to the redistribution of water through the soil profile, and the positioning of these coarser layers with silt and finer sand layers. The correlation seen in Figure 4.9 suggests that finer-grained materials at the study sites are likely to hold greater volumetric water contents, which is likely to influence the reflectors seen in the radargrams.

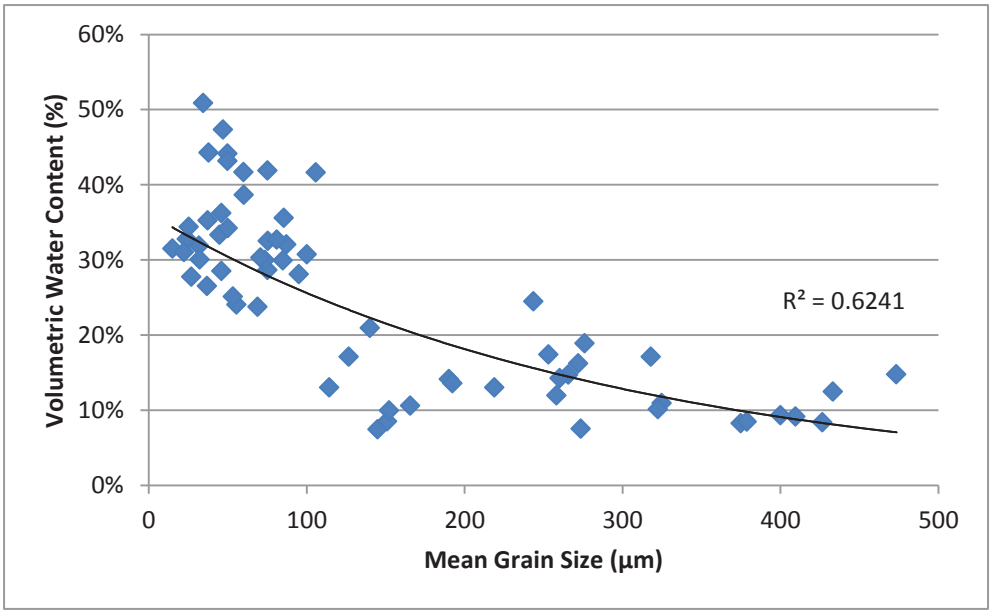

Figure 4.9: Volumetric water content plotted against mean grain size showing a negative exponential relationship ($R^2 = 0.6241$).

To test whether there was any strong influence of sample depth with volumetric water content, possibly expected due to differing consolidation or water availability at different depths, volumetric water content was correlated against the depth of the sample (Figure 4.10). The scatter shown in Figure 4.10, shows that there does not appear to be any relationship between volumetric water content and depth ($R^2 = 0.0025$), at least when all samples, irrespective of grain-size, are included. This is likely because of the overbearing influence that grain size has on the capacity to hold water.

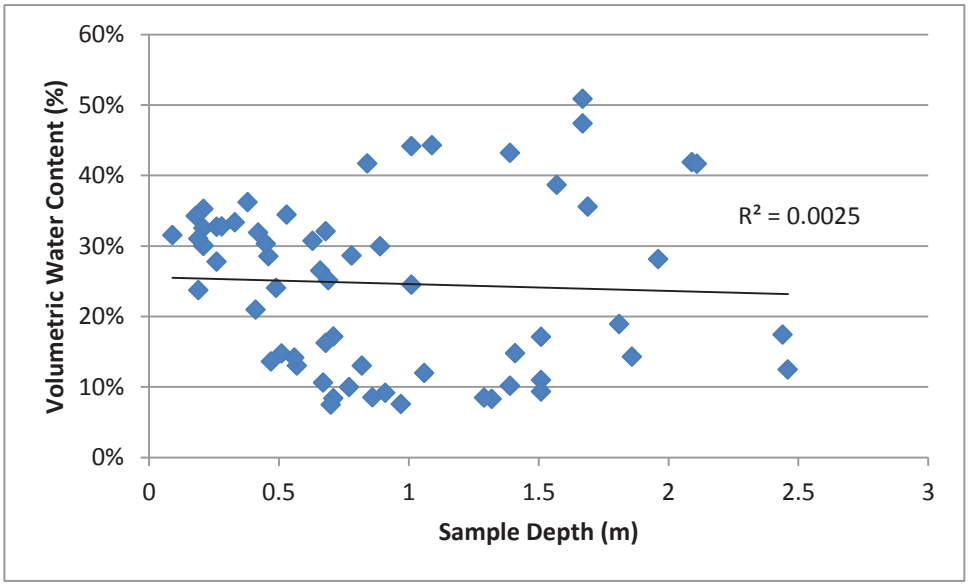

Figure 4.10 Volumetric water plotted against sample depth showing no correlation between these two variables (R^2 = 0.0025).

Bulk density across the study site varied from 1.19 Mg/m³ to 2.24 Mg/m³. Bulk density at the study site appears to be related to two factors: grain size and sample depth. There is a moderate (r^2 = 0.3549), positive, linear relationship between bulk density and mean grain size (Fig 4.11), and a weak (r^2 = 0.1928), positive, linear relationship between bulk density and sample depth (Fig 4.12). The latter is explained by bulk density increasing down the soil profile due to increasing load and decreasing soil disturbance (Marshall, 1996).

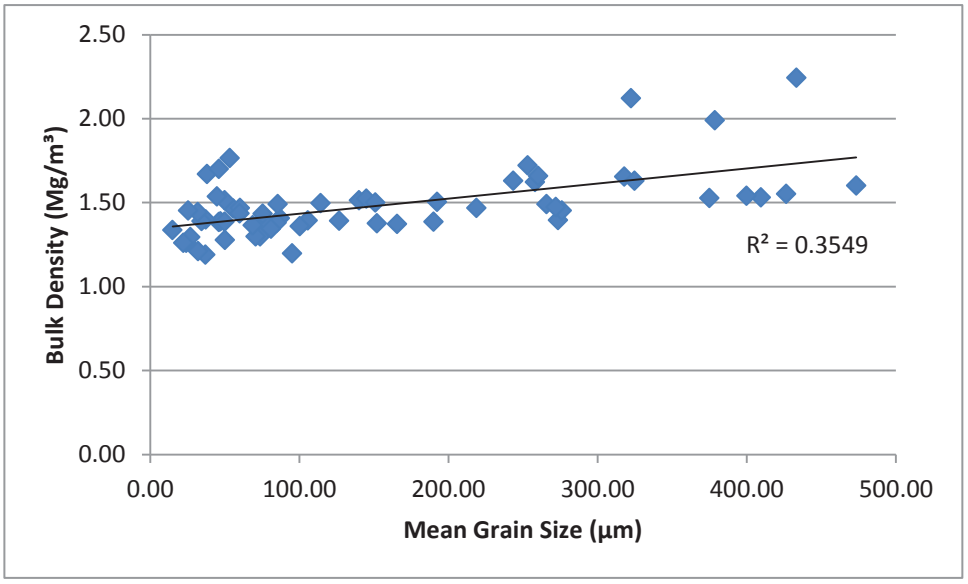

Figure 4.11: Bulk density plotted against mean grain size showing a positive linear relationship (R^2 = 0.3549).

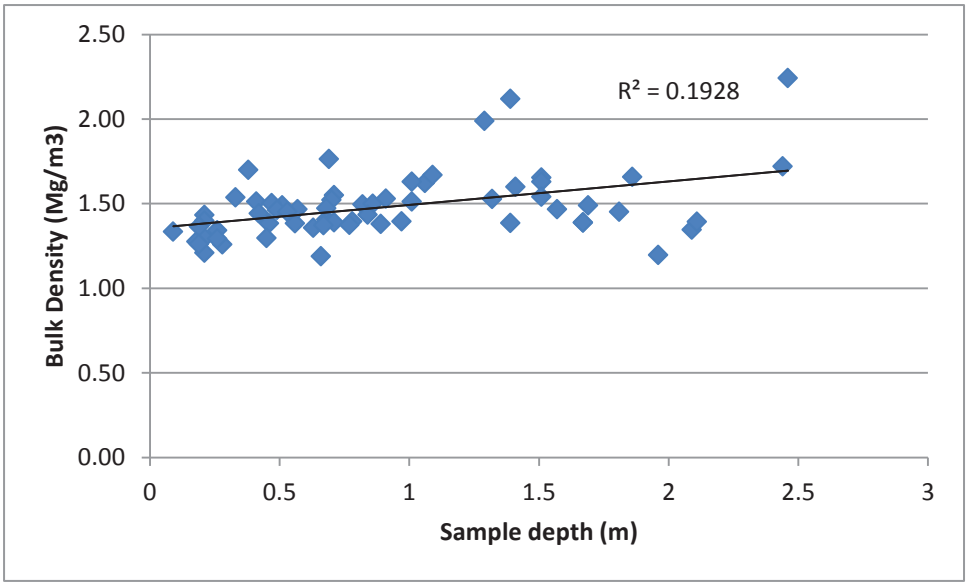

Figure 4.12: Bulk density plotted against sample depth showing a positive linear relationship (R^2 = 0.1928).

4.2 The Relationships of Radargrams to Field Measurements

4.2.1 Soil Physical Properties

To help with interpretations of radargram images, Beres & Haeni (1991) compiled a chart of reflection configurations (Fig 4.13). This chart has been modified for this research to aid in the interpretation of alluvial subsurface features. The characteristics of each radargram reflection configuration are an interpretation of the depositional sequence of sediments.

Across all radargrams, an interface or contrasting boundary layer (i.e. a sharp change in moisture content due to a change in grain size or wetting front positioned across a homogenous layer) appears as a continuous line of two to three bands (Doolittle et al., 2006; Shih & Doolittle, 1984). This is due to the oscillations in the radar signal. These bands limit the ability of GPR to detect shallow or closely spaced interfaces when using radar frequencies < 250 MHz, like that used for this research. The thickness of the bands are directly related to the dielectric constant of the material and are inversely related to the antenna frequency (i.e. a high dielectric constant and low frequency antennas will produce a thick band) (Shih & Doolittle,

1984). Finer features tend to be concealed when thicker layers of high dielectric constant material (i.e. wet sand) produce a strong reflective signal. Thus, distinguishing finer features using 200 MHz or 100 MHz antennas is limited by the strength of the radar signal and the reflective nature of the material being surveyed. Although the depth profile of a radargram can give an overall picture of the subsurface, depth should not be relied on for accurate interpretation of closely spaced interfaces.

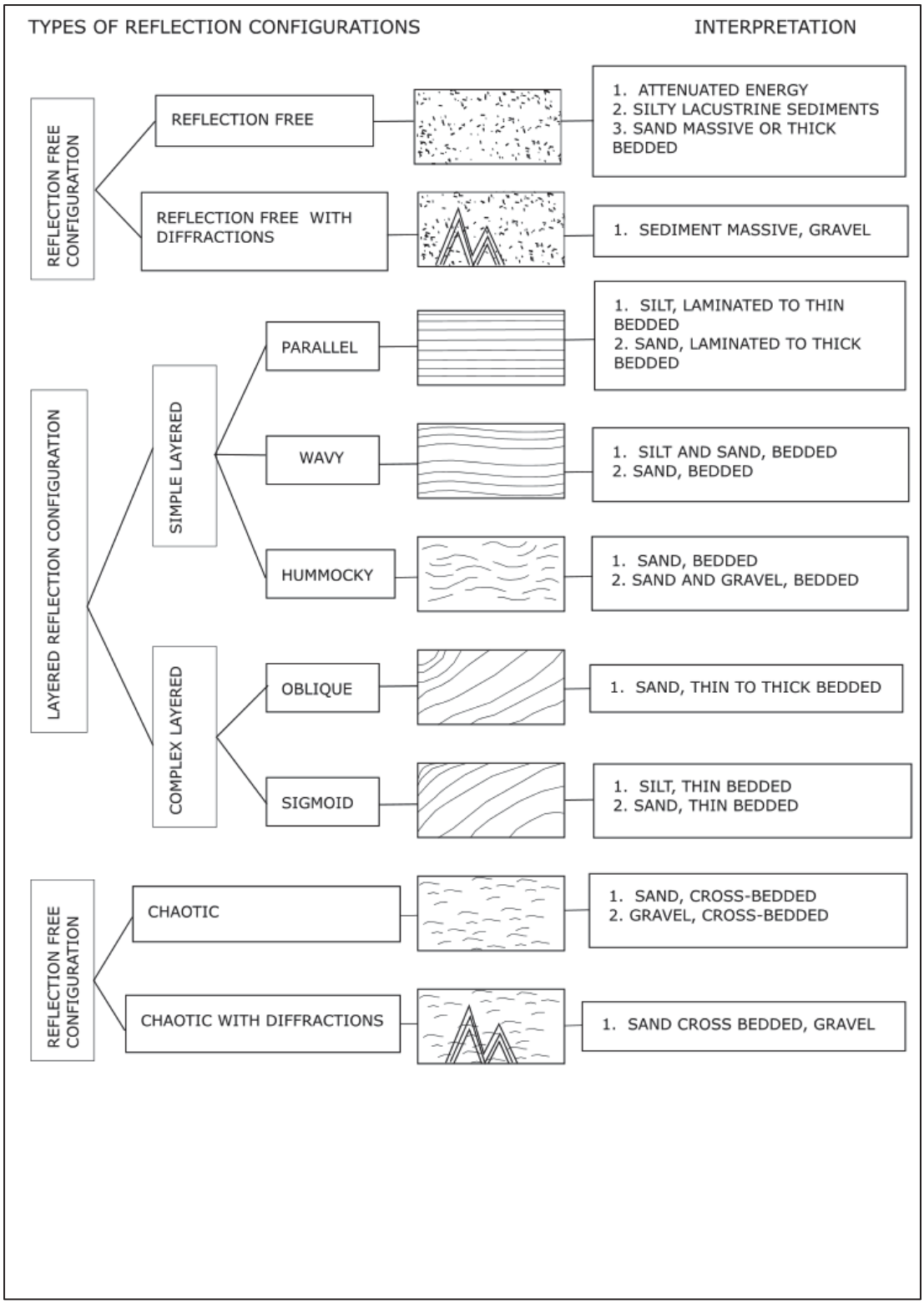

Figure 4.13: The interpretation of reflection configurations found on radargrams of the lithologic and stratigraphic properties of sediments located at Dairy 1 farm (modified from Beres & Haeni, 1991).

4.2.2 Soil Texture

Figure 4.14 shows the internal structure of the arable Long 0 line. There are three identifiable layers that have been ground-truthed with soil cores and auger samples. The simple to complex layered patterns (Fig 4.13) at the eastern end of the radargram are interpreted as medium sand and correlate with the deepest section of Core 1 (Fig 4.7). Towards the western end of the radargram, the reflection patterns become wavy and are interpreted as very coarse silt and medium sand (Fig 4.13). Further analysis as interpreted from Cores 4 (Fig 4.5) and 5 (Fig 4.15) find that these patterns correlate well with this fining throughout the mid-section of this radargram and transition to the medium sand band that was detected at the base of Core 1. Decreasing signal strength from 1.5 m to 2 m depth suggests attenuation due to the presence of gravel. The depth to gravel was identified along this attenuated zone with auger samples (green stars) and generally follow the reflection configuration.

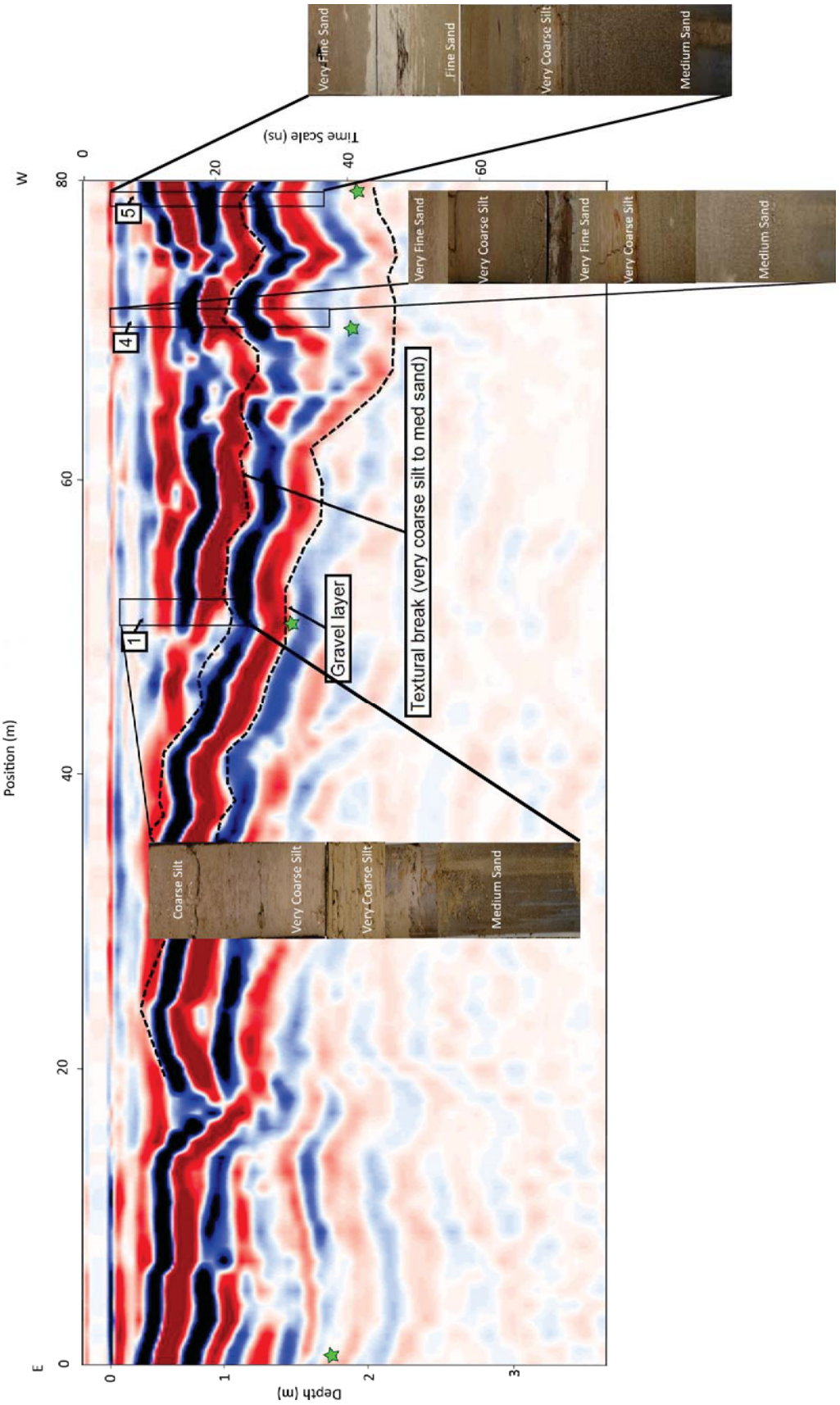

Figure 4.14: Interpreted 200 MHz radargram of arable Long 0 line, with soil Cores 1, 4 and 5. Auger samples assessed depth to gravel (green stars).

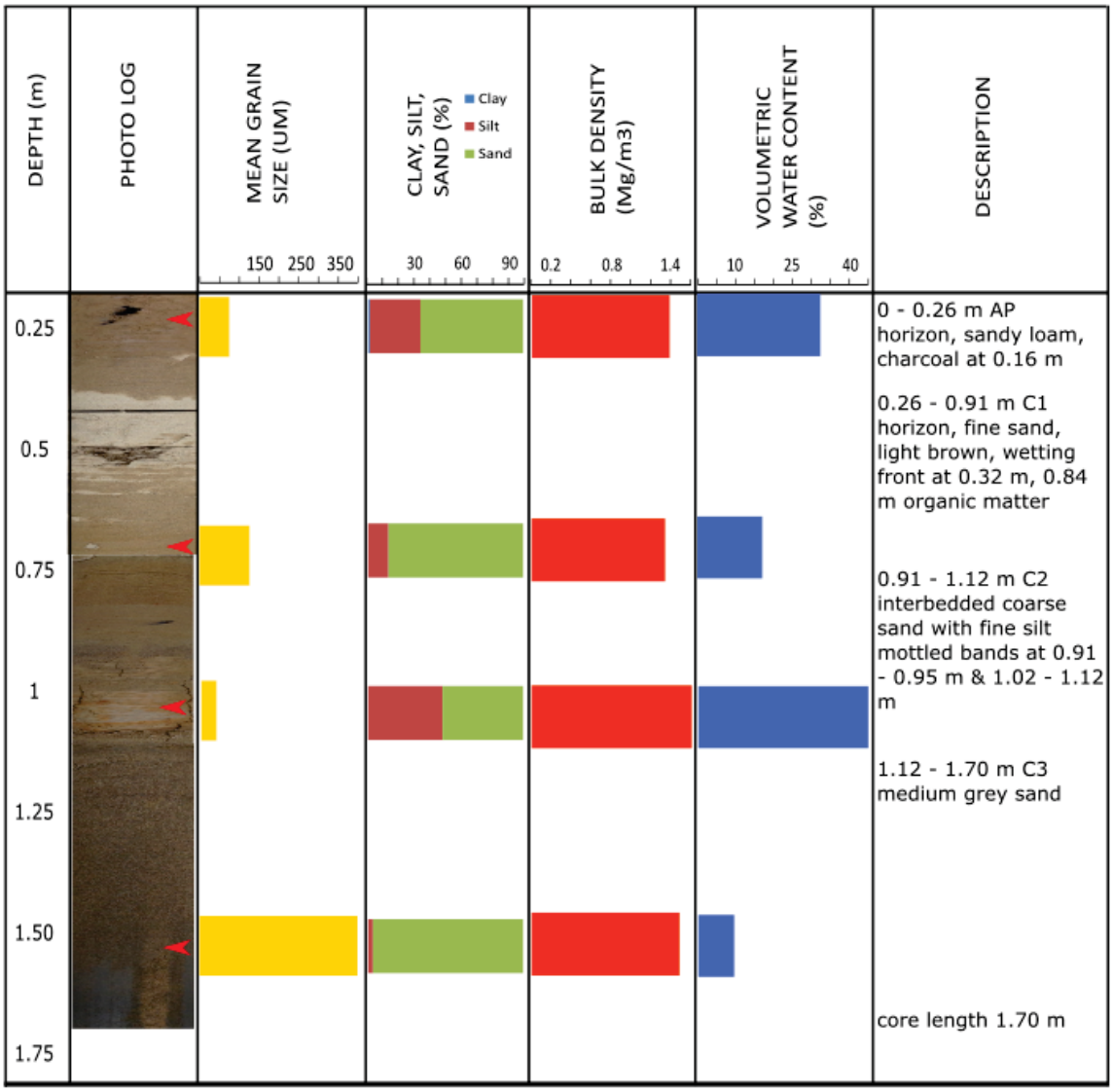

Figure 4.15: Core 5 of the arable plot showing the large textural changes within the C horizon from 1.09 m to 1.51 m depth where grain size varied from 38 µm to 400 µm respectively.

A radargram of the arable Short 50 line is shown in Figure 4.16. The reflection configuration of this radargram is simple to complex (Fig 4.13). Near the southern end of the radargram this wavy configuration is interpreted as medium sand (base of Core 1, Fig 4.7). This band tracks upwards through Core 2 (Fig 4.4) then graduates to textural changes of fine to medium sand at 0.81 m to 1.34 m as shown in Core 3 (Fig 4.17). The three bands tracking across at approx. 1.7 m to 3 m depth from south to north denote the depth to gravel as ground-truthed from auger samples. Below this depth, signal strength attenuates.

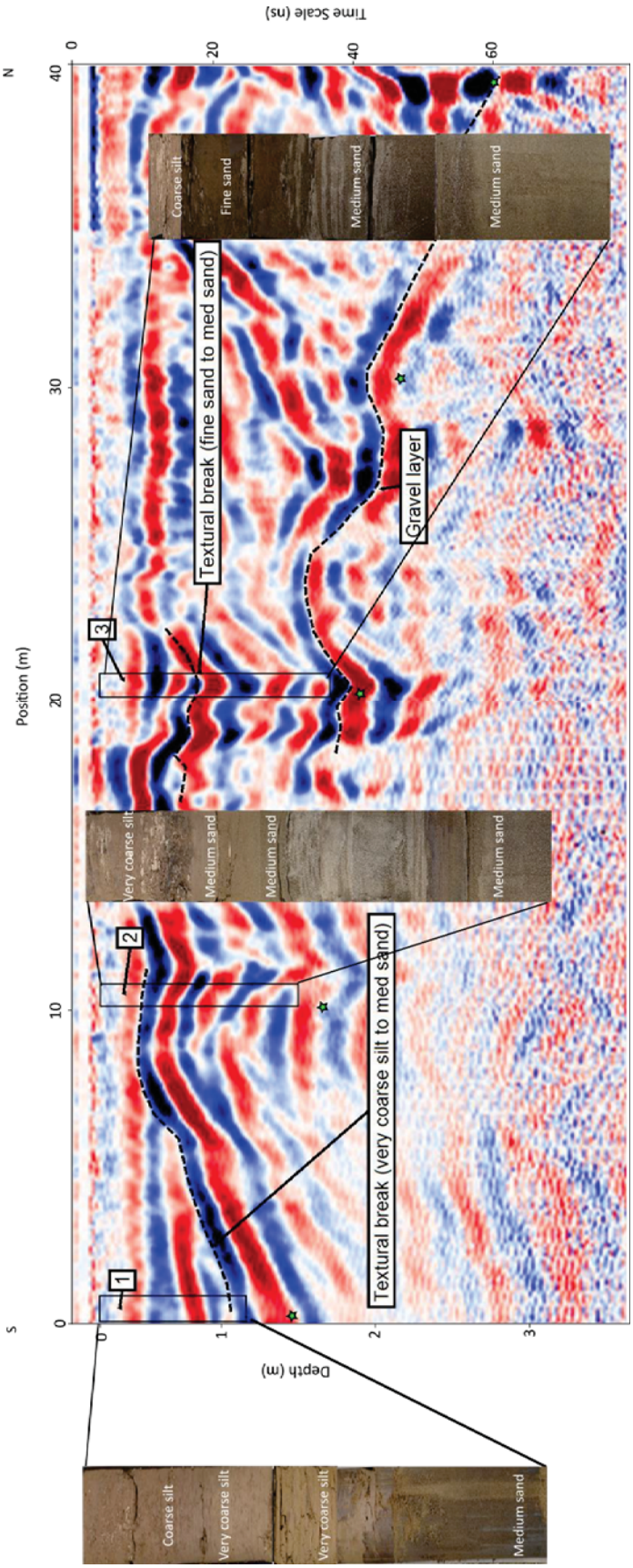

Figure 4.16: Interpreted radargram of the arable Short 50 line, with soil Cores 1, 2 and 3. Auger samples assessed depth to gravel (green stars).

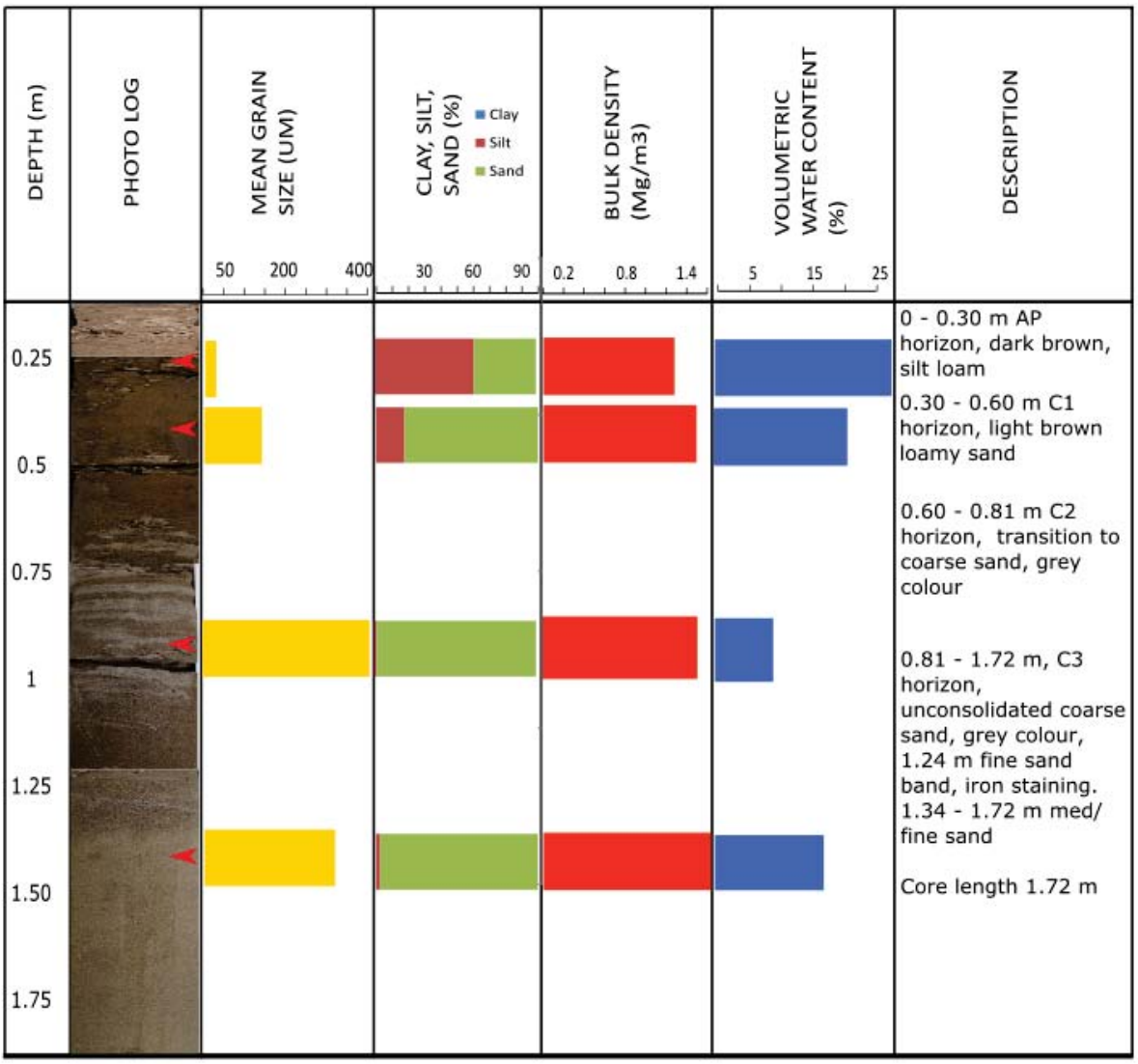

Figure 4.17: Core 3 showing a textural change between 0.81 m to 1.34 m depth from coarse sand to a fine/med sand band.

A radargram of the pasture Long 12 line (Fig 4.18) showed significant changes at approx. the 40 m position. This significant change where reflective configurations move sharply upwards from east to west is representative of an infilled channel bank. Up to 40 m from the eastern end, reflection patterns are parallel to hummocky (Fig 4.13) within the top 1.5 m and are indicative of fine sand layers (Fig 4.19). Beneath this layering at approx. 1 m, reflection configurations become complex, indicating areas of thin bedded sand and silts. Parallel reflectors are seen

at 65 ns and are indicative of signal noise due to reflections or diffractions from above-surface objects (e.g. power lines). Due to a higher electromagnetic wave velocity in the air than in the ground, their reflective arrival time could be in the time window of interest (i.e. 65 ns) (Nuzzo, 2003). In addition, the top 0.5 m is distorted as the ground and air wave have disrupted the subsurface signal reflection. Below Core 7, the detection of gravel gives an obvious strong signal where three horizontal bands are present. This same feature is found in other Long line radargram images associated with the pasture plot.

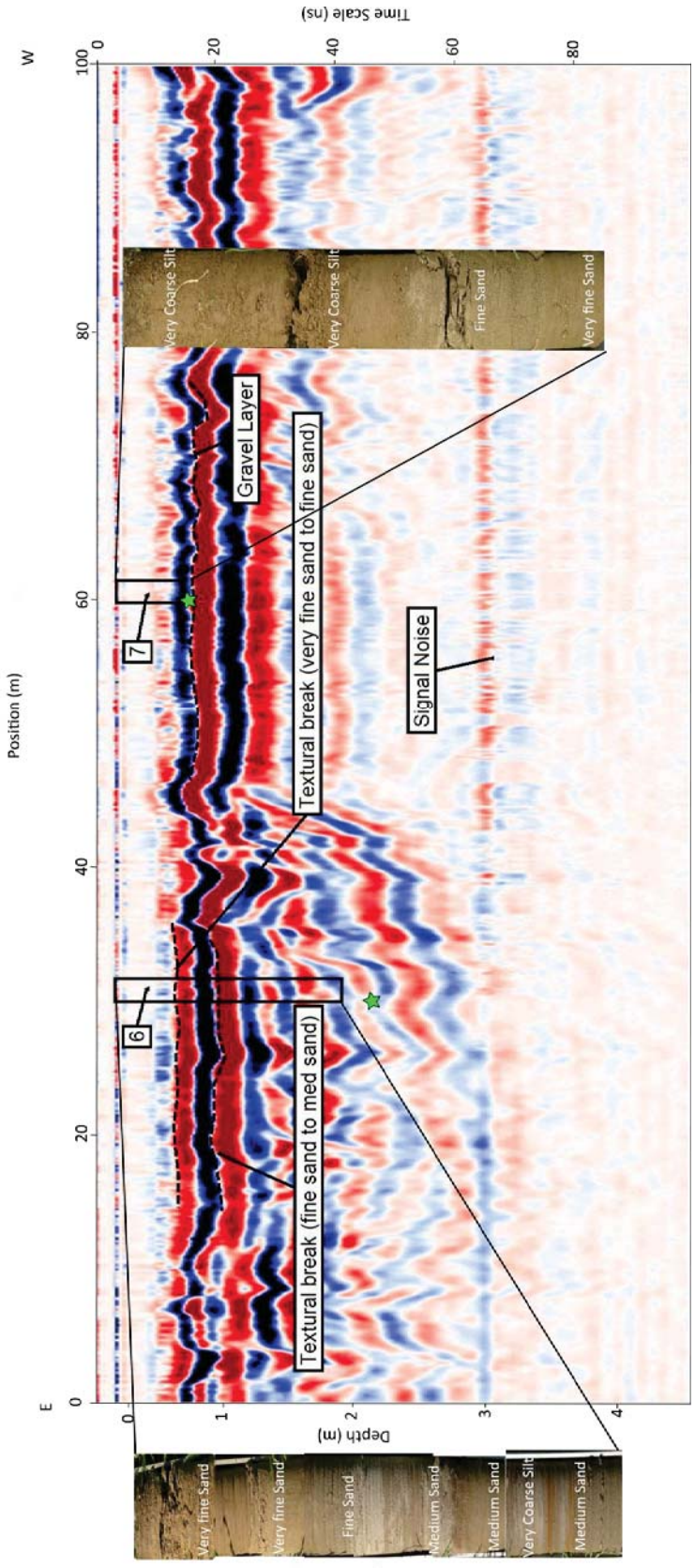

Figure 4.18: Interpreted 200 MHz radargram of the pasture plot Long 12 line, with soil Cores 6 and 7. Depth to gravel (green stars).

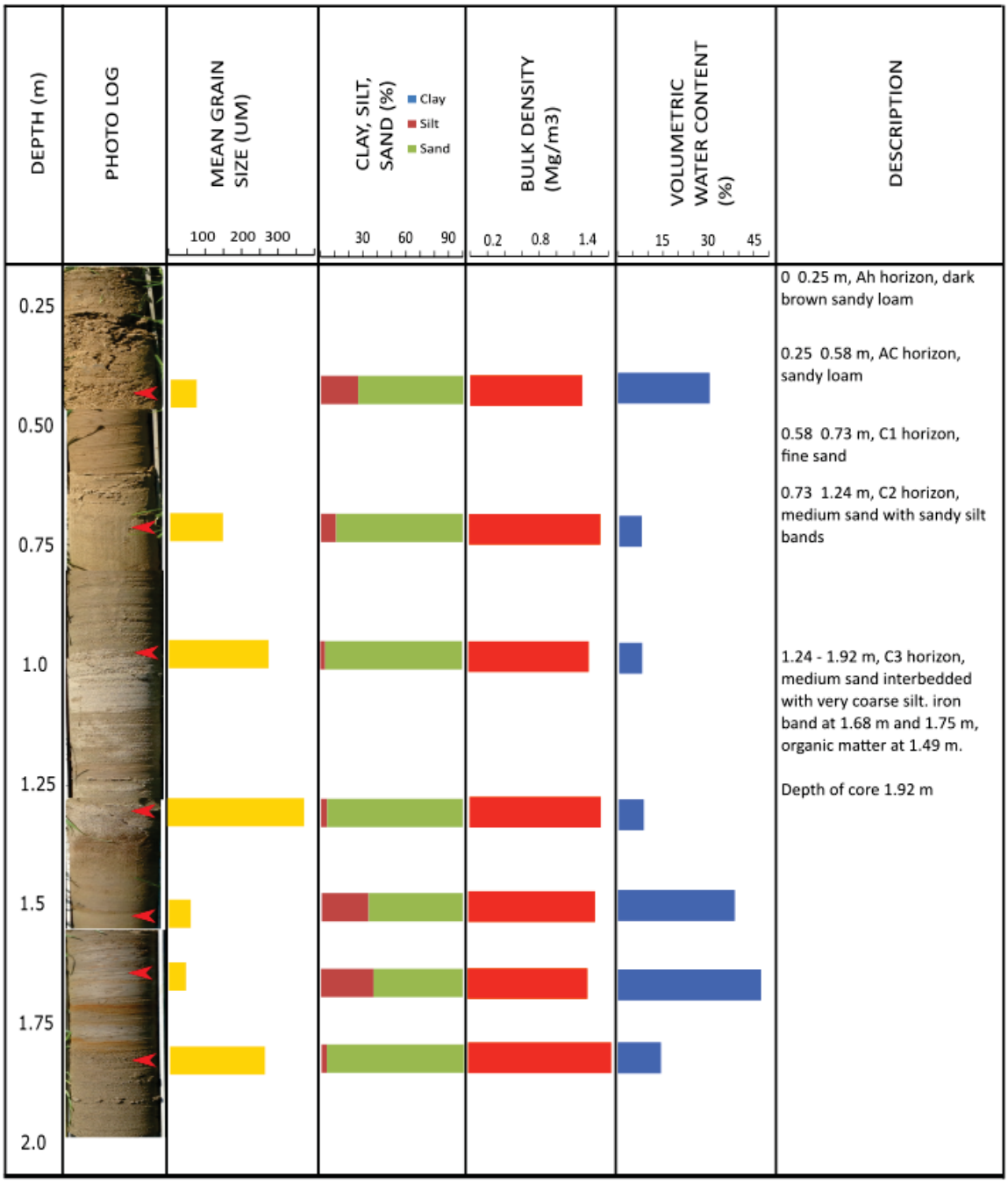

Figure 4.19: Core 6 showing interbedded layers of sands and silts throughout the C horizon.

The radar record located along the Short 36 line of the pasture plot (Fig 4.20) consists mainly of parallel to wavy reflection configurations and is interpreted as silt to fine sand laminated banding (Fig 4.13). The two sample Cores 10 (Fig 4.21) and 11 (Fig 4.22) confirm that the materials located to approx. 0.5 m depth are very coarse silt overlain with very fine sand. Core samples also identified interbedded silt and sand layering. However, these finer features were not identified on the

radargram as these were suppressed by the signal strength. The gravel layer of this radargram has been identified at the base of the three bands tracking upwards from south to north below Core 10 where the signal drastically attenuates.

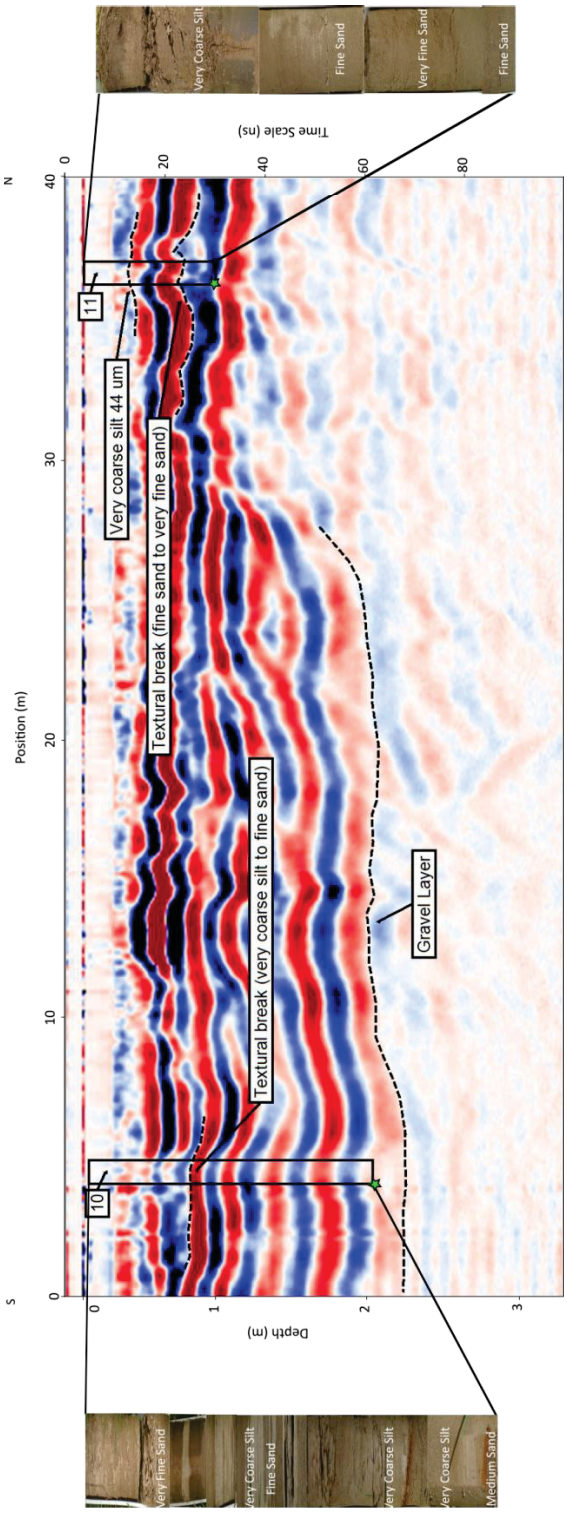

Figure 4.20: Interpreted 200 MHz radargram of the pasture plot Short 36 line. Soil Cores 10 and 11 refer to positions A and B respectively. Depth to gravel (green stars) (Velocity adjusted to 0.065 m/ns).

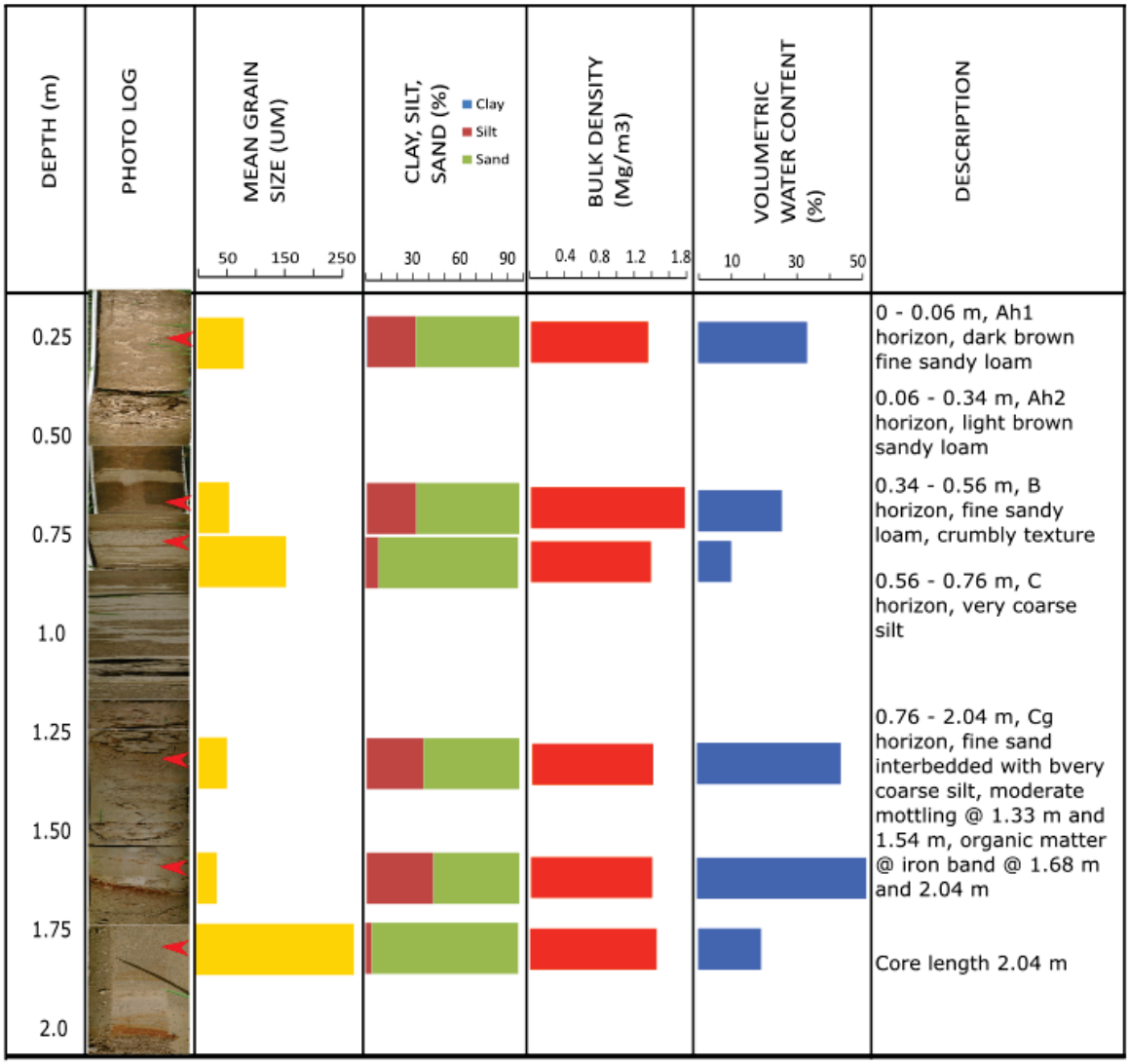

Figure 4.21: Core 10 of the pasture plot showing very coarse silt from 1.39 m to 1.67 m depth overlying medium sand at 1.81 m depth.

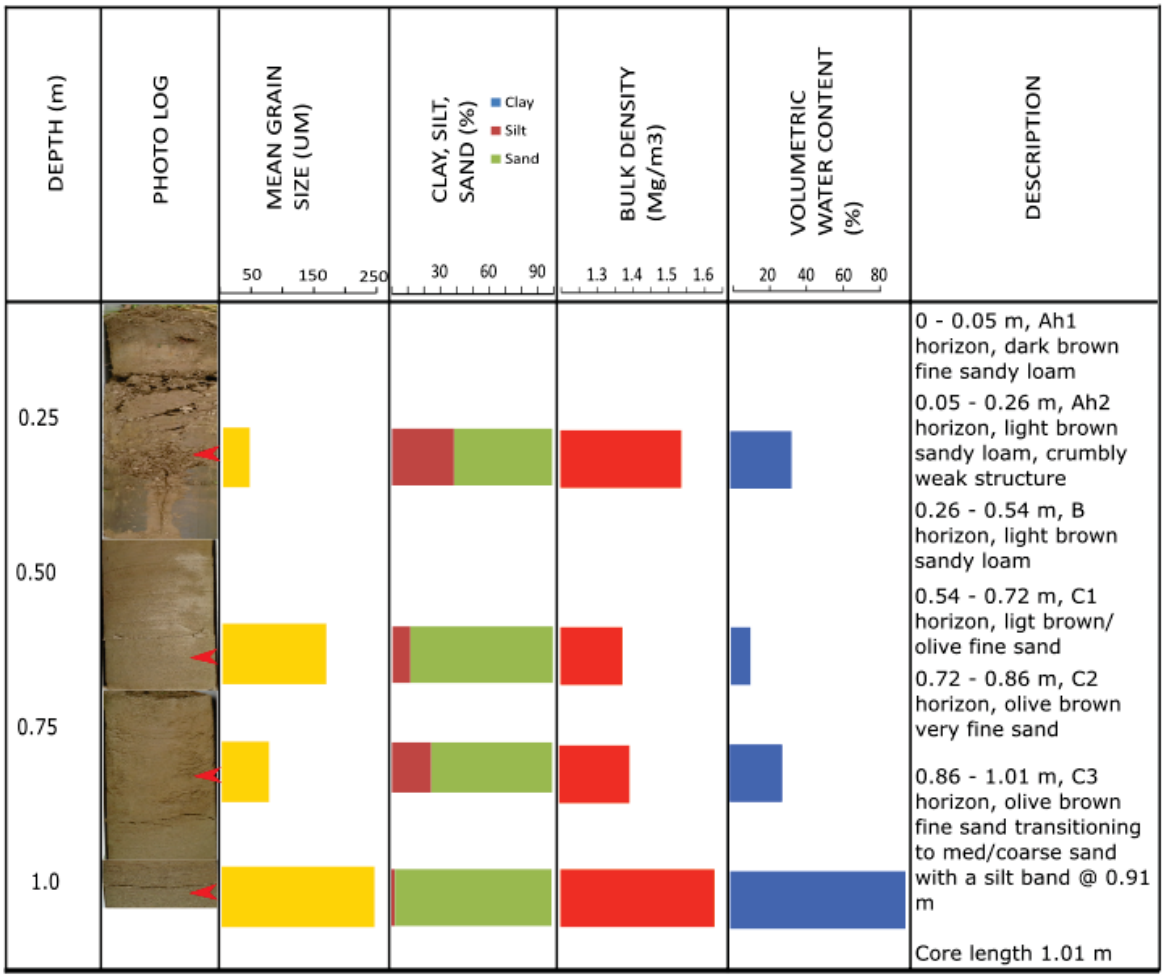

Figure 4.22: Core 11 of the pasture plot showing very fine sand at 0.78 m depth.

The radar record located along the pasture plot Short 92 line (Fig 4.23) shows strong parallel reflectors up to 20 m from the southern end along this line. These are interpreted as fine sand bands and correlate well with core 12 (Fig 4.24). Less than 20 m from the northern end of this line, the reflection configuration changes to a more wavy and hummocky pattern (Fig 4.13). These features correlate well with the bottom of core 13 (Fig 4.25) where very coarse silt is located.

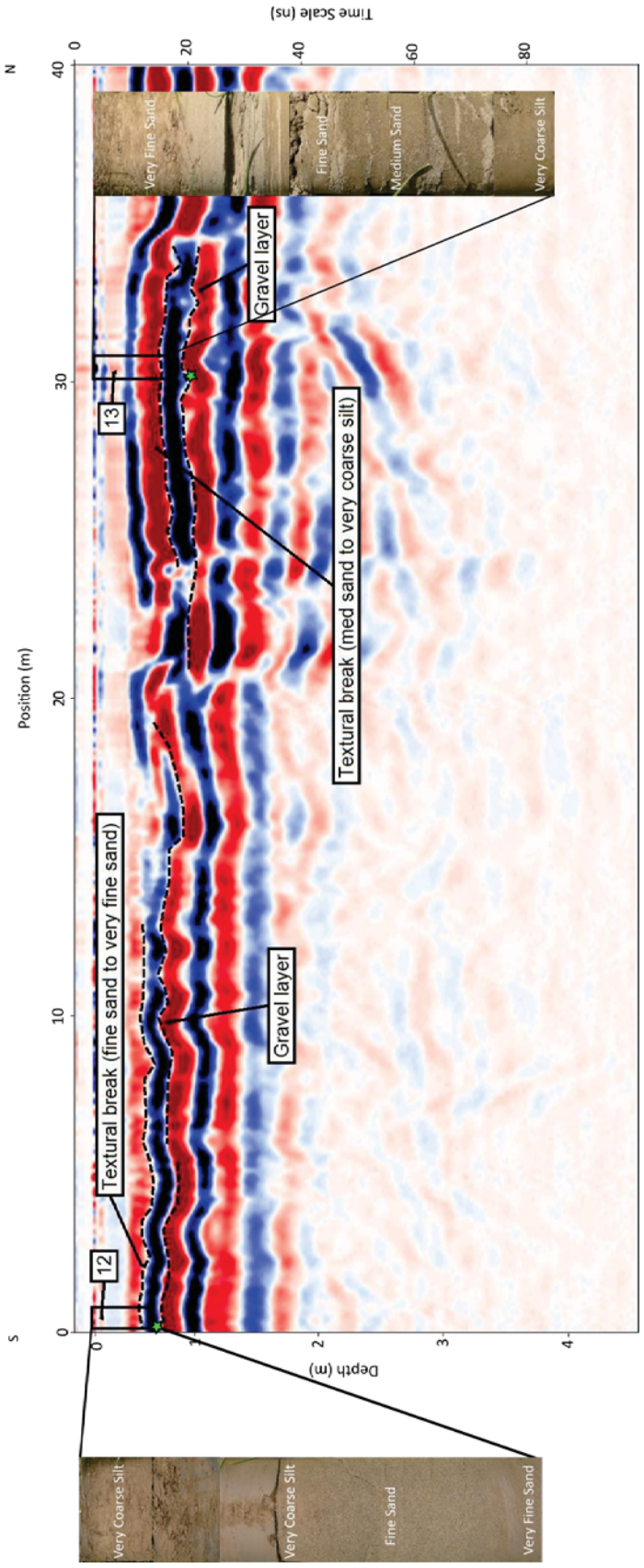

Figure 4.23: Interpreted 200 MHz radargram of the pasture plot Short 92 line. Soil cores 12 and 13 refer to positions A and B respectively. Depth to gravel (green stars).

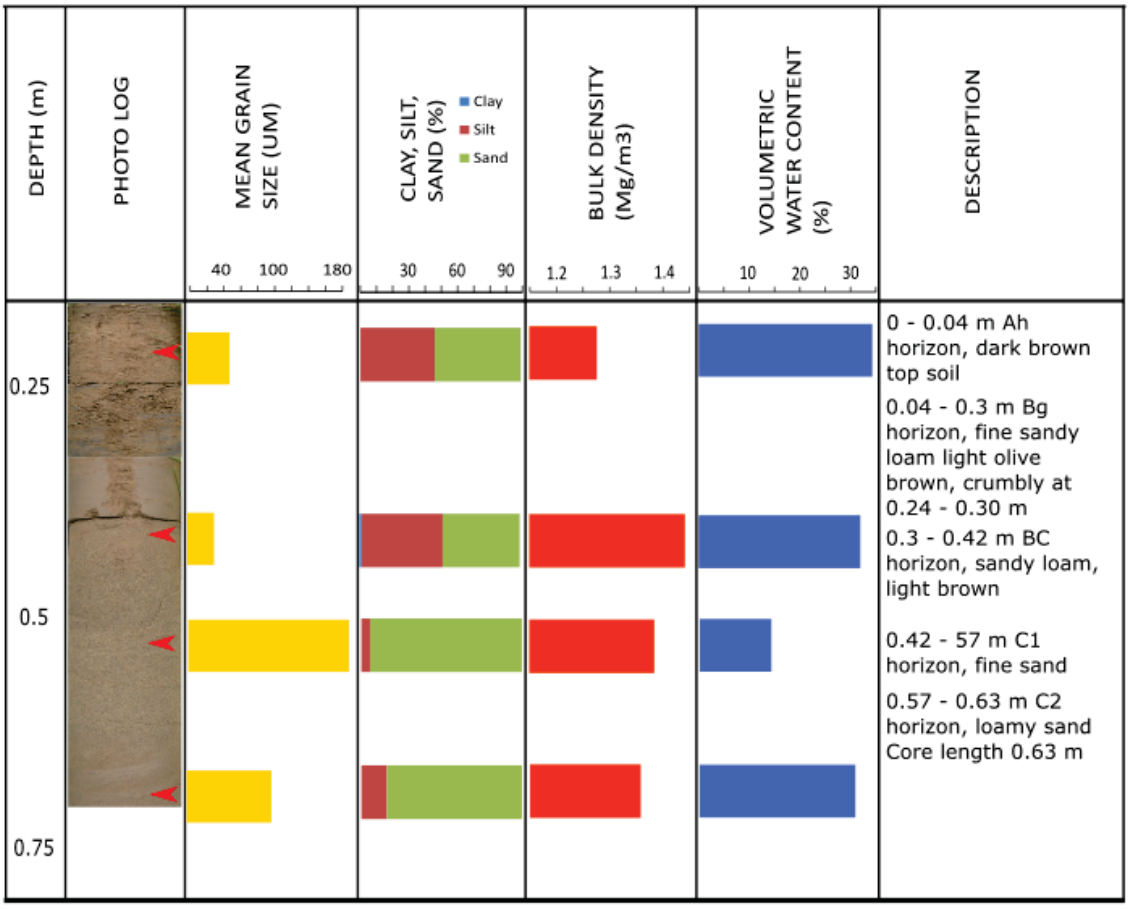

Figure 4.24: Core 12 of the pasture plot highlighting the change between fine sand at 0.56 m to very fine sand at 0.63 m depth. This fine sand layer is represented in the Short 92 radargram (Fig 4.23).

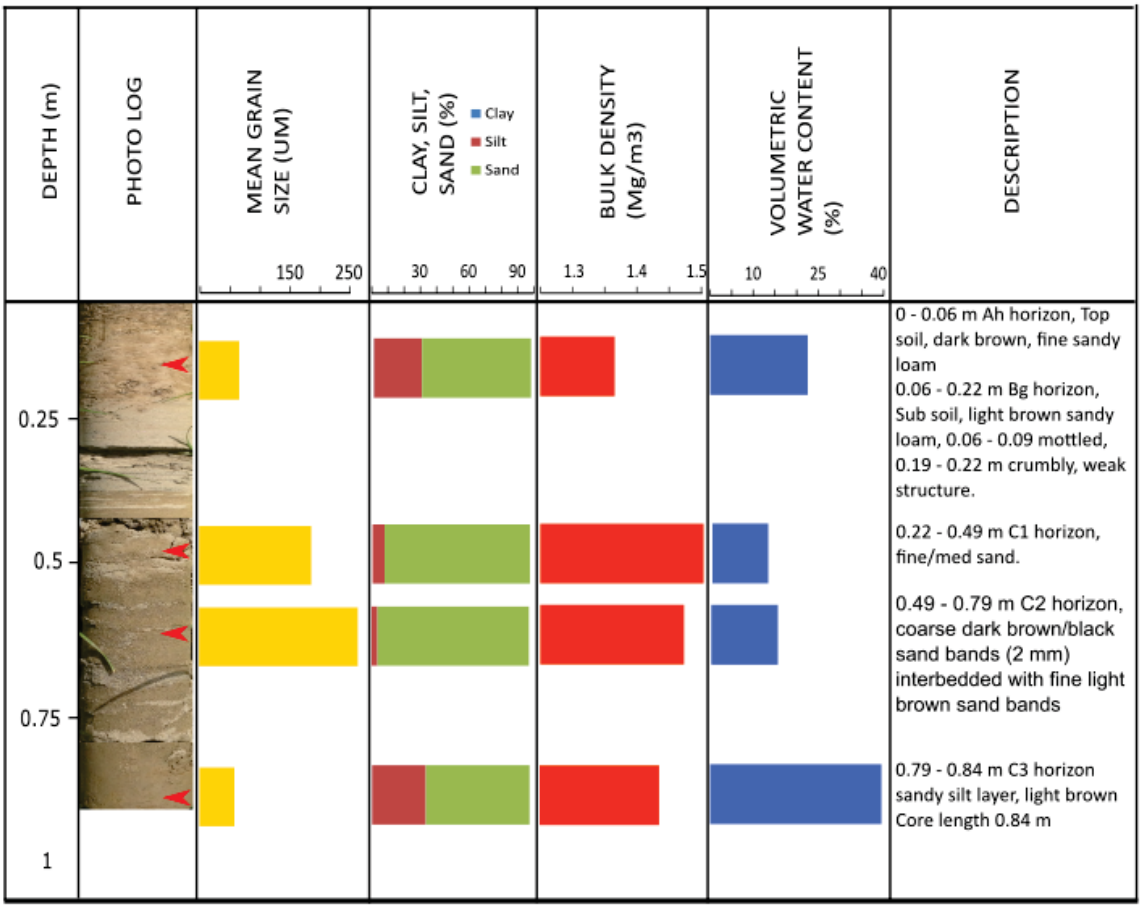

Figure 4.25: Core 13 of the pasture plot showing the very coarse silt layer at 0.84 m depth.

4.2.3 Bulk Density

Finding a relationship between bulk density and individual radargrams was inconclusive. For example, the cores located along the Short 50 line (Fig 4.26) had the highest bulk density values located in the C horizon of each core and the lowest bulk density values located in the A horizon of Core 2 (Fig 4.4) and 3 (Fig 4.17) and at the top of the C horizon for Core 1 (Fig 4.7). No significant features were identified where bulk density was at its highest or lowest along this line. A clear visual difference would be seen (i.e. strong reflective configuration) where bulk density increased (Raper et al., 1990); it is likely that the bulk density variations at the study site are too minor to produce major radar reflectors. However, within the Short 36 line of the pasture plot (Fig 4.27) strong reflectors are obvious in three of the four bulk density readings, but is not possible to assess whether these reflectors arise primarily from a change in bulk density, soil moisture, or grain size (which are

all related properties); volumetric water content and grain size both vary dramatically from 1.67 m to 1.81 m depth in Core 11 (Fig 4.22), additionally sand grain size differs in Core 10 (Fig 4.21) from 0.78 m to 1.01 m depth.

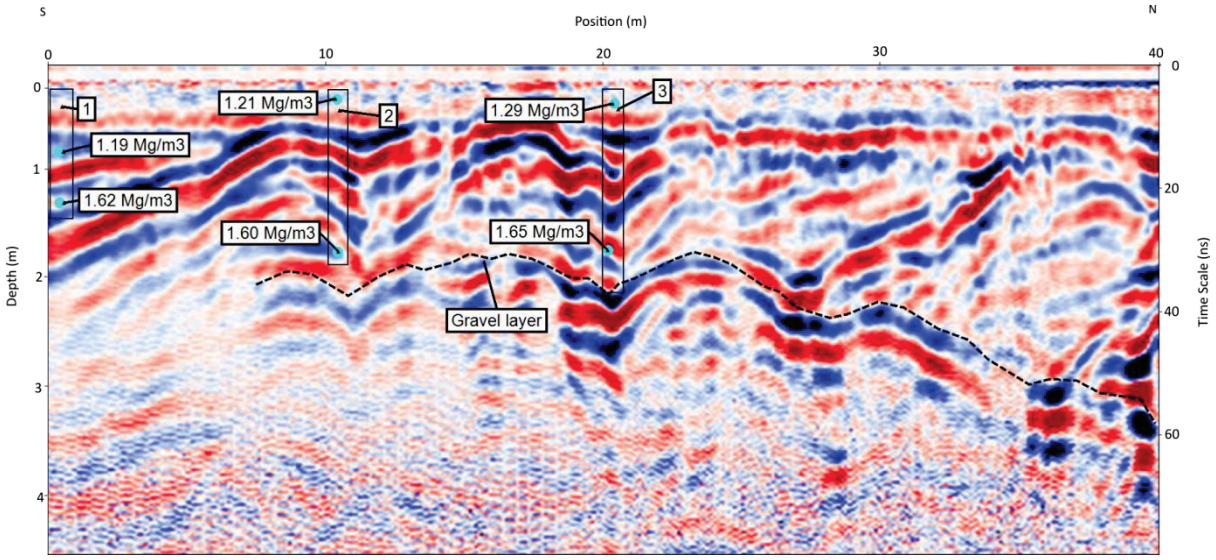

Figure 4.26: A 200 MHz radargram of the Short 50 line from the arable plot showing the location of the highest and lowest bulk density values per core with no significant features reflecting these values.

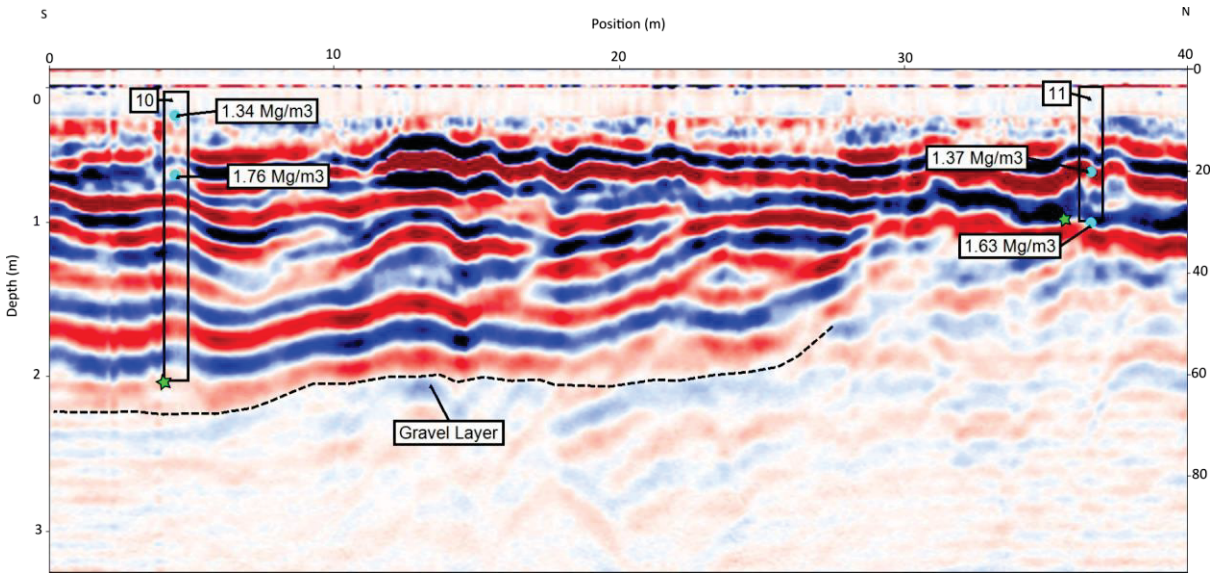

Figure 4.27: A 200 MHz radargram of the Short 36 line from the pasture plot (velocity adjusted to 0.065 m/ns). Augered gravel depth = green stars.

4.2.4 Depth to Gravel

Radargrams from the arable plot generally correlated well with the ground-truthed measurements of augered gravel depths (e.g. Short 50, Fig 4.16) where depth to gravel was identified as a three band layer. However, gravel features in the pasture plot were not as obvious (e.g. Short 92, Fig 4.23; Long 12, Fig 4.18). Although there are some reflections, a distinguished three band feature is not seen across the majority of the radargrams. Other subsurface features, such as finer silt layers or a thick sand band may impact on the identification of a defined gravel layer.

4.3 The Relationship of Hydrological Features to Radargrams

4.3.1 Soil Moisture

The Short 14 radargram of the pasture plot as shown in Figure 4.28 displays significant changes to reflection configurations. The southern end of this line shows chaotic reflections (Fig 4.13) that are interpreted as interbedded fine sands and coarse silts (Fig 4.13 and Core 8) then progresses to a more simple pattern (Fig 4.13) 20 m from the northern end. The reflection configurations become wavy and are interpreted as interbedded sand layers (Fig 4.13). This is also reflected in Core 9 (Fig 4.2) where fine sand overlays medium sand. An obvious wetting front was also detected in this core. This could be represented by the strong triple bands in the radargram at 1.95 m depth.

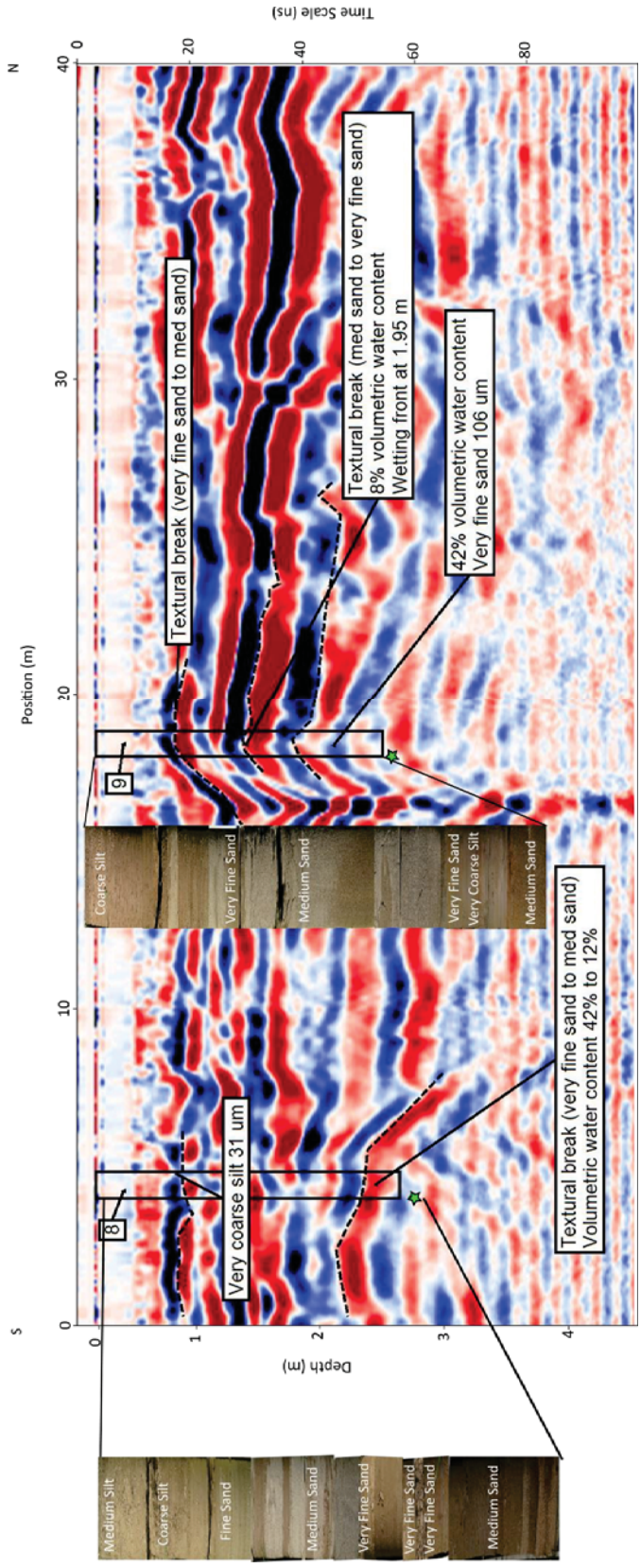

Figure 4.28: Interpreted 200 MHz radargram of the pasture plot Short 14 line showing soil Cores 8 and 9. Depth to gravel (green stars).

A sharp change in volumetric water content is seen in Core 9 (Fig 4.2) between 1.29 m and 2.11 m depth; water content varies from 8% to 42% respectively. This could be representative of the wetting front seen in Figure 4.28. Another example of reflective configurations that could be indicative of increased soil moisture includes the Short 92 line radargram (Fig 4.23). Within Core 12 (Fig 4.24), the volumetric water content changes from 14% to 31% from 0.56 m to 0.63 m depth respectively. This is representative of a change in grain size as indicated in the radargram. Core 13 (Fig 4.25) has a very coarse silt layer at 0.84 m depth as shown in the radargram of Figure 4.23. This also reflects a volumetric water content of 42%.

Radargrams collected at the pasture plot using the 200 MHz antennas were investigated to identify any effect of a change in soil moisture between spring and summer (i.e. September 2015 to February 2016). For comparison purposes all of the radargrams used in this particular analysis had the same gain applied, irrespective if they were from the September of February surveys. Velocity was set at 0.09 m/ns, to allow any changes in soil moisture levels to be shown by differences in the depth and shape of common reflectors and diffractions found in each survey. The comparison between the wet spring conditions and the drier summer conditions shows that the velocity of the radar waves travelling through the soils became faster during the drier summer conditions. For example, in the Short 36 line radargram, the reflection configurations seen at 2 m depth in September appear about 0.5 m shallower in the February surveys, interpreted to be because the velocity of the radar waves travelling through the drier soil are faster, causing the depth scale in the February radargram to contract (Fig 4.29).

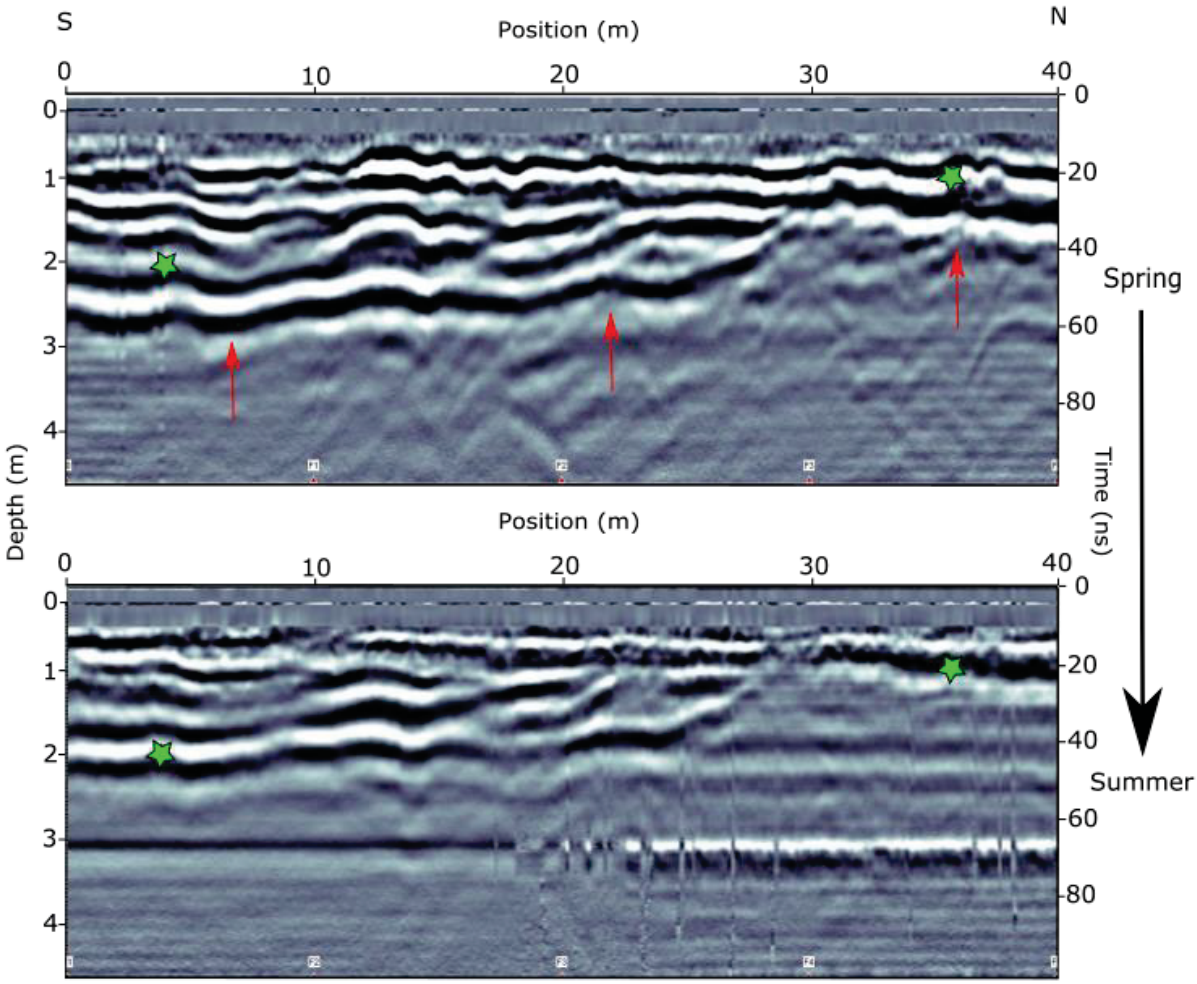

Figure 4.29: Comparison of the 200 MHz surveys conducted in September 2015 (top radargram) and February 2016 (lower radargram) at the pasture plot of the Short 36 line.

The radargrams of the Short 14 line (Fig 4.30) show a change in the shape of diffraction hyperbolas between spring and summer. The shape of a diffraction hyperbola (i.e. a diffraction pattern produced by a buried object, such as a tree or burrow) is a function of its depth and the average velocity of the materials above it. The hyperbolas seen at the 5 m position in Figure 4.30 are wider in the summer radargram, indicating a faster velocity, as a result of the soils having become drier.

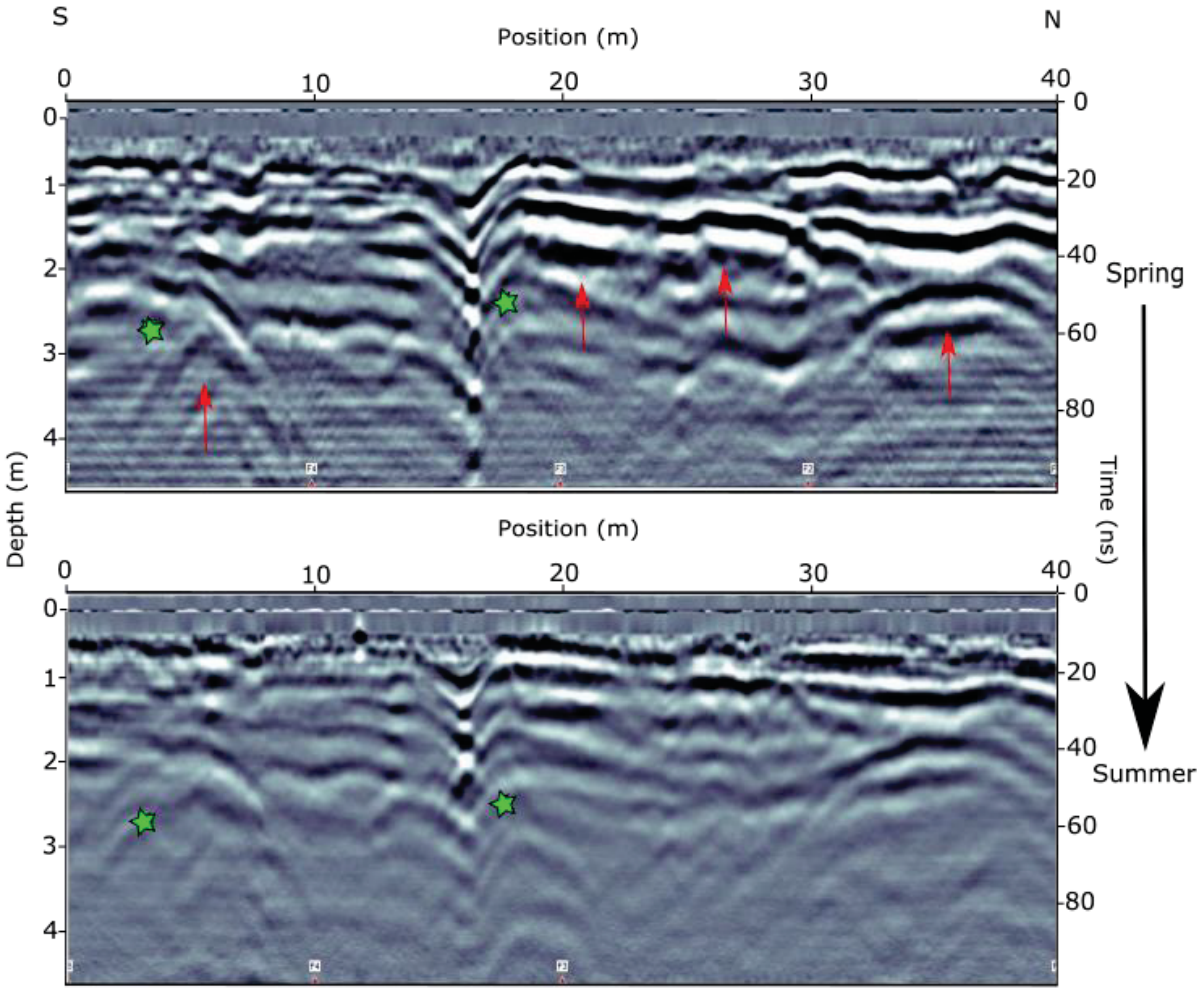

Figure 4.30: The Short 14 line showing a comparison of the 200 MHz surveys conducted in spring, September 2015 (top radargram) and summer, February 2016 (lower radargram) at the pasture plot. Red arrows indicate the greatest response seen between the spring and summer radargrams. The first arrow on the left indicates a narrower hyperbole in the spring radargram compared to the summer radargram, indicating a quickening velocity from wet to drier conditions.

The Short 92 line (Fig 4.31) shows a definite reduction in signal strength when soils are drier in summer. The hyperbolas have again widened and have become more noticeable between the 20 – 30 m positions during summer (lower image in Fig 4.31). Although signal strength has decreased in the lower radargram, between the 20 – 30 m position there is still obvious signal strength, possibly indicative of a higher soil moisture level. The banding at 3 m depth in the lower radargram is electronic noise produced from the radar antennas (Beres & Haeni, 1991).

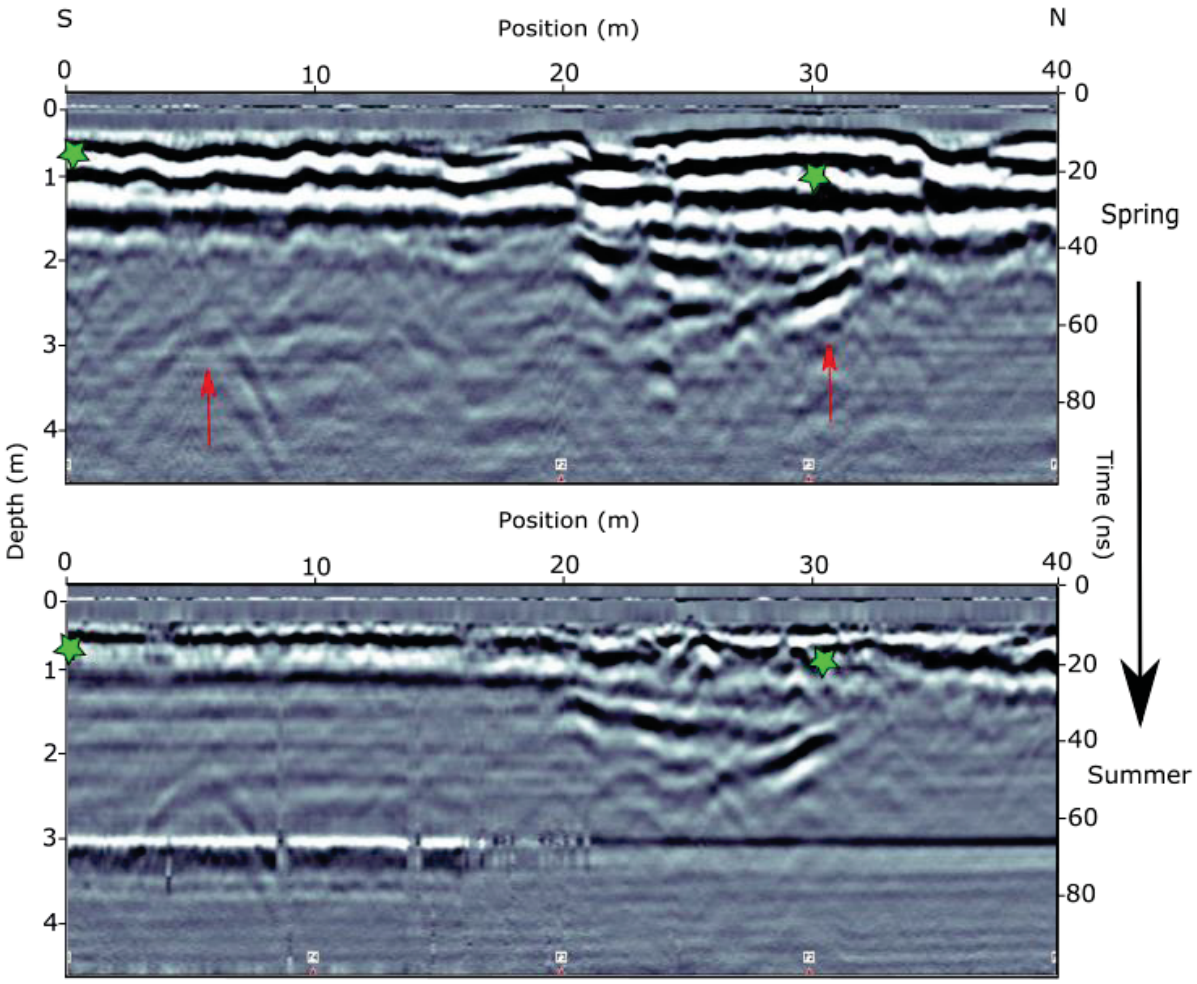

Figure 4.31: Comparison of the 200 MHz surveys conducted in September 2015 (top radargram) and February 2016 (lower radargram) at the pasture plot of the Short 92 line.

The two radargrams of the Long 12 line (Fig 4.32) located at the pasture plot show a good example of an overall change in soil moisture from spring to summer. This is indicated by the widening of the hyperbolas located at the 83 m position and the change in depth of the overall reflection configurations of the lower radargram. However, soil moisture is possibly still being held within the first 40 m of eastern side of this line as reflectors in the lower radargram are still quite prominent. This could relate to the fine silt layers having a higher water holding capacity throughout this zone. Again, electronic noise is showing up at 3 m depth.

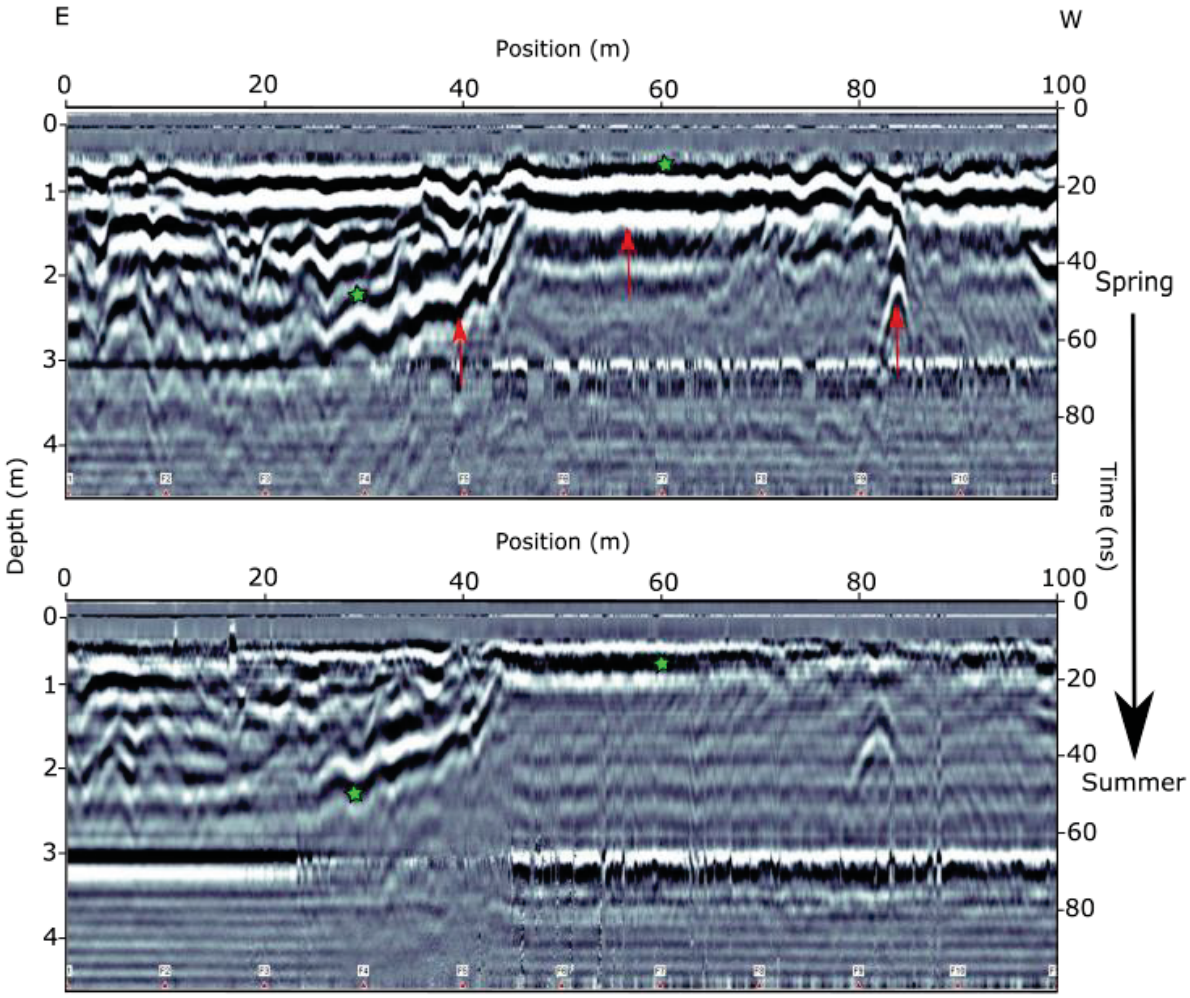

Figure 4.32: Comparison of the 200 MHz surveys conducted in September 2015 (top radargram) and February 2016 (lower radargram) at the pasture plot of the Long 12 line.

Identification of high amplitude reflectors were viewed in Slice View mode. Slice View creates GPR depth slices of grid data. Using systematic grid data, images at multiple depths are generated. This allows a birds-eye view of reflectors at varying depths throughout the subsurface. An array of high amplitude reflections are seen across the pasture plot at 0.78 m, 1.30 m and 1.56 m depth (Fig 4.33). Strong reflectors are seen approx. 30 – 45 m diagonally across the plot in September 2015. These are most noticeable at 1.30 m and 1.56 m depth (Fig 4.33). This diagonal feature forms the boundary of the infilled channel. The strong reflectors from the infilled channel location towards the western side of the plot are indicative of the initial gravel layer at approx. 0.78 m depth. However, strong reflections are also noted 20 – 40 m along the plot approx. at the Long 12 line. Comparing this area to

the Long 12 line radargram (Fig 4.18), this is evident of a fine sand layer deposited above a medium sand layer. However, this may not be the only reason why there is a strong reflector at this site. Soil moisture changes dramatically from 30% to 7% between 0.45 m to 0.70 m depth respectively and could be the reason for this strong reflection.

Velocity was adjusted from 0.09m/ns to 0.1 m/ns for the February Slice View image. This allows for an approximate comparison of the same reflectors. The Slice View images of the 200 MHz survey conducted in February 2016 highlights the lessening of signal strength as soil moisture has decreased. Gravel depth is still identified from 45 m – 100 m along the length of the plot at 0.78 m depth. At depths of 1.30 m and 1.56 m soil moisture is evident along the infilled channel bank located diagonally 45 m along the length of the plot. As previously indicated, soils within this area are finer sands and silts that are able to hold a greater amount of moisture than the sands and gravels located from 45 m to 100 m along the length of the plot.

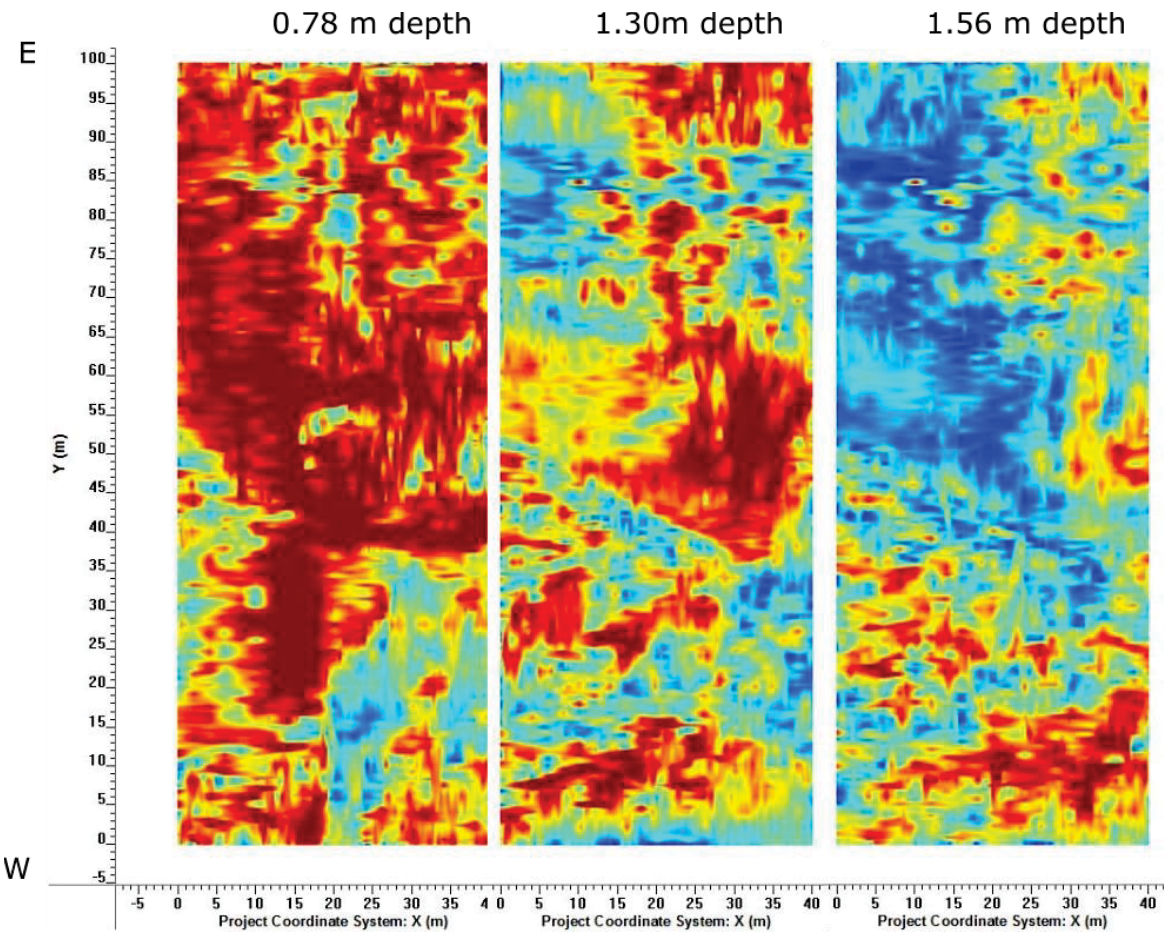

Figure 4.33: 200 MHz Slice View of the pasture plot taken in September 2015 (Velocity 0.09 m/ns). Three depths are shown for comparison with radargrams. Increased signal strength is shown in red and attenuated signal in deep blue.

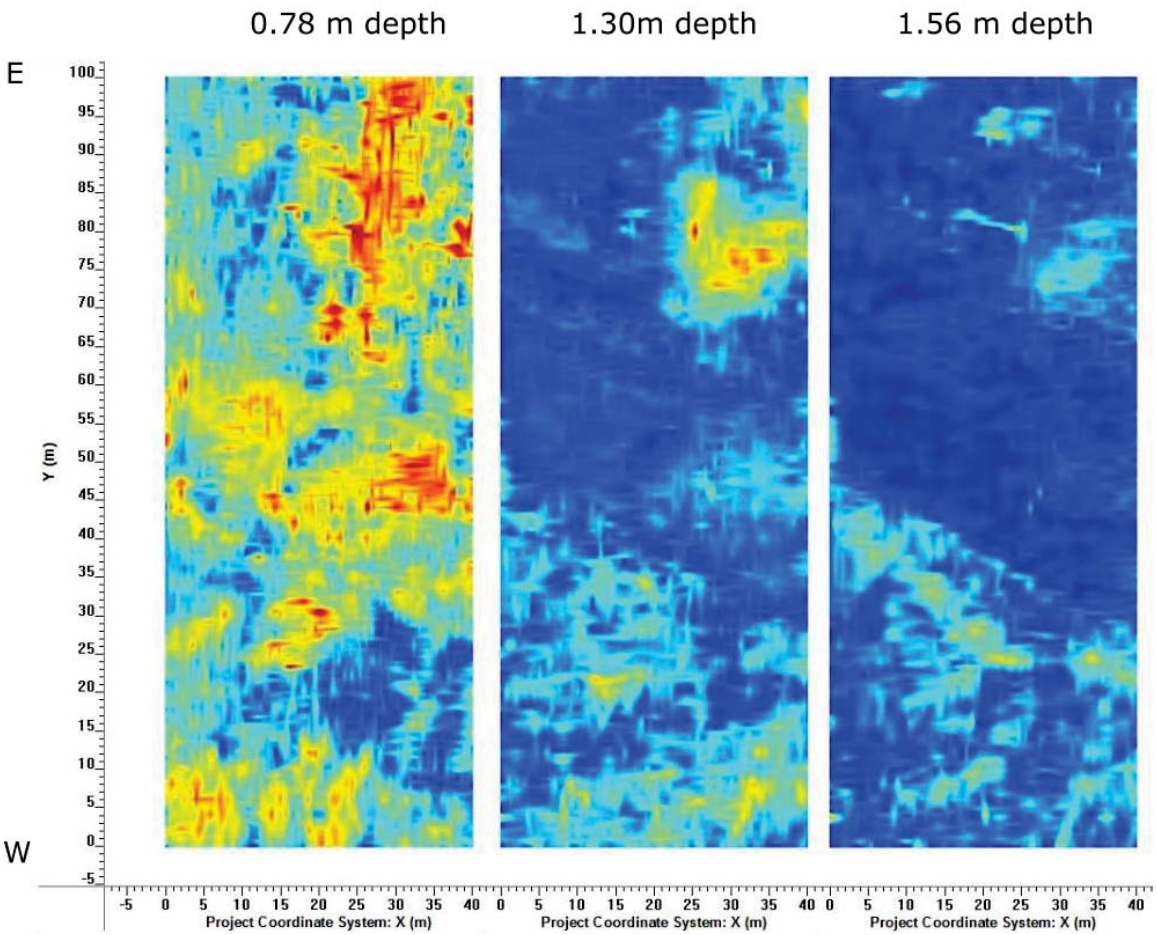

Figure 4.34: 200 MHz Slice View during February 2016 of the pasture plot showing a decrease in signal strength compared to the September 2015 images in Figure 4.33. Velocity has been adjusted to 0.1m/ns.

4.3.2 Depth to Groundwater

To identify features (e.g. water table) at depths beyond the top of the gravels, the 100 MHz antennas were deployed over the pasture plot. The longer wavelength allowed a deeper penetration of the subsurface to depths up to 182 ns (two-way travel time) or ~9.6 m (v= 0.09 m/ns). Soil moisture had decreased from the September to February surveys. This caused the radar waves to travel at a faster velocity through the subsurface in February. Thus velocity for the February survey was adjusted to 0.1 m/ns, to provide a better depth profile for analysis of reflection configurations. A radargram of the pasture plot Long 12 line (Fig 4.35) has detected the water table at 5 m depth. This is indicated by the three bar parallel lines and has been correlated with the piezometer measurements taken in conjunction with the

February surveys (Table 4.4). The contrasting boundary between the saturated and unsaturated zone at the interpreted water table depth causes diffraction hyperboles to form at this boundary.

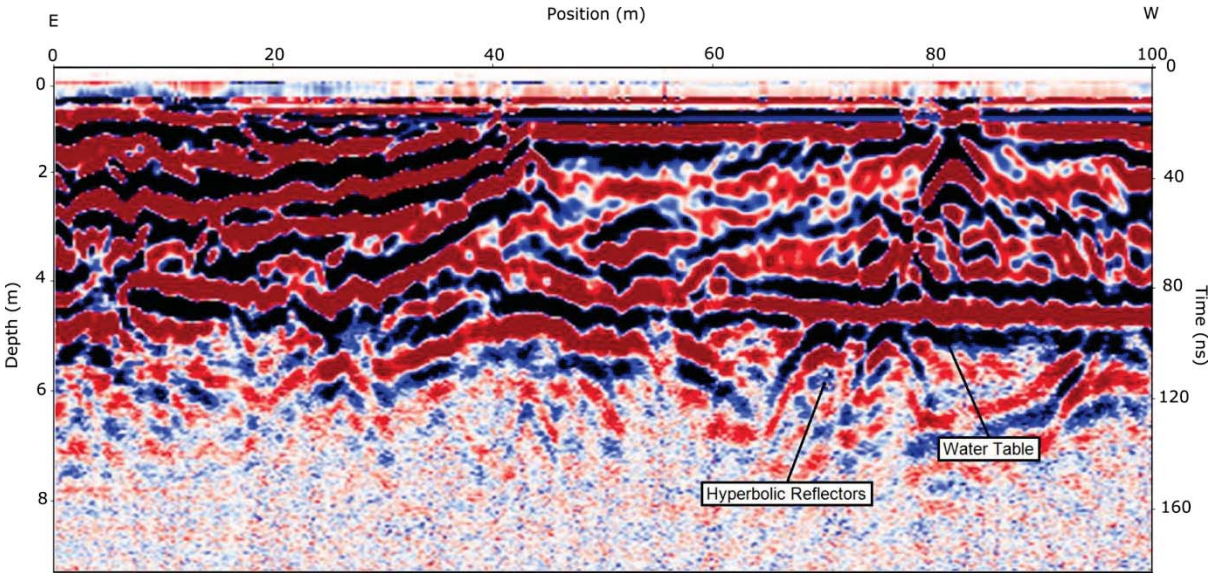

Figure 4.35: Interpretation of the 100 MHz survey of the pasture plot Long 12 line showing the groundwater reflector and hyperbolic reflectors.

A 100 MHz radargram of the Short 14 line is shown in Figure 4.36. Reflection-free patterns (Fig 4.13) are evident from approx. 5 m depth. This is indicative of the groundwater level during February 2016, with the radar signal being strongly attenuated below the water table. Above this is a transition zone where partially saturated to saturated material exists. The thickness of this zone relies on the pore size of the material. A thicker transition zone relates to an area where finer textured soil is present (Doolittle et al., 2006). Although this transition zone is below the gravel surface, fine sands and silts could be present within this area affecting capillarity. This transition zone causes a lower amplitude reflection to be recorded at the water table. Hence there is no definitive band like that in Figure 4.35 at water table depth. Hyperbolas found within this layer are indicative of large gravel fractions (Fig 4.13). The top two metres shows a section of hummocky configurations, these are indicative of sand and gravel fractions (Fig 4.13).

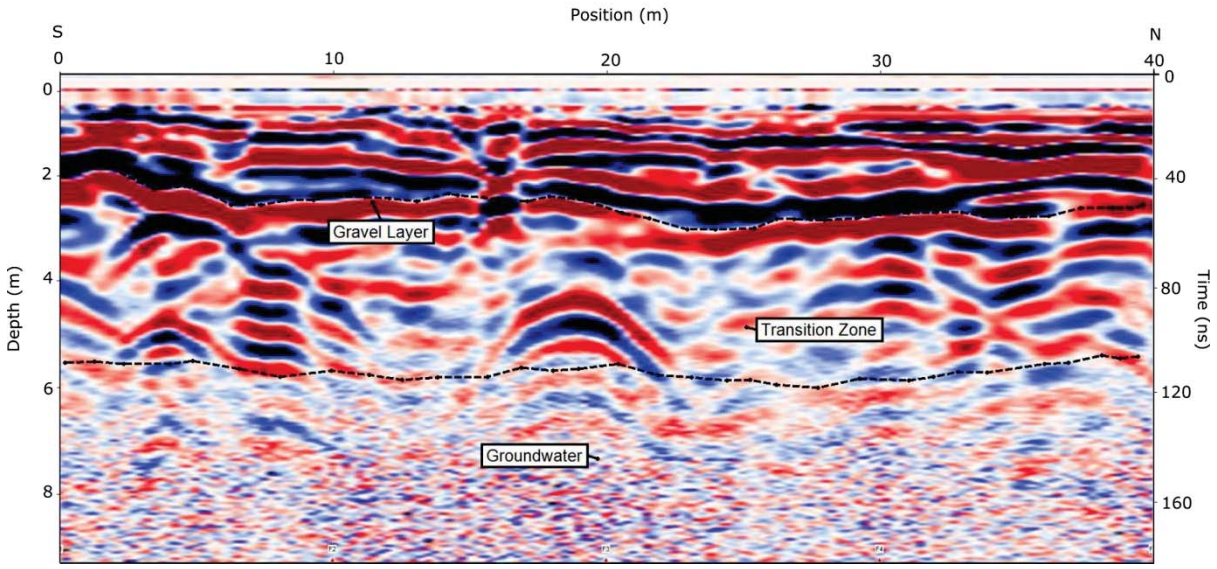

Figure 4.36: Interpretation of the 100 MHz survey of the pasture plot Short 14 m line. A transitional zone between the gravel surface and water table is represented by a slightly attenuated signal.

Subsurface slice views of the pasture plot in February 2016 using the 100 MHz antennas allowed for interpretation of depth to groundwater across the plot. Piezometer measurements indicated depth to groundwater at 5 m during GPR surveying (Table 4.4). Figure 4.37 shows the change in signal strength from 4.5 m depth to 6 m depth. The change in signal strength between these depths gives an indication into the spatial change in groundwater depth across the pasture plot during February 2016. As radar waves penetrate groundwater, the signal begins to attenuate.

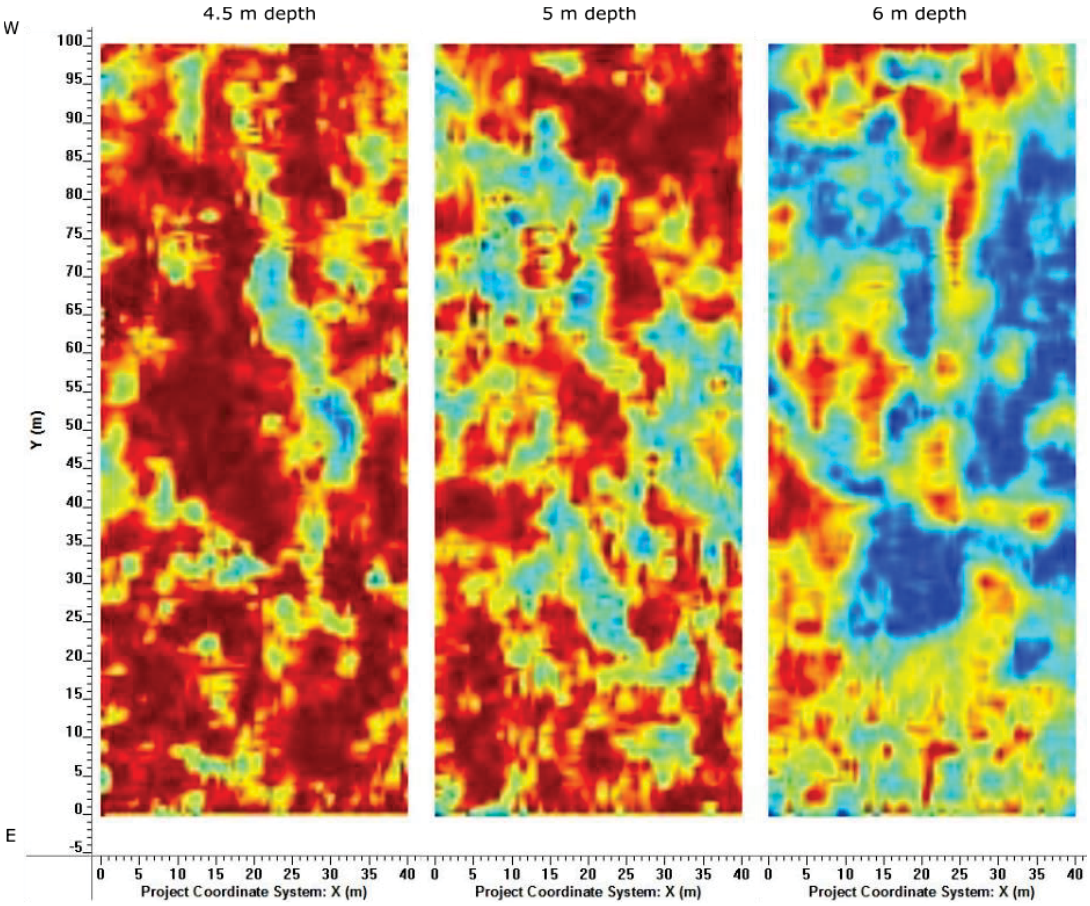

Figure 4.37: 100 MHz Slice View images of the pasture plot in February 2016. Three depths are shown for comparison with radargrams. Increased signal strength is shown in red and attenuated signal in deep blue.

4.4 Surface and Subsurface Contour and Soil Thickness

To capture the spatial variation of surface elevation and the depth to the gravel surface, geographic coordinate points including elevation, were used to produce raster's using a Natural Neighbour interpolation method (image A and B of Fig 4.38 and Fig 4.39) in ArcMap 10. By subtracting the elevation of the gravel layer from the ground surface elevation using Raster Math, a soil thickness raster was created (image C of Fig 4.38 and Fig 4.39). Visual representation of the arable ground surface shows a variation in topography from 26.7 m to 25.2 m ASL (Fig 4.38, A). The northern side of this plot has the highest elevation and tapers down to the southern and eastern side of the plot. Gravel elevation (i.e. the elevation of the top of the gravel that underlies the fine sediments and soils) varies from 24.6 m to 23 m

ASL (Fig 4.38, B). Unlike the surface contour, gravel contour has the highest elevation points located along the north-western and south-eastern sides of the plot and the lowest elevation points are at the north-eastern and south-western sides of the plot, suggesting that this relates to an infilled pool location. This is further demonstrated within the gravel layer (Fig 4.38, B) at the north-eastern side of the plot. The soil thickness map (Fig 4.38, C), calculated as the difference between the gravel surface elevation and the ground surface elevation, highlights a deeper soil present over the infilled pool at the north-eastern end of the plot.

(A)

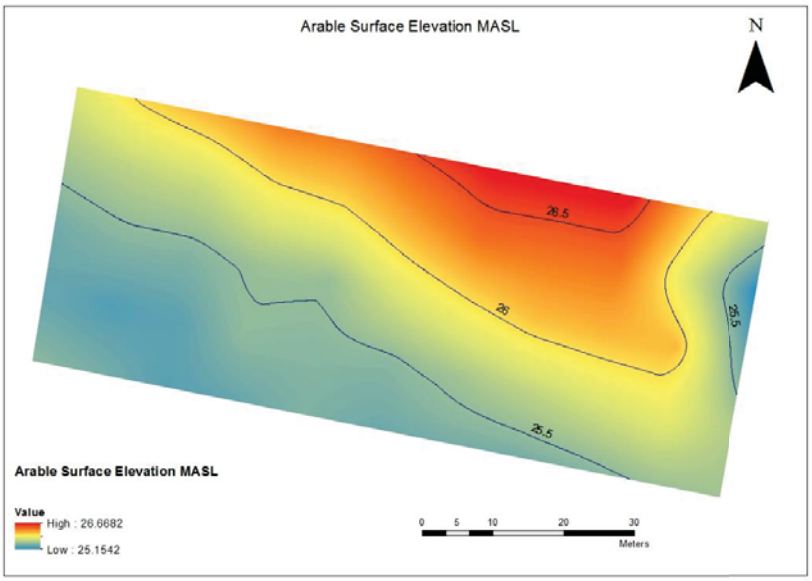

(B)

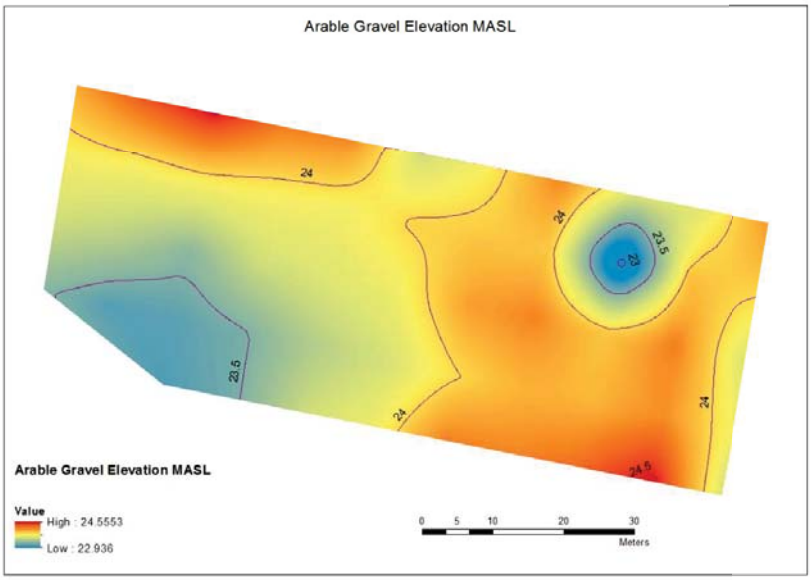

(C)

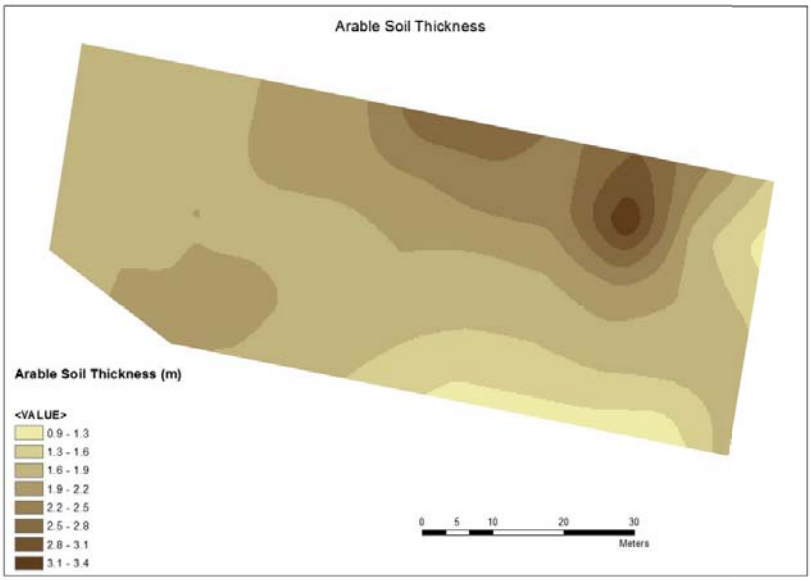

Figure 4.38: Arable surface elevation and contour (A), gravel elevation and contour (B), and soil thickness (C).

Surface elevation, gravel elevation and soil thickness of the pasture plot are represented in Figure 4.39. Surface elevation differs from 24.8 m ASL along the north-western corner to 23.9 m ASL in the south-eastern corner of the plot. Gravel elevation varies from 24.1 m ASL along the western side to 21 m ASL along the eastern side of the plot. Unlike the gravel surface in the arable plot (Fig 4.38, B) the gravel surface of the pasture plot follows a similar contour to the surface contour. Soil thickness (Fig 4.39, C) also follows this layout where the depth of soil differs from 0.6 m to 2.8 m depth. The shallowest soils are located up to approx. 60 m from the western side. Soil depth then dramatically increases towards the eastern end of the plot. This area is representative of the infilled channel identified in the Long 12 (Fig 4.18) radargram.

(A)

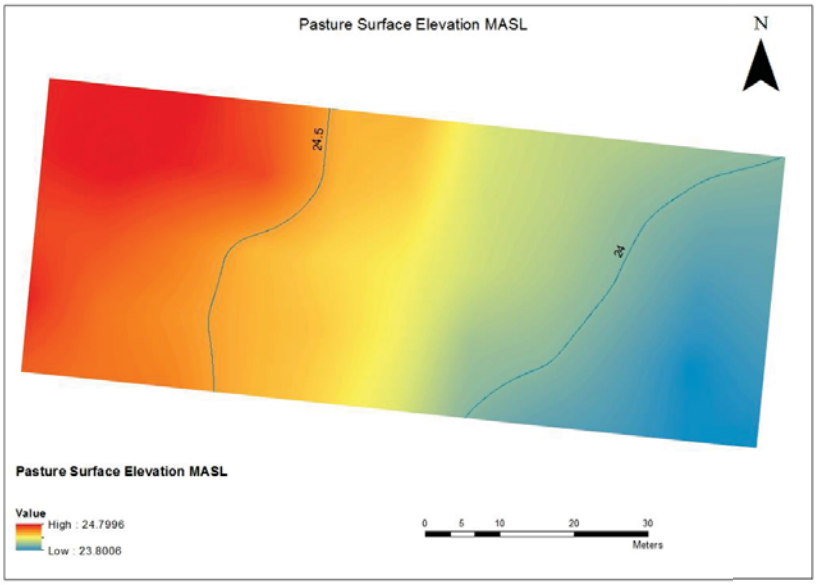

(B)

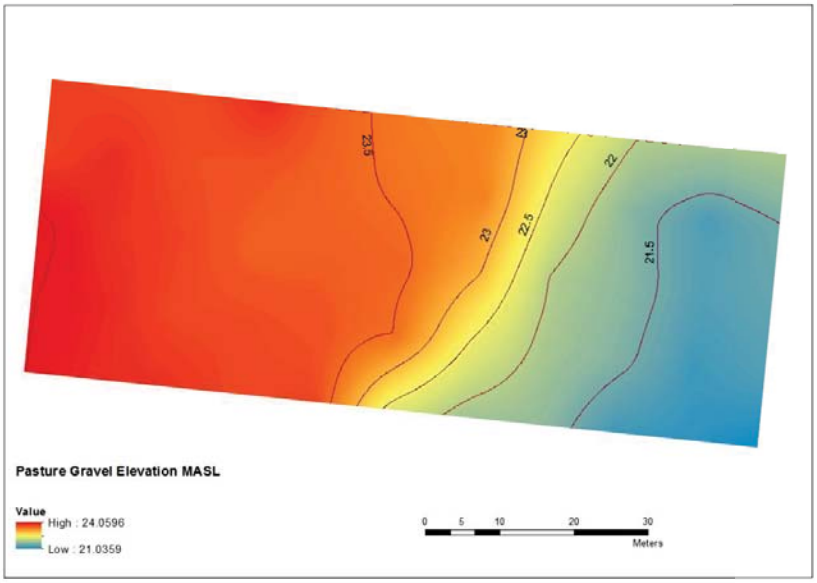

(C)

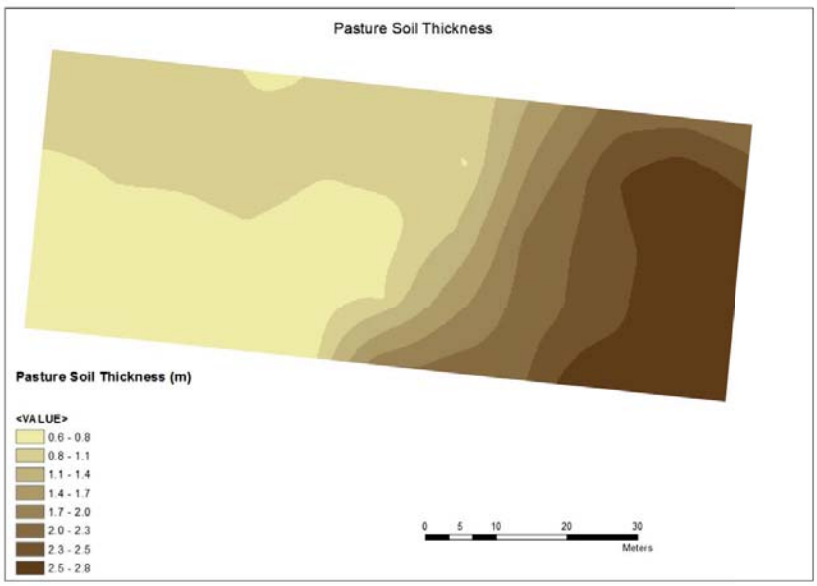

Figure 4.39: Pasture surface elevation and contour (A), gravel elevation and contour (B), and soil thickness (C).

5 Discussion

This study assessed the ability of GPR to identify soil physical and hydrological properties that control water flow pathways in alluvial soils, namely soils of the Rangitikei and Manawatu series. The use of GPR as a tool to identify soil physical features has been used predominantly in the United States in sandy and organic soils and karst landscapes (Beres & Haeni, 1991; Collins et al., 1994; Doolittle et al., 2006; Gish et al., 2002; Kung & Donohue, 1991; Zhang et al., 2014). Thus, the research presented here, extends this previous work by assessing the applicability of GPR for alluvial soils, in New Zealand.

The results from this research indicate that: i) textural and soil moisture changes within an alluvial soil profile can be detected when GPR surveying with 200 MHz unshielded antennas from ~0.5 m to ~3 m depth, allowing for masking of the top ~0.5 m of these radargram images by the ground and air waves, ii) the change in soil moisture from September (spring) to February (summer) can be identified as a change in velocity, iii) identifying features that control flow pathways (i.e. layering inclinations, depth to gravel and water table) can be identified using 100 MHz and 200 MHz antennas where groundwater depth is ~5 m.

These results are discussed below and are compared with previous literature, to explain these observations.

5.1 Identifying Subsurface Materials

Interpretation of radargrams was conducted using reflection configuration analyses and comparing soil core logs with images seen on the radargrams. Simple and complex layered patterns were interpreted as sand and silt layering and chaotic reflections referred to sand and gravel deposits. Hyperbolic reflectors indicated the presence of gravel and boundaries between gravel and the water table. These patterns have been observed by Beres and Haeni (1991).

The ability to ground-truth radargrams with soil cores has shown a correlation between strong radar signals and textural boundaries in the vadose zone (Fig 4.14).

Flow of water through the vadose zone could be significantly influenced by the changes in texture through these alluvial soil profiles irrespective of soil type (i.e. Rangitikei silt loam over sand, Manawatu fine sandy loam, Manawatu silt loam over sand or Manawatu sandy loam) as all four soil types mapped across the study site have shown a change in texture at some point down the profile. Gish (2002) identified areas of strong dielectric reflections where zones were characterised by increased water holding capacity due to differences in textural breaks (i.e. clay lens under a sandy soil). These preliminary results are encouraging and show that the use of GPR could prove to be a valuable geophysical tool to identify textural boundaries where water flow could be influenced.

The most prominent grain size over the arable and pasture plot was very coarse silt followed by medium sand (Table 5.1). Very coarse silt was generally found in thin layers and incurred some mottling or iron banding, indicating a history of perching of water. Medium sand was the second most prominent grain size and was located throughout the C horizons across both plots. This was also the largest grain size mapped across the study site, located above the underlying gravel surface. In addition to the medium sand fraction, finer sand fractions were also found across these plots (i.e. Fig 4.19).

Table 5.1: Prominence of mean grain size across the study site

Prominence	Grain Size Description	Grain Size (µm)	Location
1	Very Coarse Silt	32 - 60	All Horizons
2	Medium Sand	253 - 473	C Horizon
3	Very Fine Sand	68 - 114	All Horizons
4	Fine Sand	126 - 243	C Horizon
5	Coarse Silt	16 - 26	A Horizon
6	Medium Silt	14	Ah Horizon

Sandy soils have a higher macroporosity than soils with increased silt and clay fractions. This feature leads to an increased risk of bypass flow that increases the risk of nutrients leaving the soil vadose zone and entering water bodies (Journeaux, 2005). These sand layers are located deeper down the profile within the C horizon. Previous technology has limited the ability to identify flow pathways at depth (>2 m depth) (Doolittle & Collins, 1995). However, GPR was able to detect these layers using 200 MHz antennas when ground-truthed with soil cores. Additionally, depth to the water table was detected using the 100 MHz antennas during February (summer) across the pasture plot. Although Doolittle et al. (2006) states that the capillary fringe affects the level at which GPR will detect the water table, this should not affect the overall accuracy as radargram configurations have been ground-truthed with piezometer measurements.

Although the use of 200 MHz antennas proved useful in determining textural changes within the soil profile, and additionally highlighted layering stratigraphy of soils and depth to gravel, finer layering features (i.e. thin silt banding) have been concealed by the strong radar reflectors. The stronger signals identified on a radargram relate to features with a high electrical conductivity. These strong signals then conceal other finer features (Fig 4.14) (Doolittle et al., 2006; Shih & Doolittle, 1984). Shifting to a higher frequency with a narrower bandwidth (e.g. >300MHz), waiting for drier soil conditions, or processing the signal through higher filtration settings in post processing could eliminate this noise (Doolittle et al., 2006; Shih & Doolittle, 1984). These finer features could form important zones of water flow pathways. The use of 200 MHz antennas has proven they can be easily overlooked. This is not to disregard using the 200 MHz antennas altogether, but to include another higher frequency antennas (i.e. >300MHz) could prove useful to decrease signal noise and improve signal resolution when identifying these finer features in the shallow subsurface. The use of shielded antennas would also help to image structures in the top few decimetres of the soil profile, by removing the major intrusion of the air waves.

Alluvial soil can differ dramatically in depth and soil profile layering, as outlined from the differences in the soils across the arable and pasture plots used in this research. GPR was able to identify features of contrast (i.e. textural and soil moisture changes) accurately. Depth to gravel was generally easily identified in the arable plot where the C horizons consisted generally of sand layers (Fig 4.16) unlike the pasture plot where interbedded layers of sands and silts were common, especially within the Rangitikei series soil (Fig 4.18). Daniels (2004) describes that the depth of penetration is inversely related to the frequency of fine textured bands. These finer textured layers have the ability to store more water than that of the sandy layers and consequently attenuate the radar signal, preventing a clear image of features at depth (i.e. depth to gravel).

5.2 Seasonal Changes

The same velocity and gain settings were applied to both the September and February 200 MHz surveys. Reflection configurations were shown as 0.5 m shallower in the February survey compared to the September survey when comparing respective radargrams (e.g. Fig 4.20). This adjustment in configurations represents a change in velocity (i.e. from slower to faster) between the two survey dates. Since velocity is affected by water content, this has been hypothesised that there is a positive relationship between soil moisture and radar wave velocity. In addition to this, hyperboles have appeared wider and slightly more noticeable than in the September survey. The width of a hyperbole determines radar wave velocity. Where the hyperbole widens, this is indicative of a faster velocity and drier subsurface conditions.

The use of the Slice View tool in post processing identified areas where soil flow pathways or soil moisture was more prominent compared to other areas across the pasture plot (Fig 4.33 and 4.34). The ability to compare the changes in signal strength of Slice View images after velocity adjustment between September and February indicates possible flow pathways or zones of increased moisture. This was particularly obvious along the infilled channel bank located in the pasture plot.

The deeper penetration and lower resolution using the 100 MHz antennas allowed for identification of the water table at the pasture plot in the February surveys (Fig 4.35). In addition to the radargrams, the use of Slice View at depths close to the water table (i.e. 5 m depth) can indicate the spatial change in water table depth across the pasture plot (Fig 4.37).

The seasonal effects seen from radar wave signal changes, suggests that GPR is a useful tool to monitor soil moisture conditions between seasons and possibly determine subsurface flow pathways. In addition to this, the identification of gravel becomes more obvious in the drier season suggesting surveying in drier soil conditions can assist with identifying soil – gravel interfaces. This finding is in accord with Zhang et al. (2014) where identifying soil-bedrock interfaces and weathered-unweathered rock interfaces in shallow soils was more suited to drier soil conditions. Likewise the identification of layering within the deeper fractions of a soil profile was more prominent in September when soil moisture conditions were wet.

Overall, the importance of repeated surveys between seasons cannot be overlooked when understanding soil flow pathways, due to fluctuating soil moisture conditions and differential response of discrete soil types across seasons. This has proved beneficial when identifying the characteristics of flow pathways between wet and dry seasons as interpreted by Zhang et al. (2014).

5.3 Identifying Flow Pathways

The identification of flow pathways is reliant on changes in hydrological and physical properties. In general, volumetric water content varied down the soil profile, increasing where grain size decreased. Occasionally a sudden increase or decrease in soil moisture was found along a textural break. This is indicative of the existence of preferential flow where these pathways occur on top of a finer layer (e.g. Figure 4.5 at approx. 1m depth) (Gish et al., 2002). Additionally, these textural breaks could cause soils to be imperfectly drained, especially where finer particle sizes (i.e. silt) lay above a sand layer, leading to reduced conditions where potential

denitrification could occur (McLaren & Cameron, 1996; Stenger et al., 2013). Occasionally volumetric water content would show a sudden increase or decrease through deeper sand layers, away from any finer layering. For example, in Core 8 (Fig 4.3) at 1.96 and 2.09 m depth, changes in volumetric water content from 28% to 42% occur within a fine sand layer. This could be caused by macropore flow which only occurs vertically and not along the boundary of a possible restricting layer (Gish et al., 2002). The C horizon of the arable plot contained varying textures of predominantly sand fractions as shown through Core 2 and 3 (Fig 4.4 and 4.17 respectively). These cores showed a change in volumetric water content of 7% to 8% throughout their medium sand fraction. Although these fluctuations are small, they could potentially be showing the effects of macropore flow through a homogenous layer. As sand layers have an increased macroporosity compared with finer soil types, this could enhance water flow directly down the soil profile. Another feature that could influence flow pathways are the layering patterns of subsurface materials. A slope or slight inclination will have a gravitational effect on water movement compared with horizontal layered features (Gish et al., 2002). GPR is able to map out these sloping layers, which may otherwise be missed or be difficult to interpolate if only soil cores or pits are available. However it must be noted that topographically adjusting radargrams will give an accurate interpretation of the slope or inclination of subsurface layering. The radargrams shown in this research had minimal surface topographic differences. Therefore this feature was not added to displayed radargrams as the effect was minimal.

The arable plot provided a great example of how useful the GPR can be at capturing these subsurface undulations, with the gravel layer shown to be sloping sharply towards an infilled pool. Water flow draining down through the C horizon could potentially meet this sloping gravel layer and potentially progress towards the infilled pool. The ability of GPR for identifying subsurface layering is also useful, as Gish et al. (2002) identified that subsurface layering can influence soil moisture content. This research identified a variation in volumetric water content between respective layers, thus suggesting subsurface flow pathways will also be influenced from subsurface layering.

Surface and subsurface gravel contour and soil thickness maps from the arable and pasture plot gave a good visual representation of variation in ground surface and gravel topography, and the areas throughout both plots where soil thickness varied (Fig 4.38 and 4.39). These features could prove to be useful in identification of possible “hot spots” that control water flow instead of focusing on the entire area as a whole as emphasised by Binley et al. (2015).

As well as soil structures, GPR was also able to detect features within the underlying gravels. Areas across the two plots where the depth to gravel was shallow (<0.90 m), radargrams captured substantial information on the gravel structures. However, the radargram interpretations within the gravels are more tentative as it was not possible to extract cores of the gravels to calibrate the interpretations. The zone between the gravel surface and the water table within the gravels potentially forms an important area for water movement before it enters groundwater. The water table within these gravels was possibly identified with GPR, as supported by piezometer readings at the pasture plot, which points to the value of GPR for imaging the water table in alluvial materials.

When using the 100 MHz antennas, identification of gravel layers and water table depth were more apparent in the shallow Manawatu fine sandy loam soils of the pasture plot during February, when soil moisture conditions were drier. The water table was represented by a clear three band feature that became distorted when soil type changed from the Manawatu fine sandy loam to the Rangitikei silt loam over sand (Fig 4.35). The finer layering features within the Rangitikei silt loam over sand prevented a clear representation of the water table. This observation is supported by Doolittle et al. (2006) who states that closely spaced horizons can cause difficulty in identifying water tables.

6 Conclusions & Future Research

The geophysical technique GPR is a valuable tool for the rapid, non-invasive acquisition of subsurface information, which can be reliable when interpretations are accompanied with appropriate ground-truthing. In this study, GPR was used to assess its ability to identify subsurface features that have an impact on soil water flow pathways in alluvial soils of Dairy 1 farm, Massey University, Palmerston North, New Zealand. GPR survey data and soil physical data were collected and the following conclusions were made in regards to the ability of GPR to identify subsurface features that affect soil flow pathways:

1. The contrast between grain sizes gave the clearest and strongest radar signal. Where there was contrasting grain size, signal strength increased and was displayed as high-amplitude trace wavelets (dark red and dark blue bands in the radargrams). Where signal strength was weaker or there was minimum contrast between grain sizes, the low-amplitude signal was displayed as light red and blue in the radargram images.
2. Volumetric water content increased with decreasing grain size but sample depth had no clear relationship with volumetric water content (i.e. volumetric water content fluctuated down a soil profile), suggesting water movement was influenced from not only the surface infiltration, but from subsurface controls such as groundwater or perched water tables.
3. Bulk density had a weak relationship with mean grain size and sample depth but generally increased down the soil profile and with increasing mean grain size. This was not a feature that was obvious on the radargrams, but it is noted that bulk density correlates with grain size.
4. A sharp textural break appears to be the dominant feature highlighted in radargrams. However, not all layering features were evident on a radargram when using the 100 MHz and 200 MHz antennas. Strong signal reflectors have concealed other finer layering features.
5. The surface of the underlying gravels was identified in the radargrams and validated with augering, and this information was used to map the gravel

depth across both plots. Potential “hot spots” were identified from plot diagrams; where soil depth increased, this potentially creates a focus for soil water to drain towards. However, the surface of the gravels was not always easily identified due to finer textural layering above the gravel surface. This was more evident where soil depth increased (i.e. the Rangitikei silt loam over sand). When soil moisture conditions were drier during February, identification of depth to the gravels and depth to the water table were highlighted by the three band layering feature, when using the 100 MHz antennas. This feature was more evident within the shallow soils of the Manawatu fine sandy loam.

6. Groundwater was detected in the pasture plot using the 100 MHz antennas in February when soil moisture conditions were drier. A clear three band feature across individual radargrams was visible where gravels were shallow. Where gravels were deeper and textural banding occurred at depth, this weakened the radar signal, thus the water table was shown by an attenuated signal and a transitional zone, where partially saturated to saturated material exists. Slice View images gave an indication of the spatial change in groundwater depth across the pasture plot.
7. Radar velocity is noticeably affected by a change in soil moisture conditions between seasons. Because soil moisture is likely to be the only soil property that substantially changes across seasons, the change in velocity can therefore be used to detect and possibly map temporal soil moisture variation.

In summary, this research demonstrates the ability of GPR when using 100 MHz and 200 MHz antennas to acquire subsurface data for alluvial soils to depths >5 m. The use of GPR data coupled with minimal soil textural and piezometer data to identify soil stratigraphy and potential flow pathways has proved useful when assessing a large area. The use of GPR to identify flow pathways and water tables would provide valuable information to land users to identify potential flow pathways or zones where there is an increased risk of nutrients and pathogens that could enter groundwater via preferential flow. On the other hand, GPR could assist with

identification of potential zones where denitrification occurs (reduced conditions). This could also assist with matching land use intensity to a vadose zones capacity to convert NO^-_3.to dinitrogen (N_2) gas.

6.1 Recommendations for Future Research

The results and experience from this research lead to the following recommendations for further improvement of the application of GPR for research into soil flow pathways:

- **GPR Surveys**

Not all radargrams were linked to GPS coordinates. Initially GPS was deployed to assist with post processing in GIS software where LiDAR data were used (i.e. surface and gravel contouring). This feature could have been used more effectively if attached to the GPR during surveying to allow for accuracy with location of GPR transects. Although the method used gave an overall preliminary understanding of subsurface features and their location. If specific features were to be identified or future research was to be conducted in the area, the use of GPS jointly with GPR could provide an increased level of accuracy.

Initially, using the 200 MHz antennas gave a good indication of subsurface layering and stratification across the two plots from the September surveys. However, depth to the water table was unable to be obtained with these surveys. Identification of the water table was then excluded at this time. Identification of the water table between contrasting seasons would allow comparison of this feature as soil moisture conditions change.

Identifying finer (thin) layered features proved to be difficult using the 100 MHz and 200 MHz antennas. The value of using higher frequency antennas should be considered when identifying these finer features. Shih and Doolittle (1984) and Doolittle et al. (2006) have stated the issue with the triple band appearance affecting the identification of shallow or closely spaced interfaces and suggest using higher frequency antennas. Kung and Donohue (1991) used a 500 MHz antenna to

identify layers up to 1.85 m depth. The use of a higher frequency antenna will improve resolution in the shallow subsurface where identifying finer layers could be critical in determining soil flow pathways.

- **Soil Data Collection**

Soil physical and hydrological measurements across the study site were vital for ground-truthing radargrams albeit from limited sites. Identifying the spatial variability of grain size proved useful in identifying radargram configurations. However, temporal variables such as soil moisture and bulk density vary according to climatic and land use changes. Comparing samples between the September and February surveys would have been more beneficial and provided greater accuracy in understanding soil moisture changes between seasons. Interpreting radargrams during drier periods with soil moisture data would provide vital evidence to possible flow pathways or zones of moisture storage. In addition to analysis of radargrams, bulk density and soil moisture samples were dried at a lower temperature (75°C) instead of the recommended 105°C due to oven pre-sets. Soil cores were dried for a minimum of 72 hours which may have offset the lower temperature, although, soil cores are generally dried for 48 – 72 hours at 105°C. This may have had an effect on final weights of soil samples. For repeat surveys, oven temperatures should be set to the recommended temperature and re-weighed to check for constant weight.

Identifying radargram configurations between the depth to gravel and the water table proved difficult, as soil coring was limited to the initial depth to gravel to avoid damage to coring equipment. Estimations were then made regarding textural differences from the reflection configurations of respective radargrams. Having the ability to core through gravels to the water table may assist with radargram accuracy beyond gravel depth.

- **Radargram Imaging**

Identifying layering and comparing layering features between radargram images although useful, provided a basic understanding of subsurface features along

specific transects. To improve on this, reconstructing these radargrams and incorporating Slice View models into a 3D format would aid in the identification of flow pathways across a plot. Kung and Donohue (1991) have also identified this as an aid to improving knowledge of solute-transport within the subsurface.

References

Adamchuk, V. I., Hummel, J. W., Morgan, M. T., & Upadhyaya, S. K. (2004). On-the-go soil sensors for precision agriculture. *Computers and Electronics in Agriculture, 44*(1), 71-91.

Allred, B. J., Daniels, J. J., Fausey, N. R., Chen, C., Peters, L., & Youn, H. (2005). Important considerations for locating buried agricultural drainage pipe using ground penetrating radar. *Applied Engineering in Agriculture, 21*(1), 71-87.

Allred, B. J., Daniels, J. J., & Reza Ehsani, M. (Eds.). (2008). *Handbook of agricultural geophysics*. London: Boca Raton.

Annan, A. P., & Chua, L. T. (1992). Ground penetrating radar performance predictions

In J. A. Pilon (Ed.), *Ground penetrating radar*. Canada: Geological Survey of Canada.

Beres, M., & Haeni, F. P. (1991). Application of ground penetrating radar methods in hydrogeologic studies. *Ground Water, 29*(3), 375-386. doi: 10.1111/j.1745-6584.1991.tb00528.x

Blott, S. J., & Pye, K. (2011). Gradistat (Version 8): Kenneth Pye Associates Ltd. Retrieved from http://www.kpal.co.uk/gradistat.html

Boulding, R. (1995). *Practical handbook of soil, vadose-zone, and ground-water contamination : assessment, prevention, and remediation*. Boca Raton: Lewis Publishers.

Cameron, K. C., Di, H. J., & Moir, J. L. (2013). Nitrogen losses from the soil/plant system: a review. *Annals of Applied Biology, 162*(2), 145-173. doi: 10.1111/aab.12014

Charlton, R. (2007). *Fundamentals of fluvial geomorphology*. Abingdon, Oxon ; New York, NY: Routledge.

Chow, T. L., & Rees, H. W. (1989). Identification of subsurface drain locations with ground penetrating radar. *Canadian Journal of Soil Science, 69*(2), 223-234.

Clement, A. (2011). *Holocene sea-level change in the New Zealand archipelago and the geomorphic evolution of a Holocene coastal plain incised-valley system: the lower Manawatu valley, North Island, New Zealand*. Unpublished Thesis. Massey University.

Clement, A. J. H., & Fuller, I. C. (2007). Fluvial responses to environmental change in the North Island, New Zealand, during the past c. 30 ka recorded in river terrace sequences; a review and model for river behaviour. *New Zealand Journal of Geology and Geophysics, 50*(2), 101-116.

Clement, A. J. H., Sloss, C. R., & Fuller, I. C. (2010). Late Quaternary geomorphology of the Manawatu coastal plain, North Island, New Zealand. *Quaternary International, 221*(1–2), 36-45. doi: http://dx.doi.org/10.1016/j.quaint.2009.07.005

Collins, M. E., Cum, M., & Hanninen, P. (1994). Using ground penetrating radar to investigate a subsurface karst landscape in North-Central Florida. *Geoderma, 61*(1-2), 1-15. doi: 10.1016/0016-7061(94)90008-6

Cowie, J. D. (1964). Loess in the Manawatu district, New Zealand. *New Zealand Journal of Geology and Geophysics, 7*, 389-396.

Cowie, J. D. (1978). Soils and agriculture of Kairanga County, North Island, New Zealand. *New Zealand Soil Bureau Bulletin*(33), 92pp.

Daniels, D. J. (Ed.). (2004). *Ground penetrating radar* (2nd ed.). London, United Kingdom: Institution of Egineering and Technology.

Davis, J. L., & Annan, A. P. (1989). Ground-penetrating radar for high-resolution mapping of soil and rock stratigraphy. *Geophysical Prospecting, 37*(5), 531-551.

De Benedetto, D., Castrignanò, A., Sollitto, D., Campi, P., & Modugno, F. (2008). Non-intrusive mapping of subsoil properties in agricultural fields with GPR and EMI. *Proceedings First Global Workshop on High Resolution Digital Soil Sensing and Mapping*.

Di, H. J., & Cameron, K. C. (2002). Nitrate leaching in temperate agroecosystems: Sources, factors and mitigating strategies. *Nutrient Cycling in Agroecosystems, 64*(3), 237-256. doi: 10.1023/A:1021471531188

Doolittle, J. A., & Collins, M. E. (1995). Use of soil information to determine application of ground penetrating radar. *Journal of Applied Geophysics, 33*(1–3), 101-108. doi: http://dx.doi.org/10.1016/0926-9851(95)90033-0

Doolittle, J. A., Jenkinson, B., Hopkins, D., Ulmer, M., & Tuttle, W. (2006). Hydropedological investigations with ground-penetrating radar (GPR): Estimating water-table depths and local ground-water flow pattern in areas of coarse-textured soils. *Geoderma, 131*(3–4), 317-329. doi: http://dx.doi.org/10.1016/j.geoderma.2005.03.027

Fuller, I. C. (2005). February floods in the lower North Island, 2004: catastrophe - causes and consequences. *New Zealand Geographer, 61*(1), 40-50.

Gachter, R., Steingruber, S. M., Reinhardt, M., & Wehrli, B. (2004). Nutrient transfer from soil to surface waters: Differences between nitrate and phosphate. *Aquatic Sciences, 66*(1), 117-122. doi: 10.1007/s00027-003-0661-x

Gish, T. J., Dulaney, W. P., Kung, K.-J. S., Daughtry, C. S. T., Doolittle, J. A., & Miller, P. T. (2002). Evaluating Use of Ground-Penetrating Radar for Identifying Subsurface Flow Pathways. *Soil Science Society of America Journal, 66*(5). doi: 10.2136/sssaj2002.1620

Gish, T. J., Walthall, C. L., Daughtry, C. S. T., & Kung, K. J. S. (2005). Using soil moisture and spatial yield patterns to identify subsurface flow pathways. *Journal of Environmental Quality, 34*(1), 274-286.

Harari, Z. (1996). Ground-penetrating radar (GPR) for imaging stratigraphic features and groundwater in sand dunes. *Journal of Applied Geophysics, 36*(1), 43-52. doi: http://dx.doi.org/10.1016/S0926-9851(96)00031-6

Hedley, C. B. (2009). *The developments of proximal sensing methods for soil mapping and monitoring, and their application to precision irrigation : a thesis presented in partial fulfilment of the requirements for the degree of Doctor of Philosophy in Soil Science at Massey University, Palmerston North, New Zealand.* (Ph.D.), Massey University.

Hedley, C. B., Yule, I. J., Eastwood, C. R., Shepherd, T. G., & Arnold, G. (2004). Rapid identification of soil textural and management zones using electromagnetic induction sensing of soils. *Soil Research, 42*(4), 389-400. doi: http://dx.doi.org/10.1071/SR03149

Heerdegen, R. G., & Shepherd, M. J. (1992). Manawatu landforms - product of tectonism, climate change and process. In J. M. Soons & M. J. Selby (Eds.), *Landforms of New Zealand* (pp. 308 - 333). Auckland: Longman Paul.

Hesp, P. A., & Shepherd, M. J. (1978). Some aspects of late quaternary geomorphology of lower Manawatu valley, New Zealand. *New Zealand Journal of Geology and Geophysics, 21*(3), 403-412.

Hewitt, A. E. (2010). *New Zealand soil classification* (3rd ed.). Lincoln, New Zealand: Manaaki Whenua Press.

Hill, D. E., & Parlange, J. Y. (1972). Wetting front instability in layered soils. *Soil Science Society of America Proceedings, 36*(5), 697-&.

Horizons. (2016). Choose river rainfall chart. Retrieved 20/4/2016 from http://www.horizons.govt.nz/managing-environment/resource-management/water/river-heights-and-rainfall/Choose-river-rainfall-chart/

Huisman, J. A., Hubbard, S. S., Redman, J. D., & Annan, A. P. (2003). Measuring soil water content with ground penetrating radar: A review. *Vadose Zone Journal, 2*(4), 476-491.

Journeaux, P. (2005). *Farmed livestock as a source of microbial contamination of water*. Paper presented at the OECD Water and agriculture: sustainability, markets and policies, Adelaide, Australia.

Knighton, D. (1998). *Fluvial forms and processes a new perspective* (2nd ed.). Oxon, England: Routledge.

Kung, K. J. S., & Donohue, S. V. (1991). Imporved solute-sampling protocol in a sandy vadose zone using ground penetrating radar. *Soil Science Society of America Journal, 55*(6), 1543-1545.

Landcare Research. (2015a). *Soil report - Manawatu deep silt loam on sand, imperfectly drained phase*. Retrieved from http://smap.landcareresearch.co.nz/factsheet

landcare Research. (2015b). *Soil report - Manawatu sandy loam*. Retrieved from http://smap.landcareresearch.co.nz/factsheet

Landcare Research. (2015c). *Soil report - Rangitikei silt loam, mod deep phase*. Retrieved from http://smap.landcareresearch.co.nz/factsheet

Marshall, T. J. (1996). *Soil physics* (3rd ed ed.). Cambridge [England] ; New York: Cambridge University Press.

Massey University.). No. 1 dairy unit - Massey University. Retrieved 14/4/2016 from http://www.massey.ac.nz/massey/fms/Agricultural%20Services/No%201%20Dairy%20Farm/No%201%20Dairy%20Information%20Sheet.pdf

McLaren, R. G., & Cameron, K. C. (1996). *Soil science : sustainable production and environmental protection* (New ed ed.). Auckland: Oxford University Press.

Ministry of Health. (2008). *Drinking-water standards for New Zealand 2005*. Wellington. Retrieved from http://www.moh.govt.nz/notebook/nbbooks.nsf/0/237C397A37EFADA9CC25750600720E08/$file/drinking-water-standards-2008.pdf

Miyazaki, T. (2005). *Water flow in soils* (2nd ed ed.). Boca Raton, FL: Taylor & Francis.

Moebis, A. (2015). [Refractive Index].

NIWA. (2016). The national climate database. Retrieved 20/4/2016 from http://cliflo.niwa.co.nz/

Nuzzo, L. (2003). Coherent noise attenuation in GPR data by linear and parabolic Radon Transform techniques. *Annals of Geophysics, 46*(3), 533-547.

Page, K. J., & Heerdegen, F. G. (1985). Channel Change on the Lower Manawatu River. *New Zealand Geographer, 41*(1), 35-38. doi: 10.1111/j.1745-7939.1985.tb01067.x

Palmer, A. S. (2016, 19/4/2016). [Terraces of dairy 1 farm].

Pollock, J. A., Nelson, P., Tuohy, M. P., Gillingham, S. S., & Alexander, M. (2003a). Manawatu fine sandy loam. Retrieved 12/5/2016 from http://atlas.massey.ac.nz/soils/profiles/profile.html?P54

Pollock, J. A., Nelson, P., Tuohy, M. P., Gillingham, S. S., & Alexander, M. (2003b). Manawatu sandy loam. Retrieved 12/5/2016 from http://atlas.massey.ac.nz/soils/profiles/profile.html?P12

Pollock, J. A., Nelson, P., Tuohy, M. P., Gillingham, S. S., & Alexander, M. (2003c). Manawatu silt loam over sand. Retrieved 12/5/2016 from http://atlas.massey.ac.nz/soils/profiles/profile.html?P9

Pollock, J. A., Nelson, P., Tuohy, M. P., Gillingham, S. S., & Alexander, M. (2003d). Massey University soil map legend. Retrieved 13/4/2016 from http://atlas.massey.ac.nz/soils/legend/legend.html

Pollock, J. A., Nelson, P., Tuohy, M. P., Gillingham, S. S., & Alexander, M. (2003e). Para Rangitikei silt loam over sand. Retrieved 12/5/2016 from http://atlas.massey.ac.nz/soils/profiles/profile.html?P8

Raper, R. L., Asmussen, L. E., & Powell, J. B. (1990). Sensing hard pan depth with ground penetrating radar. *Transactions of the Asae, 33*(1), 41-46.

Rawls, W. J., Ahuja, L. R., Brakensiek, D. L., & Shirmohammadi, A. (1993). Infiltration and soil water movement. In D. R. Maidment (Ed.), *Handbook of Hydrology*. New York: McGraw-Hill.

Sensors & Software. (1999). *Ground penetrating radar - survey design*. Canada. Retrieved from http://johnrleeman.com/documents/GPR_survey_design.pdf

Sensors & Software. (2003). *EKKO view enhanced & EKKO view deluxe users guide*. Canada.

Sensors & Software. (2016). *EKKO project with processing, bridge deck condition and pavement structure models user's guide*. Canada: Sensors & Software.

Shih, S. F., & Doolittle, J. A. (1984). Using radar to investigate organic soil thickness in the Florida Everglades. *Soil Science Society of America Journal, 48*(3), 651-656.

Shukla, M. (Ed.). (2011). *Soil hydrology, land use and agriculture : measurement and modelling*. Cambridge, MA: Cabi.

Sloss, C. R., Jones, B. G., Switzer, A. D., Nichol, S., Clement, A. J. H., & Nicholas, A. W. (2010). The Holocene infill of Lake Conjola, a narrow incised valley system on the southeast coast of Australia. *Quaternary International, 221*(1–2), 23-35. doi: http://dx.doi.org/10.1016/j.quaint.2009.06.027

Stenger, R., Clague, J., Woodward, S., Moorhead, B., Wilson, S., Sholkri, A., . . . Canard, H. (2013). *Denitirification - The key component of a groundwater system's assimilative capacity for nitrate*, Massey University, Palmerston North, New Zealand.

Vale, S. S., Fuller, I. C., Procter, J. N., Basher, L. R., & Smith, I. E. (2016). Characterization and quantification of suspended sediment sources to the Manawatu River, New Zealand. *Science of the Total Environment, 543*, 171-186. doi: 10.1016/j.scitotenv.2015.11.003

Zhang, J., Lin, H., & Doolittle, J. (2014). Soil layering and preferential flow impacts on seasonal changes of GPR signals in two contrasting soils. *Geoderma, 213*, 560-569. doi: 10.1016/j.geoderma.2013.08.035

Appendices

1. Soil Core Results

Soil core results showing bulk density, volumetric water content, mean grain size, texture and soil type across all cores from the arable and pasture plot.

Core Location	Horizon Layer	Sample Depth	Bulk Density	Volumetric Water	Mean Grain Size	Grain Size Description	Texture	Soil Type
1	Ap	0.28	1.26	33%	24.12	Coarse Silt	silt loam	Manawatu silt loam over sand
	Bw	0.46	1.38	29%	46.01	Very Coarse Silt	sandy loam	
	Cu1	0.66	1.19	27%	36.92	Very Coarse Silt	sandy loam	
	Cu2	1.06	1.62	12%	258.15	Medium Sand	sand	
2	Ap	0.21	1.21	30%	32.19	Very Coarse Silt	silt loam	Manawatu silt loam over sand
	BC	0.51	1.49	15%	265.71	Medium Sand	sand	
	Cu	0.71	1.55	8%	426.60	Medium Sand	sand	
	Cu	1.41	1.60	15%	473.46	Medium Sand	sand	

3	Ap	0.26	1.29	28%	26.90	Coarse Silt	silt loam	Manawatu silt loam over sand
	Cu1	0.41	1.51	21%	140.13	Fine Sand	loamy sand	
	Cu3	0.91	1.53	9%	409.61	Medium Sand	sand	
	Cu3	1.51	1.65	17%	318.02	Medium Sand	sand	
4	Ap	0.21	1.30	30%	73.63	Very Fine Sand	sandy loam	Manawatu sandy loam
	B(w)	0.49	1.46	24%	55.60	Very Coarse Silt	sandy loam	
	Cu1	0.82	1.50	13%	114.29	Very Fine Sand	loamy sand	
	Cu2	1.01	1.51	44%	49.83	Very Coarse Silt	sandy loam	
	Cu3	1.51	1.63	11%	324.87	Medium Sand	sand	
5	Ap	0.21	1.43	33%	75.52	Very Fine Sand	sandy loam	Manawatu sandy loam
	C1	0.71	1.39	17%	126.74	Fine Sand	sand	
	C2	1.09	1.67	44%	38.02	Very Coarse Silt	sandy loam	
	C3	1.51	1.54	9%	400.00	Medium Sand	sand	
6	AC	0.45	1.30	30%	70.81	Very Fine Sand	sandy loam	Rangitikei silt loam over sand
	Cu1	0.7	1.52	7%	145.0	Fine Sand	sand	
	Cu2	0.97	1.40	8%	273.6	Medium Sand	sand	

	Cu3	1.32	1.53	8%	375.0	Medium Sand	sand	
	Cu3	1.57	1.47	39%	60.25	Very Coarse Silt	sandy loam	
	Cu3	1.67	1.39	47%	47.06	Very Coarse Silt	sandy loam	
	Cu3	1.86	1.66	14%	260.3	Medium Sand	sand	
7	Ah2	0.21	1.40	35%	37.27	Very Coarse Silt	sandy loam	Manawatu fine sandy loam
	B1	0.38	1.70	36%	46.01	Very Coarse Silt	sandy loam	
	B2	0.57	1.47	13%	218.8	Fine Sand	sand	
	C(g)	0.68	1.41	32%	87.08	Very Fine Sand	loamy sand	
8	Ah	0.09	1.34	32%	14.98	Medium Silt	silt loam	Rangitikei silt loam over sand
	Cu1	0.53	1.45	34%	25.40	Coarse Silt	silt loam	
	Cu3	0.86	1.50	9%	151.0	Fine Sand	sand	
	Cu3	1.39	2.12	10%	322.4	Medium Sand	sand	
	Cu3	1.69	1.49	36%	85.46	Very Fine Sand	loamy sand	
	Cu3	1.96	1.20	28%	95.15	Very Fine Sand	loamy sand	
	Cu3	2.09	1.35	42%	75.18	Very Fine Sand	loamy sand	
	Cu3	2.46	2.24	12%	433.3	Medium Sand	sand	

9	Ah	0.19	1.26	31%	22.31	Coarse Silt	silt loam	Rangitikei silt loam over sand
	Cu2	0.89	1.38	30%	84.90	Very Fine Sand	loamy sand	
	Cu2	1.29	1.99	8%	378.7	Medium Sand	sand	
	Cu2	2.11	1.39	42%	105.8	Very Fine Sand	loamy sand	
	Cu2	2.44	1.72	17%	253.1	Medium Sand	sand	
10	Ah	0.26	1.34	33%	81.01	Very Fine Sand	sandy loam	Rangitikei silt loam over sand
	Cu1	0.69	1.76	25%	53.26	Very Coarse Silt	sandy loam	
	Cu2	0.77	1.38	10%	152.1	Fine Sand	sand	
	Cu2	1.39	1.39	43%	49.85	Very Coarse Silt	sandy loam	
	Cu2	1.67	1.39	51%	34.54	Very Coarse Silt	sandy loam	
	Cu2	1.81	1.45	19%	276.1	Medium Sand	sand	
11	B	0.33	1.54	33%	44.77	Very Coarse Silt	sandy loam	Manawatu fine sandy loam
	C1	0.67	1.37	11%	165.6	Fine Sand	sand	
	C2	0.78	1.40	29%	75.18	Very Fine Sand	loamy sand	
	C3	1.01	1.63	24%	243.5	Fine Sand	sand	
12	Bg	0.18	1.28	34%	50.20	Very Coarse Silt	sandy loam	Manawatu fine sandy loam

	BC	0.42	1.44	32%	31.78	Very Coarse Silt	sandy loam	
	C1	0.56	1.39	14%	190.1	Fine Sand	sand	
	C2	0.63	1.36	31%	100.2	Very Fine Sand	loamy sand	
13	Bg	0.19	1.37	24%	68.84	Very Fine Sand	sandy loam	Manawatu fine sandy loam
	C1	0.47	1.50	14%	192.4	Fine Sand	sand	
	C2	0.68	1.47	16%	271.9	Medium Sand	sand	
	C3	0.84	1.44	42%	60.05	Very Coarse Silt	sandy loam	